Field Emission Current Analysis for the Assessment of Dielectric and Switching Performance of Vacuum Interrupters

Vom Fachbereich 18
- Elektrotechnik und Informationstechnik -
der Technischen Universität Darmstadt

zur Erlangung der Würde eines
Doktor-Ingenieurs (Dr.-Ing.)

genehmigte

Dissertation

M.Sc. Masoumeh KOOCHACK ZADEH
geboren am 13. Dezember 1979 in Teheran

Referent:	Prof. Dr.-Ing. Volker Hinrichsen
Korreferent:	Prof. Dr. René Smeets
Tag der Einreichung:	18. Januar 2011
Tag der mündlichen Prüfung:	27. April 2011

D17
Darmstadt 2011

Part-project 1: Diagnostic of Vacuum Quality ("DVQ") was sponsored by "*Deutsche Forschungsgemeinschaft* (DFG)" under the priority program "*Zustandsbewertung von Betriebsmitteln und Anlagen der elektrischen Energieversorgung*" (SPP 1101).

Part-project 2: Impact of Capacitive Switching ("ICS") was an industry cooperation partly sponsored from KEMA T&D Testing Services as well as Siemens AG Energy Sector, Power Distribution Division, Medium Voltage.

Acknowledgment

The present thesis is the outcome of my work as a scientific assistant at the Department of High Voltage Laboratories of the *Technische Universität Darmstadt*. I am pleased at this moment to acknowledge those who have contributed to this work.

First and foremost, I would like to thank my advisor Prof. Dr.-Ing. Volker Hinrichsen from *Technische Universität Darmstadt* for his ongoing support and encouragement in this research project. I was very fortunate to have had an advisor who gave me the freedom to explore my own ideas and at the same time the guidance that I needed to stay on course.

I am also deeply grateful to Prof. Dr. René Smeets from the "KEMA R&D High Power Laboratory" for his continuous support. I am very honored that he had agreed to to be my co-referee.

Special thanks go to "German Research Foundation (DFG)", "KEMA T&D Testing Services" as well as "Siemens AG Energy Sector", without whose financial support this project would not have been possible. Special thanks go to Mr. Andreas Lawall, Mr. Dr. Roman Renz, Mr. Dr. Jörg Teichmann and Mr. Ulf Schümann from "Siemens AG Energy Sector" for the helpful discussions during this research work, as well as Mr. Sander Kuivenhoven from "KEMA Development Engineer T&D Testing Services" for his valuable input to the "software compensation" of this work. Further thanks to "GSI Helmholtzzentrum für Schwerionenforschung GmbH" for the hardware support and help in design of the vacuum circuit.

Furthermore, I would like to express my gratitude to the employees of the mechanical and electronic workshops at the Department of High Voltage Laboratories, without their assistance, the project would be difficult to be concluded. In addition my thanks should go also to all participating students, employees, colleagues of our department for permanent technical support and for the very positive time that I had during my work in our department. In special, I would like to thank Ms. Simona Feier-Iova, Mr. Patrick Halbach, Mr. Thomas Wietoska and Mr. Thomas Rettenmaier for their support. Many thanks also to Mr. Günther Kloss for his assistance during the experimental measurements.

My special thanks go to family Mesbah for their support during the first two years of my stay in Darmstadt.

Last but not least, none of this would have been possible without the assistance and love of my parents Zahra Kheirkhah and Sadegh Koochack Zadeh who always provided open ear for me and thought me early in my life the value of education.

Finally, I affectionately acknowledge the support and encouragement given by my lovely husband Mehrdad Mirreza to whom I dedicate this thesis.

Contents

List of symbols

α	-	Middle shield potential factor
β	-	Field enhancement factor
β_{mac}	-	Macroscopic enhancement factor
β_{mic}	-	Microscopic enhancement factor
ϵ_0	As/Vm	Dielectric constant
ϕ	eV	Surface work function
ϕ_{I}	eV	Potential barrier without external electric field stress
ϕ_{II}	eV	Potential barrier with external electric field stress
γ	-	Covering ratio
μ	eV	Energy of electrons at Fermi level
θ	$^\circ$	Angel
ϑ	K	Temperature
ρ	kg/m^3	Material density
τ_1, τ_2	ms	Time constants
ω	rad/s	Angular frequency
A_{e}	m^2	Emitting area
C_0, L_0	µF, mH	Capacitance and inductance of the arc-polishing circuit
$C_{0,1}$, $C_{0,2}$	nF	Capacitances
C_1, C_2	µF	Capacitor banks
C_{c}, C_{ms}, $C_{\mathrm{k\text{-}ms}}$	pF	Interrupter capacitances
C_{cou}	pF	Coupling capacitance
C_{i}, L_{i}	µF, µH	Impulse capacitance and inductance
C_{k}	pF	Compensation capacitance
C_{p1}, C_{p2}	pF	Parasitic capacitances
C_{r}	nF	Range capacitance
C_{s}	µF	System capacitance
C_{sr}	µF	Source capacitance
d	mm	Interrupter's gap spacing
d_0	mm	Gap spacing by pre-arc ignition
d_{r}	mm	Rated gap spacing
d_{w}	mm	Contact to middle shield distance
E_{i}	eV	Ionizing energy
E_{EN}	eV	Electro negativity
E_{m}	V/m	Surface electrical field stress
E_{hom}	V/m	Homogeneous electrical field stress
E	V/m	Electrical field stress
f	Hz	Frequency

h_e	µm	Hight of the micro-emitter
i_break	A	Breaking current
i_c	A	Capacitive load current
i_cap	µA	Capacitive current component
$i_\mathrm{cap,equ}$	µA	Equivalent capacitive current
i_F	µA	Field emission current
i_F1	µA	Field emission current before arc-polishing
i_F2	µA	Field emission current immediately after arc-polishing
$i_\mathrm{F,stab}$	µA	Stabilized field emission current
i_h	kA, A	High current
i_inrush	kA	Inrush current
i_HF	kA	High frequency current
i_tot	µA	Total current
j_oF	$\mathrm{A/m^2}$	Field emission current density at low temperatures
j_F	$\mathrm{A/m^2}$	Field emission current density
k_c	pF	Compensation factor
k_f	-	Fluctuation factor
L_1	mH	Current limiting reactor
L_i	µH	Impulse inductance
L_par	µH	Parasitic inductance
L_s	µH	System inductance
L_sr	µH	Source inductance
m	-	Slope of the Fowler-Nordheim line
$\tilde{n}$	$1/\mathrm{m^2}$	Density num. of particles adsorbed on a solid surface
$\tilde{n}_\mathrm{mono}$	$1/\mathrm{m^2}$	Area rel. density num. of particles in mono molecular layer
p	mbar	Pressure
Q_p	As	Acquire charge of a particle
R_3, R_4, R_5, R_6, R_7	Ω	Decoupling resistances
R_d1, R_d2, R_d3	Ω	Decoupling resistances
R_k1, R_k2	Ω	Compensation resistances
R_L, R_L1, R_L2	Ω	Current limiting resistances
R_s	Ω	System resistance
R_sr	Ω	Source resistance
R_sh	Ω	Shunt resistance
r_e	µm	Radius of the micro-emitter
r_k	mm	Radius of electrode edge
r_p	µm	Particle's radius
T, T_1, T_2	K	Temperatures
t	s	Time
$t_{0.5}, t_{1.2}$	ms	Time parameters
t_mono	ms	Formation time of a mono molecular layer on a solid surface
$t_\mathrm{p\text{-}a}$	ms	Pre-arcing time
V_ch	kV	Charging voltage
V_r	kV	Rated voltage
v	kV	Voltage

$v_{2,\,\mathrm{vac}}$	V	Interrupter voltage at secondary side of the divider
v_{b}	kV	Breakdown voltage
v_{c}	kV	Capacitive load voltage
v_{cr}	m/s	Critical impact velocity
v_{d}	V	Forward voltage of diodes
v_{i}	m/s	Impact velocity
v_{in}, v_{in1}, v_{in2}	V	Input voltage
v_{ms}	kV	Middle shield potential
v_{o1}, v_{o2}, v_{o3}, v_{out}	V	Output voltage
v_{rec}	kV	Recovery voltage
v_{s}	kV	System voltage
v_{sh}	mV	Voltage drop across the measurement shunt
v_{sr}	kV	Source voltage
v_{T}	kV	Transformer voltage
v_{vac}	kV	Interrupter voltage
w_{i}	eV	Impact energy
y	-	Field parameters from the Fowler-Nordheim equation

List of abbreviations

ac	Alternating current
CF	Conflat
DB	Dielectric breakdown
DRS	Diode-resistor-shunt
DVQ	Diagnostic of vacuum quality
dc	Direct current
EIG	Electronic impulse generator
ES	Earthing switch
exp	Exponential
FEA	Field emission current measurement immediately after arc-polishing
FNP	Fowler-Nordheim plot
GIS	Gas insulated switchgear
GA	Gas-discharge arrester
HF	High frequency
ICS	Impact of capacitive switching
IEC	International electro-technical commission
IEEE	Institute of electrical and electronics engineers
MVI	Model vacuum interrupter
RC	Rogowski coil
RV	Recovery voltage
TG	Triggered spark gap
UHV	Ultra high vacuum
VCB	Vacuum circuit breaker
VI	Vacuum interrupter

List of chemical abbreviations

CuCr	Copper-chromium
FC-72	Fluorinert^{3M} liquid
N_2	Nitrogen
O_2	Oxygen
OFHC	Oxygen free high conductivity copper

Abstract

Vacuum circuit breakers (VCB) are dominantly used worldwide in medium voltage levels. However, in the recent years, there is a marked increase in interest to use VCBs also in sub-transmission voltage levels. This is mainly due to the environmental issues. However, the existing medium voltage VCB technology cannot be directly applied to the high voltage VCB due to the different design features which face an increase in difficulties as the voltage rises.

One very important issue in this regard could be the lack of an appropriate diagnostic tool for the evaluation of the vacuum interrupters' internal pressure. The users in the transmission voltage levels often want to know more about the up-to-date state of the high-voltage devices during their whole service life. Although in case of vacuum interrupter, it is difficult to decide upon the necessity of such diagnostics, and further discussion is required. According to current findings of the Cigré working group A3.27 "The impact of the application of vacuum switchgear at transmission voltages" (established 2009; work not yet finished), besides some technical and economical concerns, the non-availability of vacuum quality diagnostic tools might be one of the reasons for transmission system operators not to apply vacuum circuit breakers in their high-voltage transmission systems. Therefore, more investigation should be performed to develop an applicable diagnostic method for the internal pressure verification and vacuum quality tests, without demounting the interrupter from the switchgear. This investigation is the first part of the presented work, which is abbreviated in the whole work as "**DVQ**" for the diagnostic of vacuum quality. In this regard, a promising method, based on the measurement of field emission current immediately after arc-polishing of the contacts (named here as "FEA" method) is studied, which was firstly proposed by Frontzek and König. The results show that for a model vacuum interrupter with inhomogeneous electrode configuration (tip-plate), the decay rate of the field emission current after arc-polishing can be used for identifying the vacuum quality. However, for commercially available vacuum interrupters having more complex gap and contact geometries, it was not possible at all to define a test method or any test parameter configuration based on the chosen method, respectively, which would reproducibly cause a decay of the field emission current after arc-polishing. For statistically reliable evaluation on commercial interrupters extremely large number of trials would be necessary, which is totally unacceptable. Therefore, the investigated method has no practical meaning for monitoring purposes. Though the effects, which were published earlier, are basically present, the reproducibility is unfortunately too low. The search for a practical on-site diagnostic tool must therefore go on.

Another challenging issue with regard to the applicability of VCBs in high voltage systems, is the performance of the interrupter during capacitive switching test duty and the

avoidance of dielectric breakdowns (restrikes). Even in the medium voltage level, there are severe requirements for this test duty according to the IEC circuit breaker standard. To design an interrupter with very low probability of restrikes, especially at higher voltages, it is necessary to understand the physical origins of restrikes occurrence. Therefore, systematic research is performed to identify different electrical activities (especially field emission current) in the vacuum gap during the recovery phase of the interrupter after capacitive switching. The influence of pre-arcing during closing as well as arcing during opening on the dielectric performance and field emission characteristics of the gap for different types of vacuum interrupters are studied. This investigation is the second part of this dissertation, which is abbreviated as "**ICS**" for the impact of capacitive switching. The results of the investigation shows that the capacitive arc current and its time duration have significant influence on the field emission current during recovery. The impact of the inrush (making) current on the field emission current during recovery is observed to be large and to be clearly related to its amplitude. It was also found that the average value of the field emission current (according to the proposed procedure "(10×10)measurement") is a good measure for dielectric instabilities of the interrupter. However, no solid one-by-one relationship can be established between breakdown probability and field emission current in the available types of the interrupters. Furthermore, it is observed that the likelihood of restrikes during capacitive switching is a proper figure to control the production quality of vacuum interrupters. Hence, by using this method the stability of the production process of vacuum interrupters can be evaluated.

In both part-projects (DVQ and ICS), measurements, analysis and modeling of very small field emission currents (microampere up to milliampere range), as prognosticated by the quantum mechanical Fowler-Nordheim theory, in a high voltage environment under severe electromagnetic interferences, are the basis of the investigations. For this purpose, an especial measurement system as well as the required circuit for compensation of the capacitive current component, caused by the interrupter stray capacitance, are developed.

Kurzfassung

Vakuumschalter werden derzeit überwiegend in der Mittelspannungsebene eingesetzt. Jedoch zeigt sich in den letzten Jahren ein steigendes Interesse für Anwendungen in der unteren Übertragungsebene. Dies liegt vor allem an den umweltschädigenden Eigenschaften von SF_6. Die Technologie der heutigen Mittelspannungs-Vakuumschalter kann allerdings nicht ohne Weiteres für die Hochspannungsebene verwendet werden, da diese grundlegend andere Anforderungen an den Aufbau und die Dimensionierung von Betriebsmitteln stellt.

Als ein Nachteil der Vakuum-Technologie gegenüber der SF_6-Technologie wird von den Übertragungsnetzbetreibern gelegentlich das Fehlen eines geeigneten Werkzeuges zum Überwachen der Vakuumqualität in der Schaltröhre während der betrieblichen Lebensdauer gesehen. Darüber hinaus besteht bei Übertragungsnetzbetreibern häufig der Wunsch, über Diagnosemittel zu verfügen, obwohl es technisch gesehen bei Vakuumschaltern zur Zeit keine konkreten Anhaltspunkte bezüglich der Notwendigkeit gibt. Laut aktueller Erkenntnisse der Cigré Arbeitsgruppe A3.27 *„The impact of the application of vacuum switchgear at transmission voltages“* (gegründet 2009; noch nicht abgeschlossen) könnte, neben technischen und wirtschaftlichen Aspekten, das Fehlen von Diagnoseverfahren zur Überwachung der Vakuumqualität mit ein Grund für die aktuell seltene Anwendung von Vakuumschaltern in Übertragungsebenen sein. Aus diesem Grund sollen weitere Untersuchungen auf diesem Gebiet unternommen werden, um ein geeignetes Werkzeug für die Vakuumbeurteilung zu finden, ohne dass die Schaltröhre aus dem Schalter ausgebaut werden muss. Diese Untersuchung stellt den ersten Teil dieser Arbeit dar, welcher im Folgenden mit „**DVQ**“ (*Diagnostic of Vacuum Quality*) abgekürzt wird. In diesem Zusammenhang wird eine erfolgversprechende Methode erforscht, die auf der Feldemissionsstrom-Messung direkt nach der Lichtbogenlöschung basiert. Diese wurde erstmals von Frontzek und König untersucht. Die Ergebnisse für eine Modell-Vakuumröhre mit inhomogener Elektrodenanordnung (Spitze-Platte) zeigen, dass die Abklingrate des Feldemissionsstroms nach dem „Arc-Polishing“ genutzt werden kann, um die Qualität des Vakuums zu beurteilen. Jedoch war es im Rahmen dieser Arbeit nicht möglich, für kommerzielle Vakuumschalter mit ihren komplexeren Kontaktgeometrien, eine Testmethode bzw. eine Gruppe an Testparametern zu finden, die einen reproduzierbaren Abfall des Feldemissionsstroms verursachen können. Für statistisch verlässliche Beurteilungen der kommerziellen Schalter wäre eine enorme Anzahl an Versuchen notwendig, was nicht akzeptabel wäre. Aus diesem Grund erweist sich diese Untersuchungsmethode für Diagnosezwecke als nicht praktikabel. Obwohl die in vorangehenden Veröffentlichungen beschriebenen Effekte grundsätzlich vorhanden sind, ist ihre Reproduzierbarkeit leider zu gering. Die Suche nach einem geeigneten Mittel für die Diagnose von Vakuumschaltern im eingebauten Zustande ist somit noch nicht abgeschlossen.

Eine weitere Herausforderung für die Nutzung von Vakuumschaltern in der Hochspannungsebene ist die kapazitive Schalthandlung. Diese unterliegt selbst in der Mittelspannung gemäß dem gültigen ICE-Standard scharfen Richtlinien. Um Rückzündungen, speziell bei hohen Spannungen, zu vermeiden, ist es notwendig, deren physikalischen Ursprung zu bestimmen. Aus diesem Grund wurden systematisch Untersuchungen durchgeführt, um verschiedene elektrische Vorgänge (speziell den Feldemissionsstrom) während der Wiederkehrspannung nach einer kapazitiven Schalthandlung in der Schaltkammer zu bestimmen. In diesem Zusammenhang wurde der Einfluss der Lichtbogenzeit beim Öffnen und Schließen auf das dielektrische Verhalten und die Charakteristik des Feldemissionsstroms für verschiedene Vakuumröhren untersucht. Diese Untersuchungen sind der zweite Teil dieser Arbeit, welche im Folgenden mit „**ICS**“ (*Impact of Capacitive Switching*) abgekürzt sind. Die Ergebnisse der Untersuchungen zeigen, dass der kapazitive Strom und seine Dauer erheblichen Einfluss auf den Feldemissionsstrom während der Wiederkehrspannung haben. Die Auswirkung des Ausschaltstroms auf den Feldemissionsstrom konnte als sehr groß und mit deutlicher Abhängigkeit von der Amplitude beobachtet werden. Zudem wurde auch deutlich, dass der Mittelwert des Feldemissionsstroms (wie in der (10×10)-Methode vorgestellt) ein guter Indikator für die dielektrische Instabilität des Schalters ist. Allerdings konnte keine Eins-zu-eins-Beziehung zwischen der Durchschlagswahrscheinlichkeit und des Feldemissionsstroms in den zur Verfügung gestellten Schaltern hergestellt werden. Des Weiteren wurde beobachtet, dass sich die Wahrscheinlichkeit der Rückzündung während des kapazitiven Schaltens gut für die Qualitätskontrolle in der Vakuumschalter-Herstellung eignet. Folglich kann bei der Anwendung dieser Methode die Qualität des Herstellungsprozesses bewertet werden.

In beiden Teilprojekten (DVQ und ICS) werden als Basis der Untersuchung die Messung, die Analyse und die Modellierung kleiner Feldemissionsströme im Mikro- bis Milliampere-Bereich – wie in der quantenmechanischen Fowler-Nordheim-Theorie prognostiziert – in einer Hochspannungsumgebung bei großen elektromagnetischen Störungen durchgeführt. Daher wurden ein spezielles Messsystem für derartige Messungen, sowie ein System zur Kompensation der durch die Streukapazität des Schalters hervorgerufenen kapazitiven Stromkomponente entwickelt.

1 Introduction

Vacuum circuit breakers (VCB) are extensively installed in medium voltage levels since end of the twentieth century. However, in the recent years, there is a marked increase in interest to use VCBs in sub-transmission voltage levels. This is mainly due to the environmental issues over SF_6 technology, which is at the moment more dominant for applications at high voltages [Falk 06]. The vast number of publications from literature (e.g. [Itur 09], [Renz 06], [Wang 06], [Ohki 07], [Sche 06]) are proof of the interest and intensive research activities pertaining to the application of vacuum technology to these high voltages as a possible replacement for SF_6. A number of companies, especially in Asia, have produced or are developing single break VCBs for voltages up to 145 kV [Falk 06]. Some of these breakers have been installed by system operators or are already in use in industrial applications.

However, the existing medium voltage VCB technology cannot be directly applied to the high voltage VCB due to the different design features which face an increase in difficulties as the voltage rises. In this context, the interrupting performance, the dielectric behavior as well as the electrical and mechanical life of the device have a great importance.

One very important issue in this regard is the lack of an appropriate tool for the monitoring of the high degree of vacuum state in the interrupter during its service life, which is after a requirement of the users in high-voltage transmission systems. Unlike SF_6 breakers, which can be monitored for adequate SF_6 density for safe operation, vacuum interrupters are sealed for their service life. They are not connected to the pumping device after seal off and rely on being hermetically sealed. As the device becomes bigger in size (at higher voltages), there are more difficulties to handle, and hence more careful designs of the components, seals, and assembly techniques are required [Falk 06]. Moreover, the users in the transmission voltage level often want to know more about the up-to-date state of the high-voltage devices during their whole service life, although in case of vacuum interrupter, it is difficult to decide upon the need of such diagnostics, and further discussion is required. According to current findings of the Cigré working group A3.27 “The impact of the application of vacuum switchgear at transmission voltages” (established 2009; work

not yet finished), besides some technical and economical concerns, the non-availability of vacuum quality diagnostic tools might be one of the reasons for transmission system operators not to apply vacuum circuit breakers in their high-voltage transmission systems [Cigr 10]. Therefore, more investigation should be performed to develop an applicable diagnostic method for the internal pressure verification and vacuum quality tests, without demounting the interrupter from the switchgear. This investigation is the first part of the presented work, which is abbreviated in the whole work as "**DVQ**" for the diagnostic of vacuum quality. In this regard, a promising method, based on the measurement of field emission current immediately after arc-polishing of the contacts (named here as "FEA" method), which was firstly proposed by Frontzek and König, is studied [Fron 93a]. The preliminary results indicated that the decay rate of the field emission current after arc-polishing may be used for identifying the vacuum quality in a model vacuum interrupter. Further investigations were required for the verification of applicability of this method on commercial interrupters having more complex gap and contacts geometries.

Another challenging issue with regard to the applicability of VCBs in high voltage systems is the performance of the interrupter during capacitive switching test duty and the avoidance of dielectric breakdowns (restrikes) [Ryu 10]. Even in the medium voltage level, there are severe requirements for this test duty according to the IEC circuit breaker standard [IEC6 08]. To design an interrupter with very low probability of restrikes, especially at higher voltages, it is necessary to understand the physical origins of restrikes occurrence. Furthermore, it is practical to have more detailed information (than "pass" or "not pass") on the performance of the interrupter during testing. For these reasons, systematic research is performed to identify different electrical activities (especially field emission current) in the vacuum gap during the recovery phase of the interrupter. This investigation is the second part of this dissertation, which is abbreviated as "**ICS**" for the impact of capacitive switching. In this regard, the influence of pre-arcing during closing as well as arcing during opening on the dielectric performance and field emission characteristics of the gap for different types of vacuum interrupters are studied.

2 Theory and background

2.1 Vacuum circuit breakers

Vacuum circuit breakers are dominantly used worldwide in medium voltage levels ($1\,\mathrm{kV} < v < 52\,\mathrm{kV}$ [Kuch 05]) in contrast to the other types of breakers. Their reliability and safe performance are due to the advantage of switching in vacuum and the absence of an arc-quenching medium. **Figure 2.1** shows a typical cross-section of a vacuum interrupter, which is the switching element of a VCB[1]. It consists of a vacuum chamber, formed by ceramic hollow insulators, with two electrical contacts. One contact is fixed within the chamber, the other one is movable and connected through the metal bellows to the moving terminal. Thus, the contacts can be closed and opened by a mechanism connected to this terminal. In medium voltage level, vacuum interrupters with contact gap spacing of only few millimeters have high dielectric strength and small overall size in comparison with other kinds of interrupters [Slad 08], [Korn 08]. Because of this high dielectric strength they are capable to withstand the required power frequency and lightning impulse voltages by just a few millimeters contact gap spacing [Lipp 03].

Vacuum interrupters have no arc-quenching medium. After contact separation, the current continues to flow through a plasma (arc) until current zero crossing. As the switching gap is placed inside a vacuum chamber there are no ionisable gas molecules and the arc consists only of vaporized contacts material. This kind of arc is known as vacuum arc or metal vapor arc. Near current zero crossing, the metal vapor loses its conductivity as the feeding's energy decays and thus, the arc can be extinguished. This happens within a few microseconds as the charge carrier ions recombine [Mull 04] and the dielectric strength of the gap is restored. Therefore, the vacuum interrupter is also known as a zero-quencher. After arc extinguishing, the metal vapor condenses mainly on the contacts surfaces with also a portion on the metallic middle shield (see Figure 2.1), which has the function to prevent condensation of the metallic vapor onto the ceramic insulators.

[1] Vacuum circuit breaker (VCB): Whole breaker consisting of three poles (three vacuum interrupters) and a mechanical drive. Vacuum interrupter: one vacuum bottle of the VCB

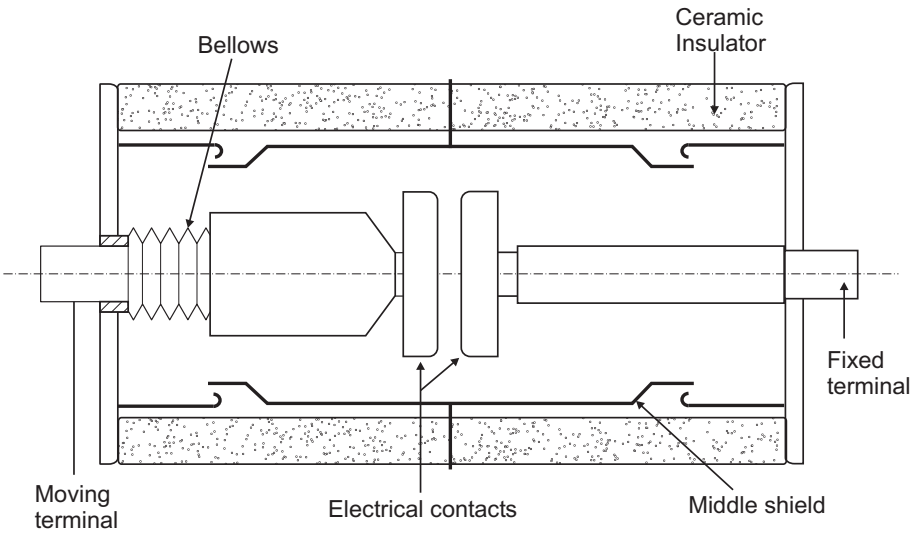

Figure 2.1: Cross-section of a vacuum interrupter

Vacuum interrupters are required to fulfill the following main functions:

1. providing high electrical insulation in open position
2. conducting currents in closed position without dissipating energy
3. interrupting different ranges of currents (load currents up to short circuit currents) with different kinds of transient recovery voltages (TRV)
4. circuit energizing under high inrush currents

A very important requirement for the interrupter's proper functioning is to maintain a low enough internal pressure (about 10^{-7} mbar) during its entire service life. Another important point to be considered is the contacts surface condition, which has also a significant effect on the withstand voltage of the interrupter. The gap history, number and kind of the making and breaking operations during service life, affect the contacts surface condition and hence have remarkable influence on the dielectric behavior of the vacuum interrupter [Lipp 03].

2.2 Electrical insulation in vacuum

As mentioned, a high dielectric strength is one of the main requirements of vacuum interrupters, which not only depends upon the macroscopic parameters such as contact

material, contact geometry, gap distance and residual gas pressure but also on the microscopic conditions of the contact surfaces. The preparation procedure of the contacts during the manufacturing process as well as their operational history determine the microscopic parameters of the gap [Lath 81].

In the following, different physical phenomena, which have significant influence on the dielectric performance of the vacuum interrupter, are presented. Generally, for an electrical breakdown to occur, two conditions must be fulfilled [Slad 08]: Firstly, a source of electrons must be present. Secondly, generation of enough ions in an ionization process must be provided to have quasi-neutralized plasma.

2.2.1 Electrical field

The electrical field applied to the contact surfaces is more complex than the homogeneous field of a plate-plate electrode configuration. Due to the gap geometry (contacts, shields, ...) as well as because of existence of micro-protrusions on the contact surface the exact value of the surface electrical field stress E_{m} is the enhanced value of the homogeneous electrical field E_{hom}:

$$E_{\mathrm{m}} = \beta \cdot E_{\mathrm{hom}} = \beta \frac{v_{\mathrm{vac}}}{d} \tag{2.1}$$

Where v_{vac} is the applied voltage between the contacts, d is the contact gap spacing and β is the enhancement factor, which consists of two components:

1. β_{mic} is the microscopic enhancement factor due to the micro-protrusions on the contact surface.
2. β_{mac} is the macroscopic enhancement factor due to the gap geometry and the middle shield floating potential. Therefore:

$$E_{\mathrm{m}} = \beta_{\mathrm{mic}} \beta_{\mathrm{mac}} \frac{v_{\mathrm{vac}}}{d} \tag{2.2}$$

Microscopic enhancement factor

The magnitude of the microscopic enhancement factor β_{mic} depends on the dimension and geometry of the micro-protrusions. **Figure 2.2** shows the distortion of electrical field on a conical micro-protrusion. In [Lath 81] and [Slad 08], β_{mic} is calculated for various idealized micro-protrusions' geometries according to their dimensions. Due to the contact surface erosion during the interrupter's service life, the microscopic enhancement factor can even

reach values in the range of a few thousands. Micro particles, existing in the gap, may also affect the microscopic enhancement factor due to both "in-flight" and "impact" phenomena (see 2.2.2).

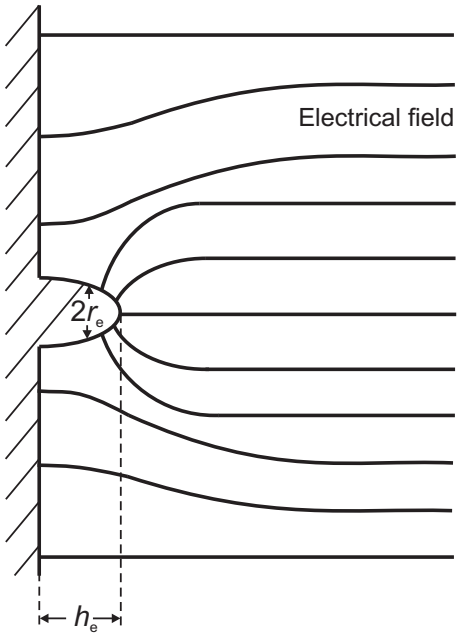

Figure 2.2: Distortion of electrical field around a micro-protrusion acc. to [Lath 81]

Macroscopic enhancement factor

The macroscopic enhancement factor β_{mac} depends on the internal design of the vacuum interrupter (geometric factor), as well as on the momentary value of the middle shield potential. In 9.4.1, the influence of the floating potential of the middle shield on the enhancement factor is described in detail.

2.2.2 Pre-breakdown effects

Field emission current

As mentioned, the first requirement for breakdown initiation is a source of electrons. Since there is no gas in the vacuum interrupters, the only source of electrons are metallic surfaces, e.g. micro-protrusions on the cathode's surface. Normally the electrons are held in the metal due to the potential barrier ϕ_{I} (see case I in **Figure 2.3**). However, they are able to leave the metal surface if having enough energy $\phi_{\mathrm{I}} = \phi + \mu$. Where, ϕ is the surface

work function and μ is the energy of the electrons at Fermi-level (FL) in eV. In case of the presence of an external electric field E acting on the metallic surface, the potential barrier becomes lower (ϕ_{II}) and narrower (see case II). According to quantum mechanical tunneling mechanism, for sufficiently high external electric field strength values $E \geq 3 \cdot 10^9\,\mathrm{V/m}$, the barrier width is sufficiently narrow that with certain probability electrons at Fermi-level can tunnel trough the barrier into vacuum. This phenomenon is known as field emission and was firstly formulated by Fowler and Nordheim in 1928 [Lath 81].

Figure 2.3 shows the potential barrier without (case I) and with (case II) an external electric field of $E \geq 3 \cdot 10^9$ V/m. Due to this external electric field, the potential barrier for electrons at Fermi-level is limited to the length x_{b}. The possibility that one electron tunnels trough the potential barrier is dependent on the width of the barrier [Ried 67] and therefore on the electrical field.

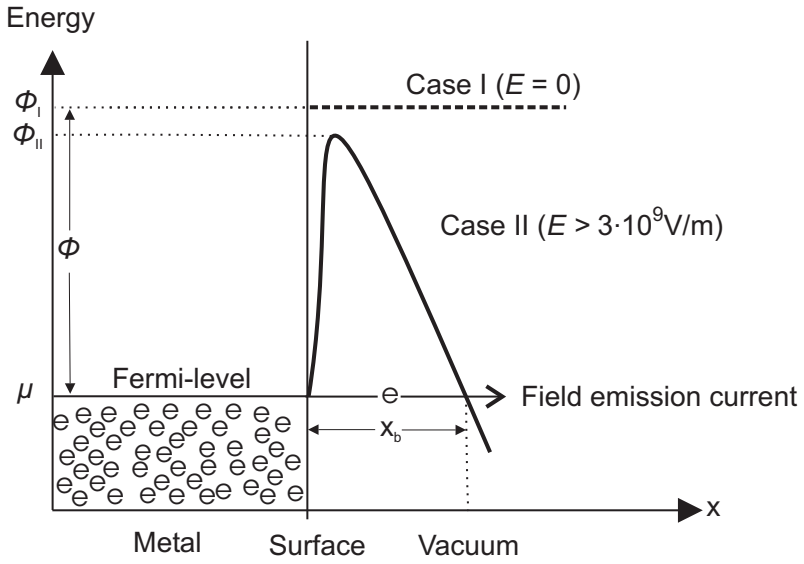

Figure 2.3: Schematic representation of the quantum mechanical tunneling effect acc. to [Eich 89] with and without external electric field

Below, the field emission current density according to Fowler and Nordheim (Fowler-Nordheim equation, FNE) for temperatures $\vartheta \leq 300\,\mathrm{K}$ is given:

$$j_{0\mathrm{F}} = \left(\frac{1.54 \cdot 10^{-6} {E_{\mathrm{m}}}^2}{\phi \cdot t_{(\mathrm{y})}^2} \right) \cdot e^{\left(\frac{-6.83 \cdot 10^9 \phi^{1.5} v_{(\mathrm{y})}}{E_{\mathrm{m}}} \right)} \tag{2.3}$$

where $j_{0\mathrm{F}}$ is the field emission current density in $\mathrm{A/m^2}$, E_{m} is the surface electric field strength in V/m and ϕ is the work function of the emitting surface in eV. The functions $t_{(\mathrm{y})}$ and $v_{(\mathrm{y})}$ are depending on the field parameter $y = \frac{\phi_{\mathrm{I}} - \phi_{\mathrm{II}}}{\phi}$ [Lath 81], [Eich 89]. At high

enough external electric field the potential barrier has a reduction down to the Fermi-level ($\phi_{\mathrm{I}} - \phi_{\mathrm{II}} = \phi$ and $y = 1$), which means possibility for free electron emission (see Figure 2.3). The simplified form of *equation 2.3* is shown below [Lath 81]:

$$j_{0\mathrm{F}} = C_1 {E_{\mathrm{m}}}^2 \cdot e^{\left(\frac{-C_2}{E_{\mathrm{m}}}\right)} \tag{2.4}$$

where C_1, C_2 are parameters depending on the work function:

$$C_1 = \frac{1.54 \cdot 10^{-6} \cdot 10^{4.52\phi^{-0.5}}}{\phi} \tag{2.5}$$

$$C_2 = 6.53 \cdot 10^9 \cdot \phi^{1.5} \tag{2.6}$$

At higher temperatures ($\vartheta > 300\,\mathrm{K}$) more electrons in metal reach energies above Fermi-level. These electrons are required to tunnel shorter distances through the potential barrier and consequently have higher emission probability. Therefore, the field emission current density has a strong temperature dependency for this range of temperatures, which is not taken into account according to the FNE [Lath 81].

Assuming a single emitter in order to find out the current-voltage-characteristic of the gap, the surface electrical field and the current density is substituted in *equation 2.4*:

$$j_{0\mathrm{F}} = \frac{i_{\mathrm{F}}}{A_{\mathrm{e}}} \tag{2.7}$$

where A_{e} is the emitting area, and i_{F} is the field emission current through the contact gap. The result of the substitution in logarithmic form is as shown below [Lath 81]:

$$\log\left(\frac{i_{\mathrm{F}}}{v_{\mathrm{vac}}^2}\right) = \log\left(\frac{1.54 \cdot 10^{-6} \cdot 10^{4.52\phi^{-0.5}} A_{\mathrm{e}} \cdot \beta^2}{d^2 \cdot \phi}\right) - \frac{2.84 \cdot 10^9 \cdot d \cdot \phi^{1.5}}{\beta \cdot v_{\mathrm{vac}}} \tag{2.8}$$

Plotting the field emission current i_{F} and the interrupter voltage v_{vac} in the form of a Fowler-Nordheim plot (FNP), i.e. $\log\left(\frac{i_{\mathrm{F}}}{v_{\mathrm{vac}}^2}\right)$ versus $\frac{1}{v_{\mathrm{vac}}}$, a straight line, as shown in **Figure 2.4**, will be the outcome. With the help of the slope of this line $m = \tan(\theta)$ and its Y-axis intercept Y_0, it is possible to calculate the field enhancement factor β and emitting area A_{e} for a known value of work function ϕ and contact gap distance d [Lath 81]:

$$\beta = \frac{-2.84 \cdot 10^9 d\phi^{1.5}}{m} \tag{2.9}$$

$$A_{\mathrm{e}} = \frac{10^{Y_0} d^2 \phi}{1.54 \cdot 10^{-6} \cdot 10^{4.52\phi^{-0.5}} \beta^2} \tag{2.10}$$

For the more complicated situation with several micro-emitters distributed on the cathode surface, the FNP will no longer be expected to result in a straight line. However, in practice the reverse is found to be true and as the voltage approaches the breakdown voltage of the gap v_b, it is noticeable that only one or two protrusions will become more dominant [Lath 81], [Slad 08].

From the discussion above, it is seen that the field emission current is depending on different parameters: applied gap voltage, microscopic and macroscopic field enhancement factor, gap distance as well as the work function of the emitting surface, which not only depends on the contact material but also on the presence of oxide layers and adsorbed gases. In [Slad 08] the sensitivity of the field emission current to the variations in the work function is shown.

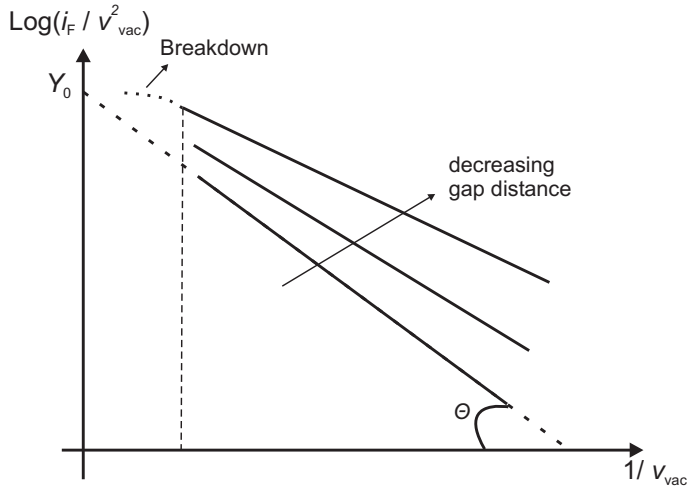

Figure 2.4: Current-voltage characteristic of the vacuum gap in the logarithmic form of the FNP for different gap distances acc. to [Lath 81]

Micro-particles

Micro-particles are always present in practical vacuum interrupters [Slad 08]. They are normally attached to the vapor shields or contact surfaces. Due to the mechanical vibrations during contact opening they can be detached from the surface and accelerated by the electric field. This may lead to late breakdowns in the interrupter after contact opening.

Micro-particles have several origins. They can be left over from the different stages of mechanical polishing and machining or they may be dust particles which are attached to the metal surface by van der Waals forces. Micro-particles may also be produced because of thermal instabilities on the electrode surfaces (cathode and anode hot spots). Impact of an

accelerated micro-particle in the electric field on the contact surfaces may also produce new micro-particles [Lath 95]. In [Slad 08] the distribution of micro-particles left on machined CuCr contact surfaces is given. Their diameter is usually in the range of several ten micrometers.

The charge of a micro-particle depends on the surface electrical field at the particle's original position before its detachment from the surface. Since the surface electrical field itself is dependent upon the geometry of the micro-protrusion/particle, the charge acquired by the particle depends also strongly on its shape. In [Lath 95] the charge acquired by different micro-particle geometries is given. For a spherical micro-particle resting on the contact surface the acquired charge is calculated as below:

$$Q_\mathrm{p} = 6.6\pi\epsilon_0 E_\mathrm{m} r_\mathrm{p}^2 \tag{2.11}$$

where Q_p is the charge acquired by the micro-particle, r_p is the radius of the micro-particle and ϵ_0 is the dielectric constant. Detachment of this charged particle from the contact surface and its acceleration towards the other contact result in the impact energy W_i and impact velocity v_i according to the following equations [Slad 08]:

$$W_\mathrm{i} = Q_\mathrm{p} v_\mathrm{vac} = 6.6\pi\epsilon_0\beta {v_\mathrm{vac}}^2 r_\mathrm{p}^2/d \tag{2.12}$$

$$v_\mathrm{i} = \sqrt{\frac{3Q_\mathrm{p}v_\mathrm{vac}}{2\pi r_\mathrm{p}^3\rho}} \tag{2.13}$$

where ρ is the density of the particle. Substituting *equation 2.11* in 2.13 and assuming the acquired charge Q_p being conserved, the impact velocity v_i is given as:

$$v_\mathrm{i} = \sqrt{\frac{9.9\epsilon_0\beta {v_\mathrm{vac}}^2}{d r_\mathrm{p}\rho}} \tag{2.14}$$

Acceleration of micro-particles in the gap by the applied electric field contributes notably to breakdown's initiation. Basically, there are two important phenomena to consider. The first one is the so called "in-flight" phenomenon, the second one is the impact phenomenon [Lath 95].

During the flight phase of micro-particles, different mechanisms may occur, which lead to loss of particle's charge or mass as described by Latham in [Lath 95] ("in-flight" phenomena). As a charged micro-particle approaches one electrode, it results in the enhancement of the electric field between the particle and the electrode and consequently in an increase of the field emission current and the possibility of a breakdown. In this mechanism, the

magnitude of the electrical field is more dominant for the initiation of the breakdown than the kinetic energy of the particle. Another effect, which may also occur during the flight phase, is the electron bombardment of the particle. As a micro-particle accelerates towards the cathode, due to the bombardment heating from the electron beam (field emission current between the two electrodes), a "mid-gap" vaporisation of the particle may occur [Lath 95]. Ionization of this metal vapor may lead to instabilities inside the gap and thus may increase the possibility of a breakdown.

Another phenomenon that must be considered is the interaction between the micro-particle and the contact surface (impact phenomenon). This phenomenon is explained in [Lath 95] and [Slad 08] comparing the particle's impact velocity v_i with the critical impact velocity v_cr, which depends on the material constants of the colliding surfaces (for copper $v_\mathrm{cr} = 200\,\mathrm{m/s}$):

1. Low impact velocity ($v_\mathrm{i} < v_\mathrm{cr}$) leads to semi-elastic non destructive bouncing impact. The particle may either stick to the surface or it may bounce. There is also the possibility of inelastic reflections and multiple transits in the gap as explained by Latham in [Lath 95] and [Lath 72].

2. Intermediate impact velocity ($v_\mathrm{cr} < v_\mathrm{i} < 5v_\mathrm{cr}$) leads to permanent mechanical deformation of the colliding surface:

   - generation of micro-craters in the surface or a micro-protrusion if a particle is welded to the surface, which results in enhanced local field enhancement factor (β). If this happens on the cathode surface, it results in an increase of the field emission current.

   - generation of secondary micro-particles during the impact, which could also be accelerated to the backing electrode.

3. High impact velocity ($v_\mathrm{i} > 5v_\mathrm{cr}$) leads to evaporation of the particle or electrode material and therefore, generation of a cloud of metal vapor, which allows regenerative ionization process and increases the possibility of a micro-discharge or even a full breakdown.

Micro-discharges

The pre-breakdown condition of a vacuum gap is also determined by the phenomenon of micro-discharges. These occur due to the applied voltage across the vacuum interrupter, and their possibility of occurrence increases at higher voltages. Micro-discharges are not

full breakdowns, but fast current spikes with amplitudes up to several ten milliamperes [Ziom 93]. The process, which causes these micro-discharges to occur, is not precisely known. For such discharges to occur, sufficient charge carriers must be produced for a short duration of time. A summary of different theories about the origin of micro-discharges is given below [Slad 08]:

1. Sub-critical explosive electron field emission from a cathode micro-protrusion. This could e.g. be the result of particles approaching the cathode and giving rise to local microscopic field enhancement and field emission current for a short duration of time. Another example for explosive emission of electrons may be an explosive destruction of a protrusion caused by a high current density flow through it.

2. Ion exchange process as a result of secondary emission of positive and negative ions from adsorbed gases on the contact surface. One random positive ion is accelerated towards the cathode in the electrical field and it may release negative ions by impacting with the cathode. In turn, the negative ions will also be accelerated in the field and may release more positive ions on impact with the anode surface. Therefore, if the multiplication of the number of ions generated at both cathode and anode is greater than unity, the process will develop to an avalanche resulting in a micro-discharge.

3. Release of gas, which is trapped in a contact's subsurface, could lead to a local electron avalanche.

2.2.3 Vacuum breakdown

While increasing the voltage across the vacuum interrupter, the different pre-breakdown effects as described above become more intensive until finally a full breakdown between the contacts occurs. As previously explained, two requirements for a vacuum breakdown are an existing cathode region that continuously supplies electrons and a source of gas in which ionization process for providing enough ions occurs. Therefore, a quasi-neutral plasma in vacuum can be built up. If these conditions are not fully achieved, only a micro-discharge occurs or in case of an existing arc, it extinguishes again [Slad 08]. In a vacuum gap, the main gas sources are metal vapor from the electrodes surface (cathode micro-protrusions or anode hot-spots) or micro-particles.

At very high electrical field stress, due to the high field enhancement factor β, a breakdown is caused by the field emission current flow. At sufficiently high field stress the potential barrier is reduced down to the Fermi-level i.e. $y = 1$, which means free possibility for

electron emission from the metallic surface (see Figure 2.3). Therefore, metal electrons can freely travel in the vacuum gap. This abrupt increase of the field emission current becomes noticeable as "field" breakdown [Eich 89].

A further breakdown mechanism is determined by the evaporation of the micro-protrusions existing on the cathode surface. In the literature this mechanism is known as "cathode" initiated breakdown. As the field emission current flows through a micro-protrusion, different energy exchange processes occur: thermal cooling due to conduction and radiation, resistive heating due to high field emission current density in the tip of the protrusion and "Nottingham" heating or cooling effect (explained briefly in Latham [Lath 81]). At high field emission currents, the micro-protrusion becomes unstable, resulting in its explosion. Evaporation of a micro-protrusion on the cathode surface occurs, if the thermal energy introduced to the protrusion is greater than its evaporation energy. In [Will 72] critical emission currents I_s, in which the temperature of the protrusion reaches its boiling temperature, are calculated for different protrusion geometries (cylindrical and conical emitters).

Another mechanism is due to anode instabilities. Due to the field electron emission there is an electron beam from the cathode impacting on a small anode area and heating it. If the input energy to this small anode area is high enough, it is possible to release metal vapor from it. Thus ionization could occur as a result of interaction between emitted electrons and the metal vapor. For contact gaps greater than 10 mm, as the gap voltage approaches the breakdown voltage, electrons will reach the anode surface at energies above 100 keV. In this case, the impacting electrons will even penetrate below the anode surface and deposit their energy in this sub-surface volume. In [Slad 08] the time to reach the boiling temperature of copper for this volume as a function of contact gap and field emission current is given. Temperature increase and expansion of this sub-surface volume would result in a high force on the anode surface. It is then possible that it breaks out and leads to a dense metal vapor cloud, which finally results in anode plasma expansion due to the interaction between electrons and metal vapor.

As is described in 2.2.2, micro-particles have also a significant influence on the breakdown initiation. Due to both "in-flight" and "impact" phenomena, micro-particles may lead to an increase in the field emission current (electron supply) as well as generation of metal vapor (possibility of ionization process, source of ions) and consequently production of a quasi-neutral plasma which is necessary for a breakdown to occur. A vacuum breakdown can also be a result of the combinations of the different mechanisms described above.

2.3 Vacuum arc

As is described in 2.1, vacuum circuit breakers must fulfill two switching operations: closing ("making") operations under inrush current as well as opening ("breaking") operations under load or short circuit currents. In the following, the interaction of the arc with the breaker for these switching operations is discussed.

2.3.1 Pre-arcing during closing operation

During the making operation of the vacuum interrupter, the electrical field stress between the contacts rises as the contact gap distance decreases. At a certain gap spacing and a sufficiently high field stress, the vacuum gap can no longer withstand the electrical stress and dielectric breakdown between the contacts occurs (pre-arc ignition). From this moment on until the first contacts touch, the making inrush current flows through the vacuum arc (pre-arcing) between the contacts, which carries the power circuit's current. During this time interval, the contact surface melts locally due to the arc's energy input to the contacts, if the current is sufficiently high [Slad 07]. This can lead to contact welding after contact touch, which will be broken during the next contact opening. As a result, new micro-protrusions can be built up on the contact surface. These new electron emitters increase the surface electrical field and, as is explained in 2.2, affect the dielectric properties of the gap. The duration of the pre-arcing is dependent on the closing velocity of the circuit breaker. Short duration pre-arcing is less disruptive for the contact surface. In 4.2 more details on the closing of vacuum circuit breakers under capacitive loads is given.

2.3.2 Development of the vacuum arc during opening operation

Depending on the application of vacuum circuit breakers, they have to interrupt load currents of up to several kiloamperes and short circuit currents up to several tens of kiloamperes. After contact separation the current continues to flow through the metal vapor arc (vacuum arc) until its energy input ceases. The current zero crossing in an ac system provides the opportunity for the circuit breaker to extinguish the arc. Near current zero, the metal vapor loses its conductivity as the feeding energy decays and the arc can be extinguished [Mull 04], [Slad 08], [Lane 08]. In the following, the initiation, development and finally extinction of the vacuum arc is explained.

Vacuum arc formation

As the electrodes start to separate, the contact area between the two electrodes decays. Therefore the actual cross section for current flowing through the contacts ceases and current density rises, which leads to local overheating of the electrodes surface. At a certain stage, the temperature of the contact spot will reach its melting point. Therefore, as the contacts continue to separate, a molten metal bridge will be formed between the contacts. More separation leads to instabilities of the molten bridge and finally, further extension and narrowing of the bridge results in its evaporation [Slad 08], [Haug 90], which results in a trapped and dense region of metal vapor in the small gap between the contacts close to the molten metal bridge's original position. The bridge rupture also leads to some metal particles being released from the contact surface. Due to the ionization of the originating high-pressure, high-temperature metal vapor, charge carriers are produced and a high-density, low-voltage glow discharge is built up [Puch 97], so that the current flow is sustained through this metal vapor arc. This discharge, which appears immediately after rupture of the molten metal bridge, operates in metal vapor of high densities $10^{25}-10^{22}\mathrm{m}^{-3}$ [Puch 97]. During this initial phase, the required electrons for current transport are caused by secondary emission, i.e. by ion impact on the cathode.

The glow discharge will transit to a usual arc due to the expansion of the metal vapor. This arc consists of cathode spots for electron supplement, and neutral plasma for current transport. But, there is still sufficient metal vapor in the region for the arc to be columnar (bridge column arc, 1 bar) [Slad 08]. For the stability of the bridge column arc, the arc roots have to supply enough metal vapor to replace the metal vapor, which continuously expands into the surrounding vacuum. This happens on the one hand due to the increase of the gap distance and on the other hand because of radial expansion of the metal vapor. Therefore, after a period of time, the bridge column arc will transit to a real vacuum arc. The time necessary for the initial bridge column arc to become a vacuum arc is a function of the instantaneous value of the current at contact separation, i.e. the higher the current at contact separation the longer is the conversion time. The mode of the vacuum arc after transition is also dependent on current magnitude. At higher currents, the vacuum arc after transition will remain a high-pressure columnar arc. In contrast, for low currents the transition leads to a diffuse vacuum arc. For an alternating current, it is possible that the arc mode changes between columnar and diffused mode. However, independent from the current amplitude, as the current goes to zero the vacuum arc will transit always to a diffused arc. The different modes of vacuum arc are as discussed below [Slad 08]:

- Diffuse vacuum arc for currents $i \leq 6\,\mathrm{kA}$: as is described, the vacuum arc consists

of a metal vapor plasma fed from the cathode spots. At low arc currents (about 100 A for copper), the plasma is supplied just from one cathode spot, and it moves with high speed towards the anode. The number of cathode spots increases proportionally with current. These spots move at random on the cathode surface. A new cathode spot replaces the old one as soon as it is extinguished. Once the cathode spots are distributed uniformly on the cathode surface, the plasma clouds (plasma plumes) of each spot grow together and result in a uniform neutral metal vapor plasma between the contacts. In this stage, there is just little overlapping between the plasma plumes. This kind of arc is known as a diffuse arc with many cathode spots [Lipp 03]. Here, the anode contact is basically passive and will just collect electrons over its hole surface [Slad 08]. For an alternating current, the number of spots increases as the current increases to its peak value and then decreases as the current approaches its zero crossing.

- Diffuse column vacuum arc for currents $6\,\text{kA} \leq i \leq 10\,\text{kA}$: at higher currents at a certain threshold value, interaction and overlapping between the cathode spots plasma plumes become considerable and this can change the characteristic of the arc. The threshold value depends on the contact geometry and material as well as on the external magnetic field [Slad 08], [Lipp 03]. In this overlapping plasma region, as the plasma density rises, the interaction between the plasma components increases. Due to the magnetic field, caused by the current flowing in the plasma, the arc will be confined to a defined low-pressure column. This arc has a main column with stable diameter, sometimes surrounded by individual cathode spots. The contact erosion due to the diffuse column arc shows only slightly melted craters on the cathode [Slad 08]. As the current ceases to zero, the interaction in the plasma region becomes less and the arc will thereby convert to a diffuse arc.

- Columnar vacuum arc for currents $i \geq 10\,\text{kA}$: if the contacts of the interrupter separate while carrying high currents, the bridge column arc transits into a high-pressure columnar arc. At sufficiently high currents, on one hand the energy input to the arc roots is high enough to compensate the material loss to the surrounding (caused by arc expansion), and on the other hand the arc is compressed due to its own magnetic field. This would overheat the contacts at the arc roots and cause considerable erosion on both contacts (cathode and anode). In this arc mode, both cathode and anode are providing the metal vapor for the ionization in neutral plasma and, therefore, are participating in the arc process.

In practical vacuum interrupters, in order to prevent such local overheating and erosion on the contact surfaces, special contact geometries, i.e. radial magnetic field contacts (RMF)

and axial magnetic field contacts (AMF), are used. For RMF design, the contacts are designed in a way that a radial magnetic field will be generated, which forces the arc to rotate and thus prevents local overheating. The energy input is then distributed over the whole rotating path. For higher interrupting currents AMF contacts are used. AMF design generates an axial magnetic field, which keeps the arc in the diffuse mode even at very high currents. The cathode spots spread more or less uniformly over the cathode's surface, and the energy input of the arc is distributed to the whole contact surface, so any local overheating is prevented [Mull 04], [Slad 08].

Current zero crossing and post-arc current

As in an ac circuit the current decreases to its natural current zero and the erosion of the contact material at the arc roots can no longer stand the loss of metal vapor, the arc transfers to a diffuse mode, with several cathode spots. Due to further reduction of the current, the number of cathode spots decreases and the energy input to the cathode spot extinction region ceases immediately, and its temperature reaches very fast the surrounding contact material temperature (thermal time constant in microseconds range [Slad 08]). Finally, at a certain current value (depending on the contact material), the vacuum arc consists of only one cathode spot. For further stability of the arc, the remaining cathode spot must emit sufficient electrons and metal vapor to supply the required positive ions to the plasma region. As the current in the last cathode spot declines below a minimalistic value and the energy into the spot region decays, the spot becomes unstable. This results in a lack of electron emission and metal evaporation necessary for arc stability and current continuity. Therefore the arc extinguishes suddenly and the current drops to zero sharply. In the literature this phenomenon is called as "current chopping" [Lipp 03], [Slad 08]. The value of the chopping current is dependent on the contact material and the amplitude of the breaking current. For CuCr contacts, it is in the range of a few amperes (1.5 A to 5 A) [Slad 08]. A high chopping current is undesirable, due to the associated overvoltages in the system.

During arc extinction, the cooling process of the arc roots and the molten areas begins and metal vapor production is stopped. But, in the intercontact region a certain amount of conductive charges and neutral particles in solid or even molten form (rest plasma) are still present. Decay of this rest plasma is necessary for the recovery of the dielectrical properties of the vacuum gap. The condition of the rest plasma just after current zero is dependent on the thermal stress, caused by the vacuum arc during the high current phase. Amplitude of the breaking current, duration of arcing time, appeared arc modes

and the instantaneous value of current at contact separation moment define the condition of rest plasma and consequently the recovery process. After arc extinction, the remaining neutral molecules and particles will condense on the contacts surface and partly on the vapor shield. The electrons and positive ions will partly recombine and in large part will be transported to the electrodes due to the transient recovery voltage (TRV), appearing after current zero across the electrodes. This charge transport results in a post-arcing current. The process during the post-arc phase is explained briefly below [Korn 08].

Just before current zero, the electrons and ions, launched from the last cathode spot, are moving towards the anode. Immediately after current zero, the old anode becomes the new cathode and the old cathode becomes the new anode. Whereas the ions continue their movement towards the old anode (new cathode), the electrons adapt their speed to the electric field. Therefore, their velocity is reduced and a net current of positive charges flows to the new cathode. This process continues until the electrons reverse their direction. During this time the voltage across the gap remains nearly zero because of the neutral plasma in the intercontact region. After the electrons reversed their direction, they move towards the new anode and leave behind an ionic space charge sheath. A transient recovery voltage (TRV) caused by the system circuit appears across the space charge sheath, which is, contrary to the plasma region, not neutral. This is shown in **Figure 2.5**. The post-arc current is a result of the ions in the sheath flowing towards the new cathode and the electrons in the plasma flowing towards the new anode. Due to the flow of electrons, which are faster than the ions, the space charge sheath continues to expand towards the new anode. Only after the sheath reaches the new anode, the TRV is applied across the full gap between the contacts. At this moment the current drops, since all electrons have been removed from the gap. The electric field between the contacts then transports the remaining ions to the new cathode [Slad 08], [Lane 08], [Lane 06].

Immediately after current zero, the gap may reignite if cathode spots build up on the new cathode (old anode). For a diffuse vacuum arc the old anode was passive during the arcing phase, thus, its surface has comparatively low temperatures with almost no erosion being produced. Whereas for columnar arc mode there are local melting zones on the old anode surface and significant anode erosions are to be seen [Boxm 95], [Mill 89]. Therefore, after a columnar mode arc, the possibility of forming a cathode spot on the new cathode and a consequently occurring reignition is much higher. As it has been discussed previously, the arc mode can be affected by different contact geometries due to the self-produced magnetic field. So, the thermal stress during arcing time, and thus, the breaking capability of the breaker is influenced by the contact geometry. Another important factor, having impact on the breaking capability, is the contact material. The material defines the intensity of

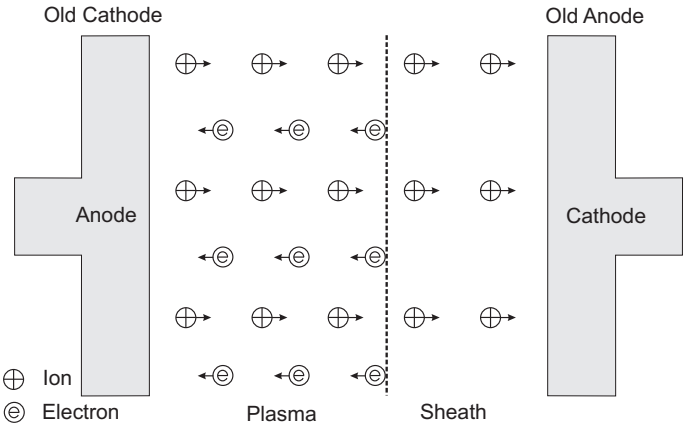

Figure 2.5: Schematic diagram showing the space charge sheath growth during the post-arcing phase acc. to [Lane 08]

the thermal stress during arcing time as well as the intensity of the cooling effect after arc extinction [Korn 08].

Failure after current interruption

After current interruption, the TRV appears across the interrupter. It contains a system frequency component and a high frequency component, which is determined by the circuit parameters and the chopping current [Korn 08]. The state of the vacuum gap and contact surface is determined by all thermal and mechanical stresses during former switching operations. If the condition in the gap is such that the interrupter is not able to withstand the recovery voltage after arc extinction, a breakdown will occur and a new arc will be formed (interruption failure). In general there are two types of failure: thermal breakdown and dielectric breakdown.

- **Thermal breakdown**: This type of breakdown is determined by the rest plasma and rest metal vapor after arc extinction. As described previously, immediately after arc extinction, the gap contains charge and metal vapor from the arc. Therefore, the maximum insulation property of the gap is not yet reached. The contact surfaces are still hot, they may even have molten metal regions on their surfaces. It takes a few microseconds for the charge particles to recombine and to be removed by the post arc current. A high residual charge density after current zero may lead to breakdowns in the post-arcing phase. The removal of the metal vapor from the intercontact region and cooling down of the electrode surfaces take even longer time (some milliseconds) [Lane 08]. Therefore, the vapor emission from the contacts and the ionization can

be continued after arc extinction for a period of time. The electrode surfaces' temperature determines the degree of vapor emission and the intensity of the molten region on the contact surfaces [Scha 02]. In case the vapor density in the intercontact region exceeds a threshold value (called as Paschen limit), immediate reignition occurs as soon as the TRV appears across the interrupter. Even below this limit, random breakdowns may occur under continuous voltage stress in the range of some milliseconds after current interruption [Scha 02]. The current amplitude in the high current phase, its steepness by current zero crossing, arcing mode and arcing time define the activities in the gap and their decay after arc extinction. The influence of the high current phase on the reignition behavior of the vacuum interrupter after current zero crossing is studied in detail in [Scha 02] and [Niay 01].

- **Dielectric breakdown**: After the charge carriers and the metal vapor are removed completely from the gap and the contact surfaces cool down, the vacuum gap will reach its full dielectric strength. It is then comparable with a cold vacuum gap [Korn 08], and the breakdown effect is determined by different phenomena, which are described in 2.2.3. These phenomena under the influence of recovery voltage may generate enough charge carriers in the gap and may even lead to a breakdown. This type of breakdown is known as dielectric breakdown. It normally occurs around the peak of the recovery voltage according to the high electrical field stress. Dielectric breakdowns may even occur several hundred milliseconds after current interruption (late breakdowns).

  Principally, there are two important phenomena. One is due to the surface condition of the contacts. Usually the contact surface has a certain roughness after manufacturing and conditioning processes. Each switching operation may change the contact surfaces due to mechanical (contact force, vibration) and thermal stresses. Breaking of contact welds (see 2.3.1) may also result in rougher contact's surface. The microprotrusions existing on the cathode surface results in electric field enhancement and consequently an increase of the field emission current, which may lead either to self evaporation of the cathode emitter (cathode initiated breakdown) or to the evaporation of a region on the anode surface, heated by the electron beam coming from the cathode (anode initiated breakdown). If the instabilities on the cathode or anode surface supply enough metal vapor, a vacuum breakdown can occur.

  Another important phenomenon is caused by the micro-particles existing in the gap. As it is described in 2.2.2, micro-particles have different origins. Mechanical vibrations after a switching operation, thermal instabilities on the contact surface or even impacting of a micro-particle with a metallic surface may detach a new

particle. During the flight phase of micro-particles (“in-flight” phenomena) or by their impact on the contact surface (“impact” phenomena), they can contribute to electron emission as well as metal vapor generation necessary for the ionization process. Thus, they cause the vacuum breakdown to occur.

3 Diagnostic of vacuum quality (DVQ) and its importance on interrupters performance

As is explained in chapter 2.1, vacuum circuit breakers are required to fulfill different fundamental functions in an electric power distribution system. However, their functional reliability may be affected by different parameters. In this regard, the interrupters' internal pressure is an important parameter, which has significant influence on the appropriate performance of the interrupter. Rise of the internal pressure above a certain threshold value ($10^{-4} \cdots 10^{-3}$mbar) [Fron 93b], [Fink 95], firstly reduces the interrupter high current breaking capability. One or two orders of magnitude higher than this threshold pressure, the vacuum interrupter also loses its insulating properties, and its functional reliability is no more guaranteed. Most vacuum interrupter manufacturers go far beyond this threshold value and produce new interrupters with residual gas pressure of less than 10^{-7} mbar (ultra-high vacuum range). On one hand, such a low residual gas pressure is a quality and reliability criterion. On the other hand, it provides a safety margin which must be sufficient for the whole service life [Fink 95].

During the last decades, many developments have been done with regard to sealing techniques, leak detection equipment and vacuum compatible materials. These developments have made it possible to produce sealed vacuum interrupters which can maintain good vacuum over their service life [Slad 08]. In medium voltage levels, vacuum interrupters are successful in real service for more than thirty years [Renz 07]. As the device becomes bigger in size (at higher voltages), there are more difficulties to handle and hence more careful designs of the components, seals, and assembly techniques are required [Falk 06]. Therefore, lack of an internal pressure diagnostic tool may become an important issue especially for the development of high voltage vacuum circuit breakers, as the transmission system operators usually want to know more about the up-to-date state of the high-voltage devices during their whole service life. According to current findings of the Cigré working

group A3.27 "The impact of the application of vacuum switchgear at transmission voltages" (established 2009; work not yet finished), besides some technical and economical concerns, the non-availability of vacuum quality diagnostic tools might be one of the reasons for transmission system operators not to apply vacuum circuit breakers in their high-voltage transmission systems [Cigr 10].

Pressure verification tests are performed after assembling of the interrupters in the factory using sophisticated and expensive equipment, usually based on the magnetron principle [Fron 93b]. In this method, voltages up to several kilovolt and magnetic fields of several hundred millitesla are applied to the interrupter simultaneously. The ion current between contacts or between contacts and middle shield is a measure for the vacuum quality. This method is not useful for users because the vacuum interrupter has to be disassembled from the switchgear with the risk of improper remounting [Dams 95]. Nevertheless, failures of vacuum interrupters during service cannot be completely excluded and it may be possible that after some years of service the interrupter internal pressure increases. Reasons for residual gas pressure rise might be out-gassing and gas desorption from different materials inside the interrupter (metallic parts and ceramic), gas permeation through the chamber walls and metallic flanges, small gas leakage caused by excessive mechanical stress or insufficiently welded or brazed junctions. For industrial applications leakage may occur by aging of the metal bellows due to the large number of operations. But also in distribution applications with few number of operations, the residual gas pressure may increase by long term diffusion or deactivation of the getter material [Dams 95]. Therefore, as the functional reliability of vacuum interrupters is ensured over their internal pressure, it would be practical to be able to recheck the pressure within the interrupters after several years of service. For this reason, simpler methods, suitable for application on the site, are required. Such a method, on one hand should allow to re-check whether the above mentioned threshold pressure is still maintained and on the other hand, it should desirably provide information about the remaining safety margin of vacuum. The method should be as simple as possible, based on measurement of only one or two electric signals, without the necessity to remove the interrupter from the switchgear and with minimum investment in equipment and time [Fron 93b].

During the last decades, various kinds of internal pressure diagnostic methods have been studied and worked out, which are based on effects of different parameters. However, new investigations in this field show that a satisfying and reliable method, which gives information about the remaining safety margin, has still not been found. In the following, different methods from the literature are briefly discussed. Among these methods, the fundamentals of a method, based on evaluating the changing rate of the field emission

current immediately after arc-polishing of the contacts are in detail discussed. This method, called here "FEA" (for field emission analysis), was firstly introduced by Frontzek and König. However, more investigations are required to verify applicability of this method on commercial interrupters.

3.1 Methods for indirect internal pressure measurement

In the following, different ideas and methods for on-site internal pressure diagnostic on vacuum interrupters are discussed. **Figure 3.1** presents an overview on physical principles and their suitability for measurements in different pressure ranges.

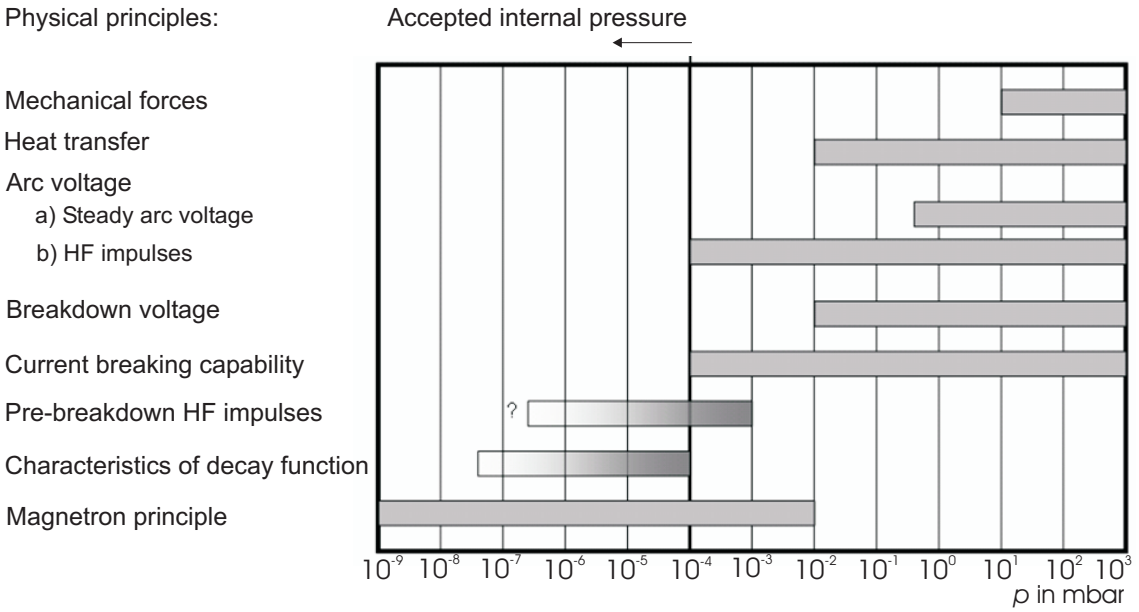

Figure 3.1: Overview of physical principles and their suitability for internal pressure diagnostic in vacuum interrupters acc. to [Fron 98]

3.1.1 Breakdown voltage

Most of the utilities have ac and dc testing devices for test voltages of several ten kilovolt [Dams 95]. But, unfortunately the breakdown voltage of a vacuum interrupter is nearly independent from its internal pressure in the ranges below 10^{-3} mbar. Only if the internal pressure rises above this value, an increase of the breakdown voltage is often observable.

For pressures higher than 10^{-2} mbar the breakdown voltage decreases again according to the Paschen's Law. This is shown schematically in **Figure 3.2**. It is obvious from this figure, that diagnostic methods based on breakdown voltage measurements can detect a pressure rise only above 10^{-2}mbar, which is about two orders of magnitude higher than the threshold pressure ($10^{-4} \cdots 10^{-3}$ mbar), where the interrupter has already lost its current breaking capability [Fron 00]. Furthermore, in case the interrupters are installed in gas insulated switchgear (GIS), where the surrounding medium is SF_6, incorrect results may be the outcome of such diagnostic methods. This is because that the impact of the entered SF_6 on the dielectric behavior of the interrupter is not clear.

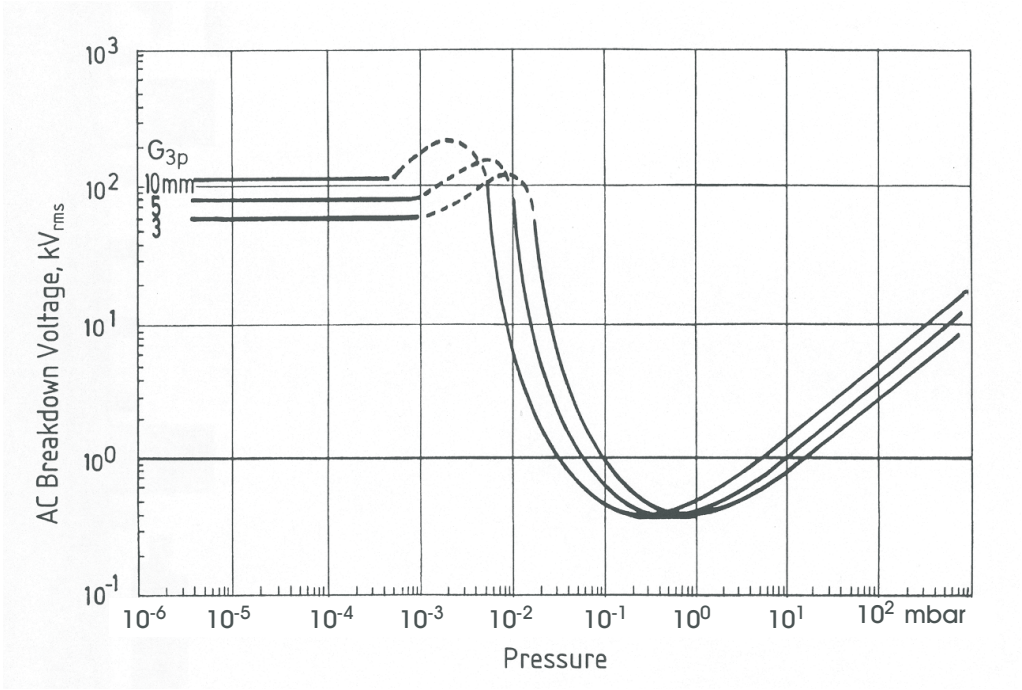

Figure 3.2: Typical Paschen curve of a vacuum interrupter acc. to [Fron 00]

3.1.2 Current breaking capability

Vacuum interrupters have high capability to interrupt the ac current at its zero crossings. However, if the internal pressure exceeds values of $10^{-4} \cdots 10^{-3}$ mbar, they lose their high current breaking capability. The state of the vacuum can principally be determined by interruption tests at high current levels and power-frequency. Nevertheless, this approach requires a synthetic test circuit with high voltages and currents. Thus, for diagnostic methods, often high frequency (HF) currents are used in order to have high current steepness

at moderate current amplitudes [Fron 93b], [Fron 93a], [Fron 00], [Dams 95].

Such methods could be applied even during closing operation of the breaker for determination of the vacuum status [KEMA]. Here, an HF current is injected into the interrupter during closing operation. Pre-ignition of an arc before contact closing and the arc extinguishing time are indicators of the high current interrupting capability of the interrupter. In case of a good vacuum inside the interrupter, the HF current is interrupted after a few current cycles. For insufficient vacuum, the arc cannot be interrupted.

Such diagnostic methods are more sensitive than methods based on breakdown voltage measurements. They are also suitable for verification of the internal pressure of interrupters installed in gas insulated switchgear (GIS). Nevertheless, they cannot determine the residual gas pressure and the remaining safety margin of the interrupter.

3.1.3 Pre-breakdown effects

Different investigations are known from the literature based on the field emission characteristics for determination of the interrupter internal pressure. In these methods, the field emission current is measured either directly, or it is substituted by measuring of X-ray radiation, as this is proportional to field emission current [Dohn 81]. In this respect, there are two main groups of methods:

- The first group is based on the absolute dependency between field emission current and vacuum state. This group of methods, all based more or less on similar principles, are introduced in different publications [Fron 00], [Sydo 02], [Walc 99], [Walc 02]. Increasing the internal pressure of a model vacuum interrupter up to a certain threshold value, a strong decrease of the field emission current will be observed. This phenomenon is due to the gas adsorption process on the cathode surface and the consequent changes in the cathode surface work function. But, if one decreases the pressure again down to the ultra vacuum range, the field emission current will not increase back to its original value (see 6.2). This threshold value depends significantly on the electrode material and the type of the residual gas. It may vary between 10^{-5} and 10^{-2} mbar for different contact-gas-systems. Furthermore, the field emission current depends strongly on electrode surface condition, electrode material, residual gas and history of the gap. Due to the lack of absolute correlation between field emission current and internal pressure, these methods are not suitable to estimate the remaining safety margin of the interrupter internal pressure.

- The second group is based on the the changing rate of the field emission current. Here, a kind of electrode surface conditioning is performed immediately before starting the field emission current measurement. This is done with the objective to remove the adsorbed gas layer from the contact surface. For instance, in the FEA method [Fron 93a], arc-polishing is applied to obtain a clean contact surface, and in [Jutt 71], [Jutt 72], [Ziyu 06] this is achieved using electron bombardment desorption. In such methods, the decay time constant of the field emission current immediately after surface conditioning, due to gas re-adsorption process, is a measure for identification of the internal pressure.

3.1.4 Other methods

In addition there are also a couple of methods [Dams 95], [Fron 00], [Kama 06], [Xing 10] based on other different parameters: arc voltage, heat transfer, force acting on the moving contact, partial discharge, current chopping of dc arcs and the shield potential. All these methods have the disadvantage that the resolution in the vacuum range (below 10^{-3} mbar) is too poor.

3.2 FEA method as a possible method for DVQ

As is shown in 2.2.2 the field emission current is influenced by many parameters, such as electrode work function, electrode surface condition, electrode temperature, gap distance and geometry, history of the gap and the applied voltage. The electrode work function itself is not only dependent on the electrode material but also on the gas layer, which covers the electrode surface even having ultra high vacuum inside the interrupter. Therefore, variation in the gas coverage layer on the contact surface results in the changes of the work function and consequently changes of the field emission current. This is the basic idea of the FEA method, which was firstly proposed by Frontzek and König [Fron 93a]. In the following, the theory of sorption and desorption processes of gases on the metallic surface is given in brief. Afterwards, the method principle and first experimental results of the authors are presented.

3.2.1 Adsorption and desorption of gases

Adsorption is the process of attraction of gas atoms or molecules to a solid surface. This process occurs either due to dipole interactions or van der Waals forces (physisorption) or because of covalent bonds (chemisorption). The process opposed to adsorption is called desorption. Desorption is a phenomenon whereby molecules or atoms are released from the surface. This occurs if a certain energy input (desorption energy) is available. The interaction energy as well as the desorption energy by chemisorption is approximately ten times stronger than by physisorption [Wutz 00], [Pupp 91].

Adsorption equilibrium will be reached when the adsorption rate becomes equal to the desorption rate. The covering ratio γ of a metal surface is defined as the ratio of the density number of particles adsorbed on a solid surface ($\tilde{n}$) to the area-related density number of particles in a mono molecular layer ($\tilde{n}_{\mathrm{mono}}$). For the density number of particles on the surface less than the mono layer density number $\tilde{n} < \tilde{n}_{\mathrm{mono}}$, the covering ratio gives values less than 1.

$$\gamma = \tilde{n}/\tilde{n}_{\mathrm{mono}} \tag{3.1}$$

Figure 3.3 shows how the covering ratio varies with the residual gas pressure in a system at adsorption equilibrium [Wutz 00]. Rise of the internal pressure results in the growth of the gas layers covering the contact surfaces and accordingly in changes of the surface work function. At higher temperatures, the surface covering ratio will be lower for a certain internal pressure.

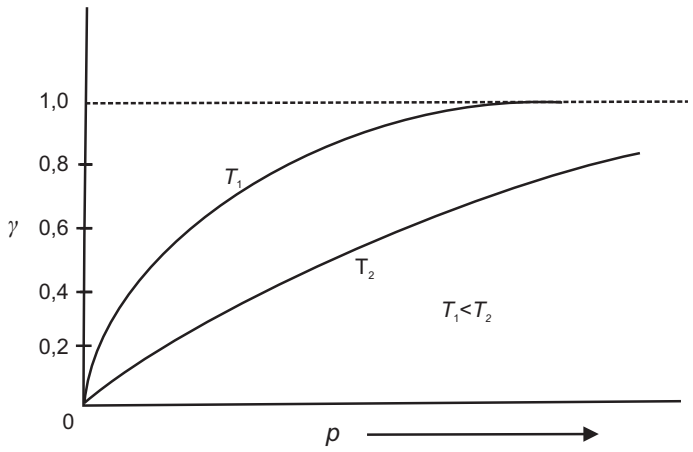

Figure 3.3: Covering ratio versus internal pressure according to Langmuir for two different temperatures [Wutz 00]

In [Wutz 00] the formation time of a mono molecular layer on a surface is calculated. For this calculation it is assumed, that every gas atom or molecule, impacting with the surface, adheres permanently to it. Assumed, having air as residual gas, which is usually the case, and having approximately room temperature $T \approx 300\,\mathrm{K}$, following formula can be estimated:

$$t_{mono}/\mathrm{s} \approx \frac{3.6 \times 10^{-6}}{p/\mathrm{mbar}} \tag{3.2}$$

It is seen that the time necessary to have a mono molecular layer is inversely proportional to pressure.

Gas adsorption and work function

Gas layers covering the cathode surface have important influence on its work function and consequently on the field emission current, especially in the semi-vacuum range. Depending on the type of the gas and surface material, adsorption may lead to an increase or decrease of the work function. In [Hein 89], changes of the work function in case of physisorption as well as chemisorption is calculated. The changes of the work function due to physisorption is dependent on the density number of adsorbed particles $\tilde{n}$ and their dipole moment. The changes of the work function in case of a chemisorption is also a function of the density number of adsorbed particles $\tilde{n}$ as well as the surface work function (ϕ in eV) and the ionizing energy (E_i in eV) and electro negativity (E_EN in eV) of the residual gas.

$$0.5 \times (E_\mathrm{i} + E_\mathrm{EN}) > \phi \rightarrow \Delta\phi < 0 \tag{3.3}$$

$$0.5 \times (E_\mathrm{i} + E_\mathrm{EN}) < \phi \rightarrow \Delta\phi > 0 \tag{3.4}$$

In [Hein 89] changes of the work function in the range of $-1\,\mathrm{eV} \cdots +1\,\mathrm{eV}$ are calculated for different systems (contact-gas), which result in significant changes of the field emission current according to the FNE. For metals with high work function values (for example copper), an increase of the work function is normally the case. Higher density number of adsorbed particles $\tilde{n}$ results in higher increase of the work function. Measurement results according to [Fron 93a] and [Hein 89] show that gases such as oxygen, nitrogen and air attached to the surface of CuCr contacts cause in most cases a rise of the work function.

3.2.2 FEA method principle and first experimental results

The method proposed by Frontzek and König [Fron 93a] is generally based on the evaluation of the changing rate of the field emission current. The principle of this method for a system with air as residual gas and CuCr electrodes is shown in **Figure 3.4**. The measurements were performed on a model vacuum interrupter in open contact position with short gap spacings (offline measurement). The procedure consists of three stages. In the first stage, the emission current is measured at a certain applied high alternating voltage with frequency of 50 Hz. Afterwards, the contact surfaces are arc-conditioned by a high frequency current, which is called "arc-polishing" (second stage). This is followed by an immediate return to the alternating voltage application of the value set before (third stage). A significant increase in the emission current is observed in the first moment. But, it decays to the value measured before arc-polishing the faster the higher the internal pressure is. Theoretically, at the end of the measurement, the field emission current decays back to values measured before the arc-polishing ($i_{F,stab} = i_{F1}$). The dependence of the decay time constant on the residual gas pressure is used for the evaluation of the vacuum state of the interrupter.

At the beginning of the test, the electrode surfaces are at adsorption equilibrium. Depending on the internal pressure, the gas layer covering ratio γ_1 and consequently the electrodes work function ϕ_1 have certain values. Thus, applying a high alternating voltage across the interrupter results in a field emission current of value i_{F1}, which depends (besides other parameters) on the surface work function (first stage). During arc-polishing phase, due to the arc energy input, the adsorbed gas layer will be removed from parts of the electrodes surface. The movement of the arc and its penetration into the attached gas layers cause this cleaning (second stage). Therefore, immediately afterwards, at those locations the covering ratio γ_2 and the work function ϕ_2 have been reduced. This results in higher emission current values i_{F2} after immediate return to the adjusted alternating voltage (third stage). However, the removed gas molecules will be re-adsorbed on the electrode surface at a certain rate until the adsorption equilibrium is reached again. The rate of formation of a new gas layer depends on the contact-gas system, on the temperature, and mainly on the residual gas pressure (see *equation* 7.5). Higher internal pressures result in a faster re-adsorption process and consequently a faster decay of the field emission current. The gas re-adsorption process and the consequent decay of the field emission current have the same time constants, which are inversely related to the internal pressure. Therefore, theoretically, from the decay time constant of the field emission current, the residual gas pressure can be evaluated.

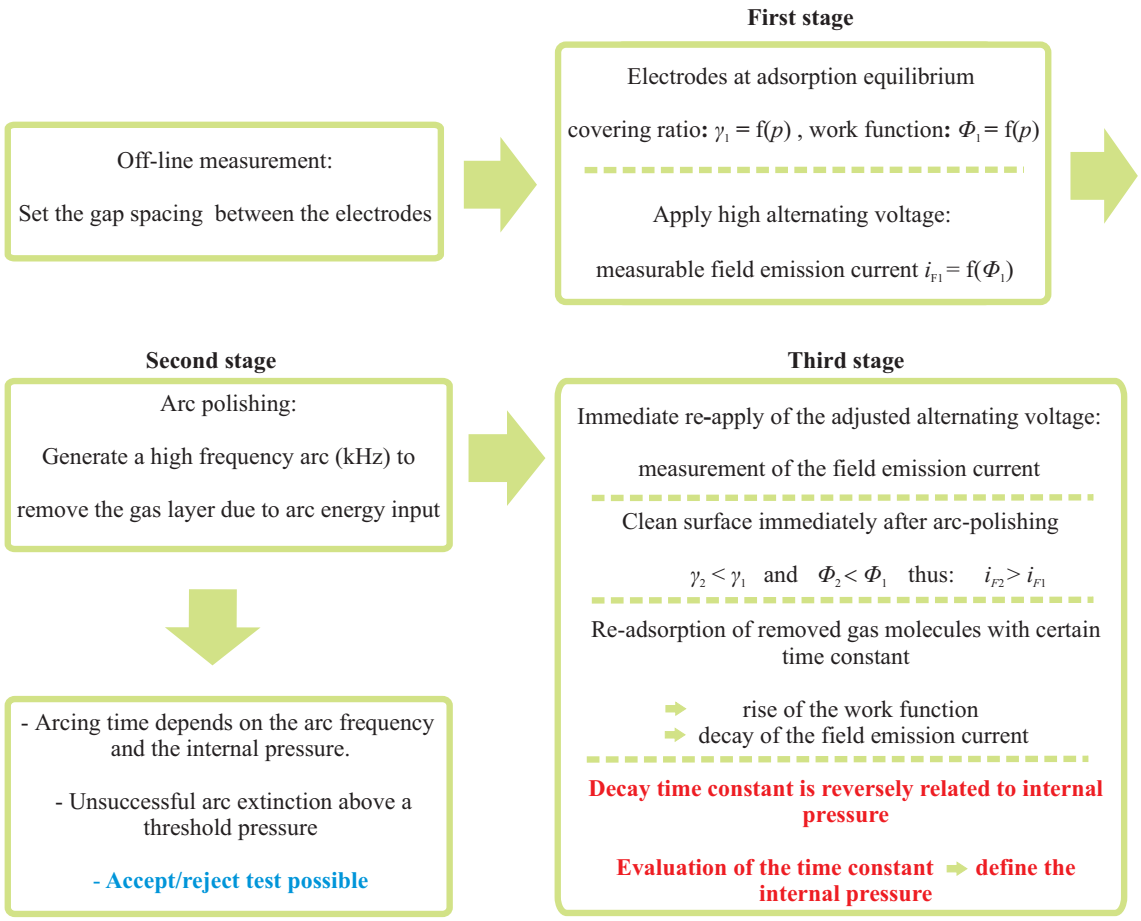

Figure 3.4: FEA method principle for a CuCr-air-system, acc. to Frontzek and König

Figure 3.5a shows expected waveforms of emission current before and immediately after arc-polishing presented by Frontzek and König [Fron 93a]. It is seen, that the field emission current increases rapidly after arc-polishing and then decays with time. For quantitative analysis of the decay time they defined two time parameters $\tau_{0.5}$ and $\tau_{1.2}$ as shown in Figure 3.5a. As a first approach, according to the measurements carried out on a model vacuum interrupter, an inversely proportional dependence between the time parameters and the internal pressure was found (see Figure 3.5c). It was also observed that the time parameters are in good agreement with the calculated formation time of a mono molecular layer. These time parameters were used for the evaluation of the residual gas pressure below 10^{-4} mbar.

Figure 3.5b shows a typical waveform of the high frequency current (1.35 kHz) during arc-polishing. At pressures below 10^{-4} mbar, the arc is extinguished after a few cycles. For higher internal pressures, unsuccessful arc extinction and damped current oscillations are observed [Fron 93a]. This phenomenon gives the possibility to detect also internal

pressures above 10^{-4} mbar. In this case the vacuum interrupter is insufficient for further service.

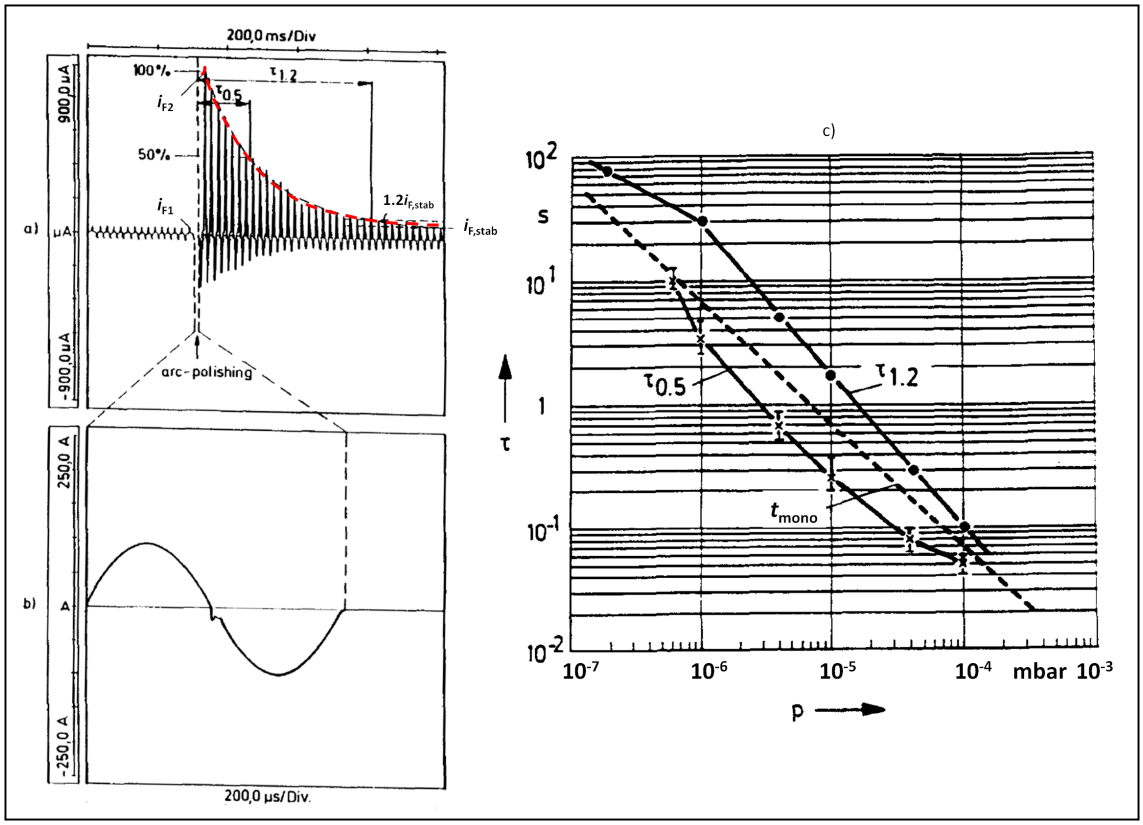

Figure 3.5: a) Typical waveform of field emission current according to Frontzek and König for CuCr-air-system b) arc-polishing HF current c) time parameters as a function of pressure [Fron 93a]

3.3 Objective of the work - DVQ

Pressure verification after several years of service requires procedures different from the sophisticated method based on magnetron principle, used by most of the manufacturers in the factory. These procedures should be as simple as possible, based on measurement of only one or two electric signals without the necessity to disassemble the interrupter from the switchgear and provide information about the remaining safety margin of vacuum. Various kinds of internal pressure diagnostic methods have been introduced before. However, a satisfying and reliable method, which also gives information about the remaining safety margin, has still not been found. In this respect, fundamentals of a promising method, based on evaluation of the changing rate of the field emission current immediately

after arc-polishing of the contacts, was suggested by Frontzek and König (FEA method). As a first approach, the method is applied on a model vacuum interrupter with certain contacts geometry, contact material (CuCr) and residual gas (air). The preliminary results indicated that the changing rate of the field emission current after arc-polishing may be used for the task of identifying the state of vacuum. It was found that the decay time constant of the measured field emission current is approximately inversely proportional to the residual gas pressure of the relevant interrupter and could be used to evaluate its internal pressure [Fron 93a]. However, it is of great importance that the method works also properly in the complex regime of commercial vacuum interrupters, with complicated contact geometries (AMF, RMF) and unknown type of the residual gas. Therefore, more detailed investigations are required for the verification of applicability of the method on commercial interrupters, which is an important part of the presented work.

For these investigations, different experimental setups (vacuum circuit, electric circuit) are designed and implemented. A special measurement shunt with the required compensation circuit is also developed, which gives the possibility to measure very low field emission currents immediately after arc-polishing of the contacts. The measurement results are verified with the help of the well-known FNE. Furthermore, the impact of the internal pressure on the current-voltage characteristic of the vacuum gap is studied.

Systematic investigations are performed to check if this method is stable and robust enough to serve as basis of a future diagnostic method. Particular aspects that had to be investigated were: sufficient sensitivity, reproducibility, parameters having impact on the results, independence of the reported effects from other parameters that cannot be controlled, applicability to the various commercial vacuum interrupters and influence of the arc-polishing current parameters (amplitude, frequency).

During the investigations, FEA method is applied firstly on a self-made model vacuum interrupter having the possibility to vary the residual gas pressure, the type of the gas and the contacts geometry and material. Thereafter, the applicability of the method in practical situations is investigated using different types of commercial interrupters with raised internal pressure. Finally, the measurement results of both the model vacuum interrupter and the commercial interrupters are compared and discussed.

4 Impact of capacitive switching (ICS) on the dielectric behavior of vacuum interrupters

Capacitive currents are switched in power systems due to different types of capacitive loads such as capacitor banks, cables and overhead lines. Capacitor banks are mainly installed in the system for reactive power compensation, voltage control and power factor correction in utility systems [Heuc 10]. A vacuum interrupter for capacitive switching duties must fulfill the following requirements: It has to be able to close under high inrush currents (up to several ten kiloamperes) for inserting the capacitive load, but needs only to break relatively low currents (up to several hundred amperes) for load interruption. As the interrupting current is low compared to the breaker interrupting capability, the interruption is normally successful even at short arcing times (contact separation just before current zero crossing). Consequently, it is possible that a half cycle later, at maximum voltage stress, the contacts are not completely open. This situation can increase the probability of arc re-establishment between the contacts. Nevertheless, even after full contacts separation, due to high voltage stress (see 4.1), still a risk of arc re-establishment (breakdown) exists [Smee 00]. Multiple breakdowns may cause high overvoltages in the system and can damage the circuit components. The following consists of a brief theory on capacitive opening and closing operations. Furthermore, the influence of capacitive switching on the dielectric behavior of the interrupter after current interruption is discussed.

4.1 Opening operation

In the case of interrupting a capacitive load, the current is very small compared to the short circuit current interruption, in the range of several ten to several hundred amperes [IEC6 08]. But, the main problem is the high electric field stress. The interrupter must

be able to withstand the power frequency recovery voltage, which has an amplitude of at least twice the peak of the system voltage. **Figure 4.1** shows a single phase diagram of a capacitive circuit. Due to the 90 degree lagging capacitive load voltage v_c, the voltage is at its maximum as the current approaches its zero crossing [Smee 00]. Therefore, after current interruption the capacitive load remains charged at system peak value $\hat{v}_s$ (in the single phase case), whereas, the system voltage continues changing sinusoidally. The resulting recovery voltage appearing across the interrupter after current zero is the difference between the system voltage and the load voltage ($v_s - \hat{v}_s$). **Figure 4.2** shows current and voltage waveforms for a single phase capacitive current interruption. The voltage across the interrupter is thus a unidirectional voltage of a $(1 - \cos \omega t)$ function, and its duration is until the next closing operation of the interrupter or rather dependent on the equivalent discharging resistor. According to the IEC circuit breaker standard [IEC6 08], a capacitive test circuit is defined as following: "The characteristics of the capacitive circuit shall, with all necessary measuring devices such as voltage dividers included, be such that the decay of the voltage across the circuit-breaker does not exceed 10% at the end of an interval of 300 ms after final arc extinction."

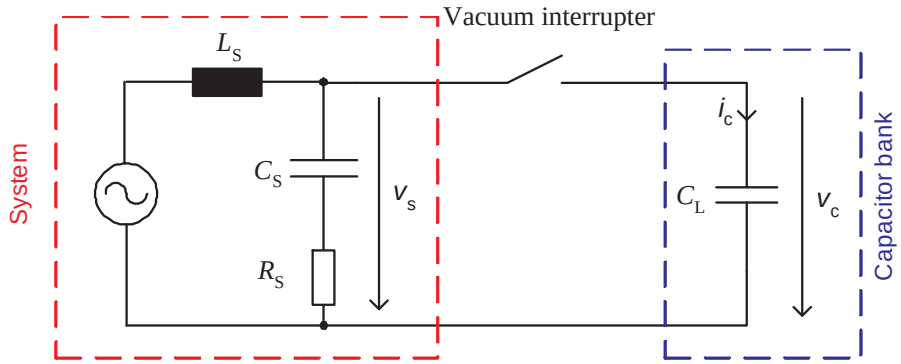

Figure 4.1: A single phase capacitive circuit. C_s: system capacitance, L_s: system inductance, R_s: system resistance, C_L: load capacitance

The initial value of the recovery voltage across the interrupter is zero with a very slow rate of rise (50 Hz). One half cycle later, the system voltage reaches the opposite polarity of the load voltage, leading to a 2 p.u. voltage stress across the interrupter (neglecting the voltage drop across the system inductance). For a three-phase ungrounded neutral the recovery voltage will even be higher, i.e. 2.5 p.u. across the first phase to clear [Slad 08]. In case of a non-simultaneous opening with a time difference greater than a quarter of a cycle, the maximum of the recovery voltage would be even higher [Cigr 94]. The interrupter is required to withstand this unidirectional voltage stress. Breakdowns in the interrupter later than one quarter cycle after current interruption, are called as "restrikes" [Smee 00].

Breakdowns within one quarter cycle are called “reignitions”, which are not as critical as restrikes [Mull 04].

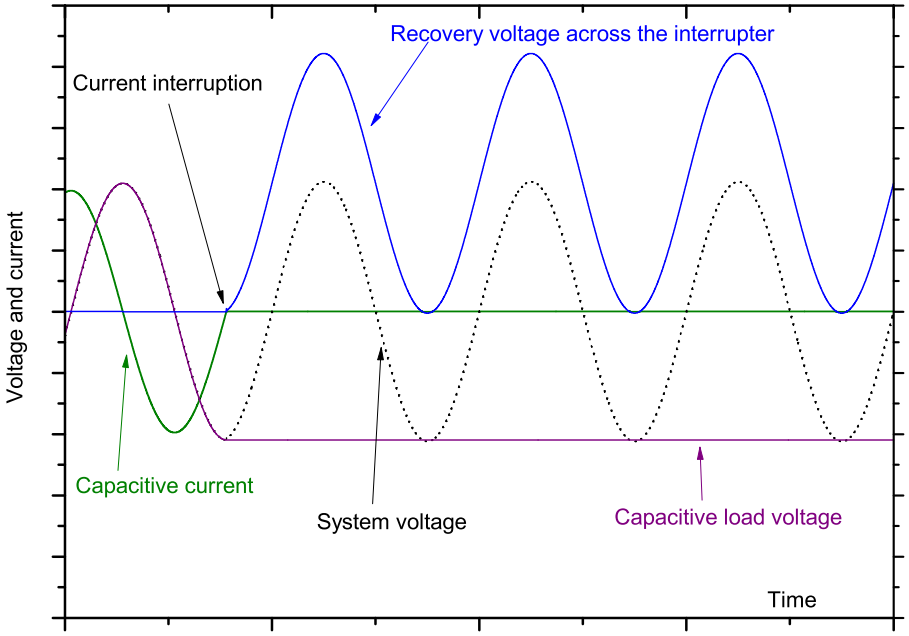

Figure 4.2: Current and voltage waveforms at capacitive current interruption

While most vacuum interrupters are able to withstand the unidirectional recovery voltage during their service life, once in a while a breakdown may occur [Slad 08]. **Figure 4.3** shows the effect of multiple restrikes during the recovery phase. In case of a restrike, the load and stray capacitances will discharge over the system and load stray inductances. This causes a high frequency restrike current flowing through the interrupter i_{HF}. The amplitude of this current is dependent upon the circuit inductances and capacitances, circuit damping and the instantaneous value of recovery voltage at the moment of restrike. It has the highest value, if the restrike occurs exactly at the peak of the recovery voltage. But, it is well possible that the voltage across the contacts at restrike's moment is less than the peak value. Amplitude and frequency of the restrike current may reach values in the range of several kiloamperes and kilohertz.

As the high frequency restrike current flows in the circuit, a capacitive transient voltage appears across the capacitive load and the system. Therefore, the load voltage is at its maximum value as the high frequency current approaches its zero crossing (see Figure 4.3). The vacuum interrupter has assumedly the ability to interrupt such a high frequency current at one of the current zero crossings. The worst case would be interruption in the first current zero crossing (as shown in Figure 4.3), where the load transient voltage is at its highest possible value. Therefore, after successful interruption of the high frequency

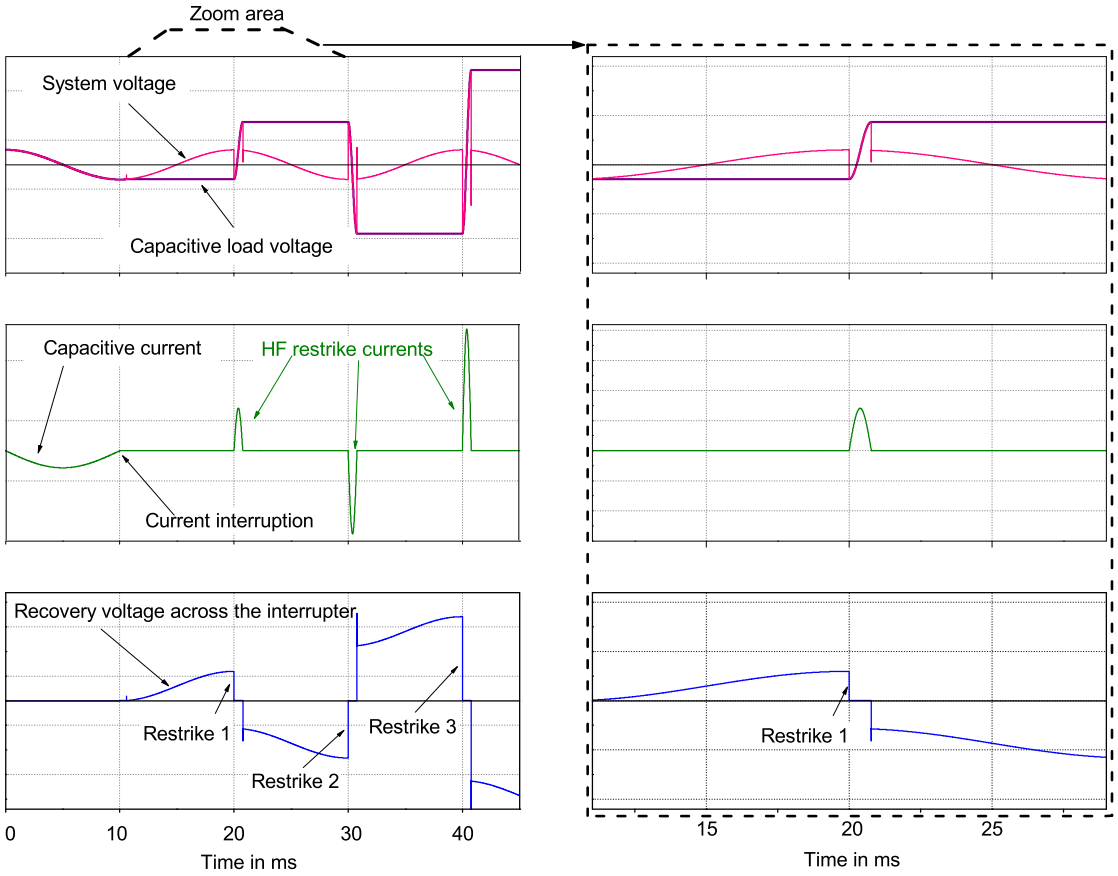

Figure 4.3: Schematic showing the effect of restrikes at capacitive current interruption

restrike current, the capacitive load has been re-charged to even higher values than before (see Figure 4.3). Thus, there is a higher risk of a new restrike and the voltage escalation could be theoretically continued.

In practice, a restrike will not necessarily occur at recovery voltage peak value, and also the restrike current will not necessarily be interrupted at the first current zero. On the other hand, due to the circuit damping the residual load voltage rise will be slower. There is, however, the possibility to develop high overvoltages and multiple restrikes, which may damage the switchgear insulation and also the capacitive load.

4.2 Closing operation

In contrast to interruption of capacitive loads at comparatively low currents of up to several hundred amperes, the making current at energizing an uncharged capacitor load is about

a few kiloamperes up to several tens of kiloamperes. Here, a charging current will flow to charge the uncharged capacitor over the system inductance. This charging current is called as "making inrush current". Its amplitude is determined by the load capacitance and system inductance as well as by the instantaneous value of the system voltage at the moment of closing operation and by the residual charge of the load. The maximum inrush current occurs when the breaker closes on the peak of the ac voltage. Depending on the load capacitance (cable, overhead line or capacitor bank) and system inductance, the inrush current has different oscillation frequencies, up to several hundred times the power frequency, and different amplitudes of up to several tens of kiloamperes. The inrush current at energizing overhead lines or cables is much lower than in case of capacitor banks. This is explained by the relatively high overhead line surge impedance of several hundred ohms and the cable surge impedance of several tens of ohms. In case of energizing capacitor banks, it is usually distinguished between two different cases [Smee 00]:

1. **Single capacitor bank switching:** In this case, only one single bank is going to be connected to the system (see Figure 4.1). The relatively large system inductance limits amplitude and frequency of the inrush current.

2. **Back-to-back capacitor bank switching:** Another parallel capacitor bank is going to be connected to a capacitor circuit, which is already active. This situation is shown in **Figure 4.4**. Due to the very small parasitic inductance L_{par} amplitude and frequency of the inrush current cannot be limited. According to the IEC circuit breaker standard [IEC6 08] for back-to-back capacitive switching tests, the amplitude of the inrush making current shall be 20 kA and its frequency shall be 4.25 kHz.

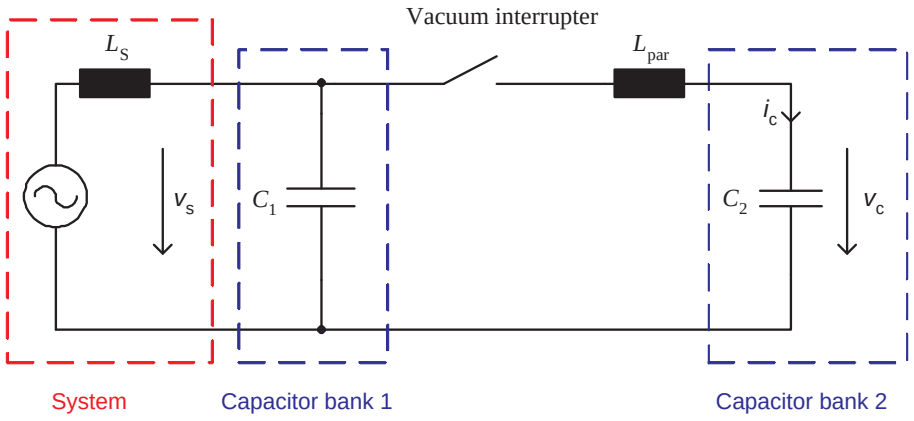

Figure 4.4: A single phase back-to-back circuit. L_s: system inductance, C_1, C_2: capacitor banks, L_{par}: parasitic inductance

During closing operation of the vacuum interrupter, the electrical field stress between the contacts rises as the gap spacing between the contacts decreases. As is explained in 2.2.1, the surface field stress is not only defined by the homogeneous field stress between the contacts i.e. $E_{\mathrm{hom}} = \frac{v_{\mathrm{vac}}}{d}$, but also is enhanced as expressed by the macroscopic and microscopic field enhancement factors. At a sufficiently low gap spacing d_0 and substantially high field stress E_0, the vacuum gap can no longer withstand the electrical stress, and dielectric breakdown between the contacts occurs. From this moment on until the first contact touch, the inrush current flows through the vacuum arc (pre-arcing time $t_{\mathrm{p\text{-}a}}$).

Figure 4.5 shows a measurement example of pre-arcing during closing operation. The homogeneous field stress is calculated using the measured gap distance d and the interrupter voltage v_{vac}. From the figure, it is seen that the pre-arc ignites at a field stress of $E_{\mathrm{hom}} =$ 13.5 kV/mm and a gap distance of $d_0 = 1.1$ mm. The pre-arcing duration is about $t_{\mathrm{p\text{-}a}} =$ 1.3 ms. During this time interval, the inrush current with maximum amplitude of 6 kA and frequency of 1.5 kHz flows through the vacuum arc. Thereafter, the current continues to flow via the closed contacts and will be damped due to the circuit damping.

During pre-arcing, the contact surface melts locally due to the arc's energy input into the contacts. At higher inrush current amplitudes and longer arcing times, energy input from the arc roots is greater. This can lead to contact welding during closing phase as well as during contact bouncing after they have touched for the first time. These contact welds will then be broken during the next contact opening. As a result, new micro-protrusions will develop on the contact surface, which may lead to higher electrical field enhancement and, consequently, reduce the dielectric strength of the gap. Therefore, a high inrush current is a risk not only for the capacitor bank but also for the circuit breaker itself [Slad 07].

The effect of the inrush current on the dielectric properties of vacuum interrupters is more pronounced, when the welds broken by contact opening have not been burned out by sufficient arcing activity. The most critical case is currentless opening of the interrupter after contact welding with high inrush currents. In this case, there is no arc during opening operation to eliminate the broken welds and to smoothen the surface. Also, at capacitive switching, interrupting current and consequently arcing energy have comparatively low values. Thus, the smoothing (conditioning) effect of the interrupting arc might not be sufficient to reduce the field enhancement after next contact opening. Another point is that the breaking current in a capacitive circuit is much lower than the breaker interrupting capability. Therefore, the current can be interrupted easily even at low arcing time. This results in low arcing energy and low possibility for contact conditioning. Thus, the low breaking current compared to high short-circuit currents is not an advantage of capacitive switching [Smee 00], [Korn 07].

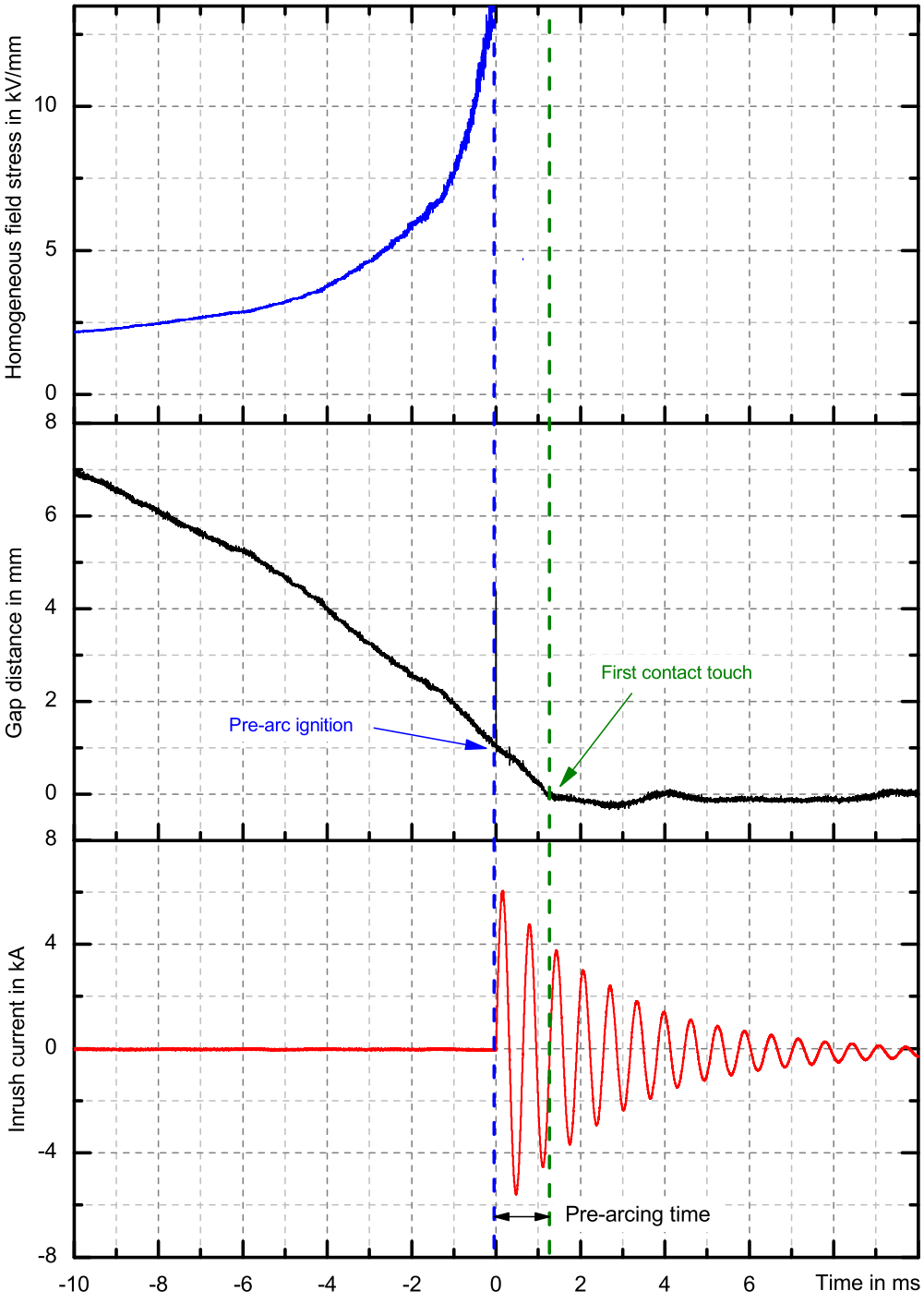

Figure 4.5: Pre-arcing at closing operation before first contact touch. Gap distance and inrush current: measured values, field stress: calculated values

4.3 Objective of the work - ICS

In spite of the low breaking current at capacitive switching, there are severe requirements on the switching capability of the vacuum circuit breakers. According to IEC circuit breaker standard [IEC6 08], "two classes of circuit breakers are defined according to their restrike performances:

- **Class C1:** low probability of restrike during capacitive current breaking;
- **Class C2:** very low probability of restrike during capacitive current breaking."

To fulfill the requirements for capacitive switching duties and to obtain a sufficiently low restrike probability, application of vacuum interrupters with greater gap distance or even series connection of two vacuum interrupters at higher system voltage levels, e.g. 36 kV or 40.5 kV, is sometimes necessary [Dull 04], [Dull 06], [Gier 01].

The recovery voltage applied across the contacts after capacitive switching is generally lower than the one minute power-frequency and lightning impulse withstand voltages. In spite of this fact, restrikes occasionally occur after capacitive interruption even up to ten seconds later [Slad 08]. More detailed information (than just to pass or not to pass a test) on the performance of vacuum interrupters during recovery phase after capacitive switching is necessary to understand the physical reasons of restrikes. Different effects like electron emission, micro-particles or even a combination of both may lead to restrike during the recovery phase. Furthermore, performance assessment of vacuum interrupters during the recovery phase after capacitive current switching is an important issue with regard to the applicability of vacuum to higher voltage levels. For utilization of vacuum interrupters in transmission systems, the restrike problem must be understood and solved [Ryu 10].

In this work, systematic research is performed to understand and identify the electrical activities in the vacuum gap during its dielectric recovery. To find out the impact of capacitive switching on the dielectric behavior of vacuum interrupters and to have more detailed information on the origin of restrikes, measurement of very low field emission currents (microampere up to milliampere range) immediately after interruption of capacitive currents (up to several hundred amperes) during the complete period of the dielectric recovery is necessary. For this reason, a special measurement system is developed to measure field emission current in a high voltage test environment under severe electromagnetic interferences. The measurements are performed both in a high voltage experimental circuit as well as in a full-power test-circuit with commercially available vacuum circuit breakers (up to 36 kV rated voltage). To compensate the capacitive current component, caused by

the stray capacitance of the interrupter, hardware (electronic, online) processing is developed. For applications under more severe electromagnetic interferences a software (offline) processing, based on MATLAB, is developed by the project partner (KEMA[1]). Finally, the results of the hardware and software compensation methods are compared.

In this context, the influence of the power frequency breaking current on the gap dielectric recovery and the contacts surface condition is studied. Moreover, the impact of pre-arcing at contact closing under inrush currents in the range of several kiloamperes and kilohertz on the field emission characteristics of the contacts is investigated.

[1]Developed by Mr. Sander Kuivenhoven

5 Test setups and measurement systems

Measurement and analysis of field emission currents in a high voltage environment under severe electromagnetic interferences are fundamentals of both part-projects (DVQ and ICS). For this reason, a special measurement system is developed that allows to measure very low field emission currents immediately after high current flow (arc-polishing phase in DVQ and load current phases in ICS). Furthermore, different test setups, experimental circuits and measurement techniques are designed and implemented for different investigations, described in the following chapters. **Figure 5.1** shows an overview of the different test setups.

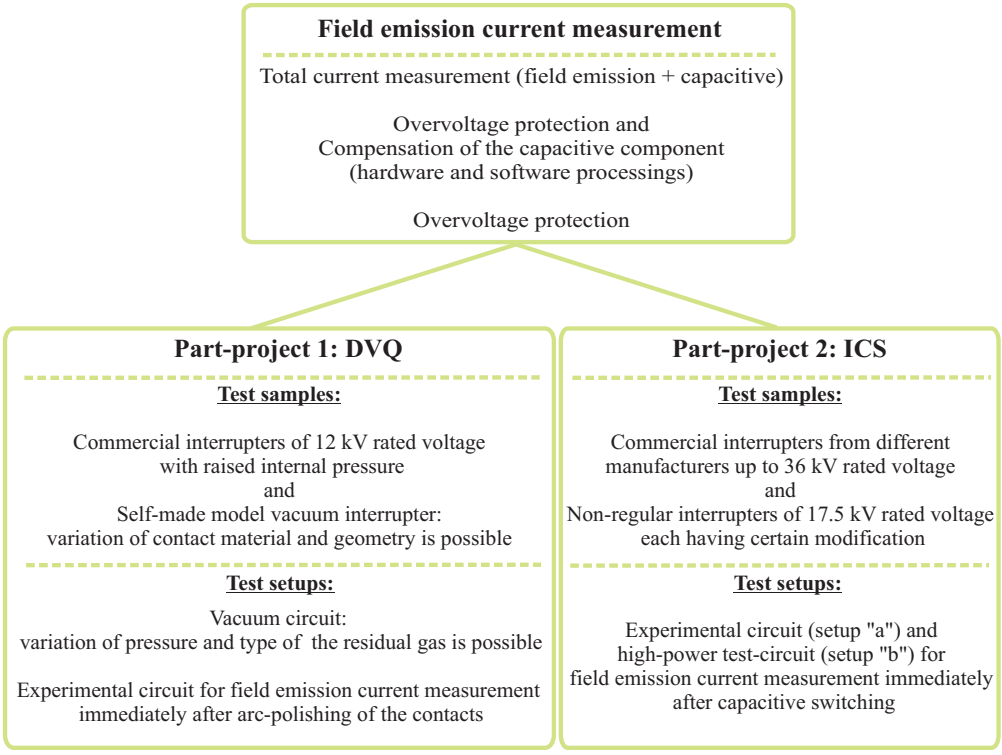

Figure 5.1: An overview of test setups

5.1 Measurement system for field emission current

The measurement principles for both part-projects (DVQ and ICS) are similar. Very low field emission currents (microampere up to milliampere ranges) have to be measured immediately after high current flow (arc-polishing phase in DVQ and load current phases in ICS). **Figure 5.2** shows the simplified circuit diagram of the measurement system, named here as "diode-resistor-shunt (DRS)", comprising a resistive part R_{sh}, gas-discharge arrester (GA) and anti-parallel bypass diodes. The resistive part is a parallel connection of ten to fifteen metal film resistors, which are placed in a brass cylinder in a low-inductive arrangement. **Figure A.1** and **Figure A.2** in Appendix A show a photo of DRS and its detailed circuit diagram, respectively. Using a coaxial cable, the measuring signal is transfered to either a digital oscilloscope or a digitizer in case of digital optical data transfer. The gas-discharge arrester with nominal static spark-over voltage of 90 V is connected in parallel to the resistors. To protect the shunt resistor R_{sh}, power diodes in anti-parallel connection are applied. By using this anti-parallel diode configuration the high current and the low field emission current, which differ by several orders of magnitude, can be measured separately. During the high current phase the diodes are conducting. Therefore, only a negligible amount of current can flow through the shunt resistor, and it is thus protected from the high currents. This current can be measured with the help of a Rogowski coil. Alternatively, during high voltage application the low field emission current shall flow exclusively through the shunt resistor and not through the diodes. For this reason the voltage drop across the shunt resistor must be lower than the diodes' threshold voltage. To increase the maximum permissible voltage across the shunt resistor and thereby the maximum measurable signal, two or three diodes are connected in series in each anti-parallel branch. Furthermore, according to the desired measurement range, different values of R_{sh} have been chosen (68 Ω and 500 Ω).

The bypass diodes are dimensioned to withstand the high current phase respective to the application. For example, in ICS using the full-power test-circuit, the bypass diodes have to withstand the power-frequency breaking current at amplitudes of several hundred amperes as well as the inrush making current at amplitudes of several kiloamperes and frequencies of several kilohertz. **Table 5.1** gives an overview of the technical data of the DRS for different applications.

It has to be taken into account that the current during high voltage phase is not a pure field emission current i_{F}, but it is overlapped with a capacitive component i_{cap} due to the stray capacitance of the interrupter. Therefore, the measured voltage drop across the

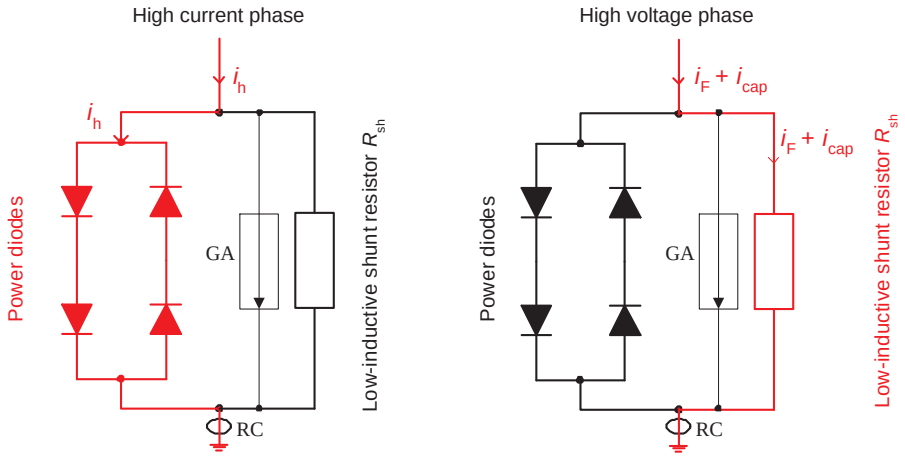

Figure 5.2: Simplified circuit diagram of the measurement system "diode-resistor-shunt (DRS)", GA: gas-discharge arrester, RC: Rogowski coil

Table 5.1: Technical data of the measurement system DRS

Application	DVQ	ICS (Experimental circuit)	ICS (full-power test-circuit)
R_{sh}	68 Ω	500 Ω	500 Ω
Metal film resistor	10 × 680 Ω	15 × 7.5 kΩ	15 × 7.5 kΩ
Max. continuous current of diodes	260 A	260 A	508 A
Max. current of diodes for 10 ms, 25°	2500 A	2500 A	5500 A
Recovery of the diodes	fast	standard	standard
Nom. dc spark-over voltage of gas arrester	90 V	90 V	90 V
Impulse spark-over voltage of gas arrester	<600 V	<600 V	<600 V

resistor shunt v_{sh} is:

$$v_{sh} = R_{sh} \cdot (i_F + i_{cap}) = R_{sh} \cdot i_{tot} \tag{5.1}$$

where i_{tot} is the total current flowing through the interrupter and the measurement system during high voltage phase. To separate the pure field emission current, the capacitive current must be subtracted from the total measured current ("compensation"). Different online and offline compensation methods for different applications are discussed below.

5.1.1 Compensation of the capacitive component

To compensate the capacitive component due to the stray capacitance of the interrupter (in the range of few ten picofarad depending on gap distance and geometry), hardware (online)

as well as software (offline) processing are applied for different applications. The idea of the both methods is similar, i.e. subtraction of an equivalent capacitive current $i_{\mathrm{cap,equ}}$ from the total current i_{tot}. For this purpose, the voltage drop across the interrupter measured by a voltage divider ($v_{2,\mathrm{vac}} = \frac{v_{\mathrm{vac}}}{\text{divider ratio}}$) as "input 1" and the measured total current through the shunt resistor ($i_{\mathrm{tot}} \propto v_{\mathrm{sh}}$) as "input 2" are the inputs to the compensation unit. The equivalent capacitive current is then derived from "input 1" and subtracted thereafter from "input 2", such that the output of the processing unit is only the field emission current i_{F}:

$$i_{\mathrm{cap,equ}} = k \cdot \frac{\mathrm{d}v_{2,\mathrm{vac}}}{\mathrm{d}t} \tag{5.2}$$

$$i_{\mathrm{F}} = i_{\mathrm{tot}} - i_{\mathrm{cap,equ}} \tag{5.3}$$

where k is the compensation factor which is adjusted such that $i_{\mathrm{cap,equ}} = i_{\mathrm{cap}}$ is achieved.

This is realized, for the hardware compensation, using electronic components. The circuit diagram is shown in Appendix B. With the help of a rotary capacitor C_{k} and two potentiometers R_{k1} and R_{k2}, the equivalent capacitive current is produced and adjusted. Using a differential amplifier, it is then subtracted from the total current. Each input of the compensation unit is protected using overvoltage protection including zener diodes. Furthermore, impedance amplifiers are installed to exclude any influence of the compensation unit on the input signals. This hardware processing is used only for applications in the high voltage lab. The circuit is placed in a shielded measurement cabin to avoid electromagnetic interferences and to be able to compensate easily during the measurements (online compensation). This is done, normally, at voltages below field emission current inception voltage, where only the capacitive current flows, with varying the rotary capacitor and potentiometers until the capacitive current is compensated.

The software compensation was basically developed by the project partner (KEMA). In this case the compensation is performed offline after each measurement. The recorded data (total current and interrupter voltage) are entered to a digital signal processing algorithm (realized with MATLAB tools). The interrupter voltage is derivated numerically and multiplied with the compensation factor k to produce the equivalent capacitive current. It is then subtracted from the total current to have the pure field emission current. This method is applied especially in the full-power test-circuit, where it is advisable not to use the hardware compensation due to the electromagnetic compatibility issues. The output of the both compensation methods, i.e. field emission current, is verified according to the well-known FNE (see 6.1 and 8.1). Furthermore, the results of the hardware and software processing are compared in 8.2.

5.1.2 Overvoltage protection

During field emission current measurements, above a certain level of the operating voltage, micro-discharges or even full breakdowns may occur inside the interrupter, which would lead to overvoltages across the DRS and accordingly cause destruction of the ICs in the electronic circuit and even deterioration of the oscilloscope or the digitizer. Therefore, all used electronic devices are required to be protected from possible overvoltages. **Figure 5.3** shows the circuit diagram of the designed four stages overvoltage protection device. Different voltage limiting components in decoupled parallel connection are combined as a cascade circuit, to obtain an optimum effectiveness of the circuit. It consists of a gas-discharge arrester GA with nominal static spark-over voltage of 90 V (first stage), a bidirectional zener diode Z_1 with nominal zener voltage of 82 V (second stage), anti-series zener diodes Z_2 and Z_3 with zener voltage of 15 V (third stage), anti-parallel diodes D_1 and D_2 with series connection of three diodes in each branch (fourth stage) and decoupling resistors between the different stages (R_{d1}, R_{d2}, R_{d3}). If an overvoltage occurs at the input of the circuit, the last stage will become conductive at first. The circuit is dimensioned such that via the voltage drop across the decoupling resistors the respective prior stage is forced to absorb the energy and protect the stage behind it. For example, the first stage protects the second stage, the second stage protect the third one, and so on.

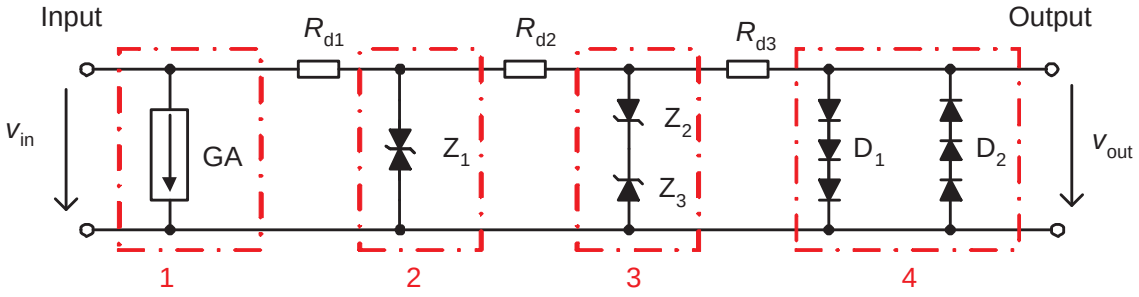

Figure 5.3: Circuit diagram of the overvoltage protection at the field emission current channel of the oscilloscope or digitizer. GA: gas-discharge arrester, Z_1, Z_2, Z_3: zener diodes, D_1, D_2: diodes, R_{d1}, R_{d2}, R_{d3}: decoupling resistors

The fourth stage is not required for protection reasons, but is necessary to avoid overloading of the oscilloscope. As the measurement of field emission current is required to be carried out immediately after a high current phase, the oscilloscope, adjusted to very high resolution, may be overloaded for some milliseconds after current interruption. This stage is thus necessary especially for the low measurement range of only several ten microamperes. The voltage at the input of the oscilloscope will then be limited to $3 \times v_d$, where v_d is the forward voltage of the diodes in the forth stage.

The overvoltage protection circuit is built up as compact as possible, placed in a metallic box, shielded from high frequency electromagnetic interferences, with BNC input and output connectors, and is connected directly to the protected device.

The whole measurement system including the shunt resistor, the compensation processing and the overvoltage protection has a low-pass characteristic with a cut-off frequency of 100 kHz, which is far in excess of the frequency of the field emission current (few hundred Hertz).

5.2 Setups for part-project "DVQ"

For the verification of the FEA method, changing rate of the field emission current after arc-polishing is measured and evaluated. For this reason, a combined experimental circuit for the generation of field emission current and the arc-polishing current is designed. The investigation is performed on both a model vacuum interrupter (MVI) and on commercial interrupters from different manufacturers with increased internal pressure. A vacuum circuit is required for studies on the MVI.

5.2.1 Test objects

Model vacuum interrupter

With the help of the MVI, it is possible to vary the residual gas pressure from atmospheric pressure down to the ultra high vacuum (UHV) range (10^{-7} mbar). For generation of such low pressures, the MVI is required to be baked-out. Therefore, only stainless steel and refractory ceramic can be used. Moreover, for the sealing of flange connections, conflat (CF) flanges are installed. For stainless steel CF-flanges baking temperatures of 450°C can be achieved. The MVI can be easily disassembled, so that different contact geometries and materials can be investigated. **Figure 5.4** shows the MVI. A similar design of MVI was also used in previous works of [Schm 87], [Hein 89] and [Ball 92].

The upper contact's terminal (1) is fixed and is connected to high voltage. The lower contact's terminal (2) is movable through the metal bellow (3), and thus, the contacts gap distance can be adjusted. The contacts (4) are screwed to the terminals via stainless steel contact supports (5). The MVI has a height of 685.5 mm and is constructed using CF-flanges (6) with diameter of 100 mm. For high voltage insulation, two ceramic insulators (7) are installed. The middle section (8) is made from stainless steel and has the same

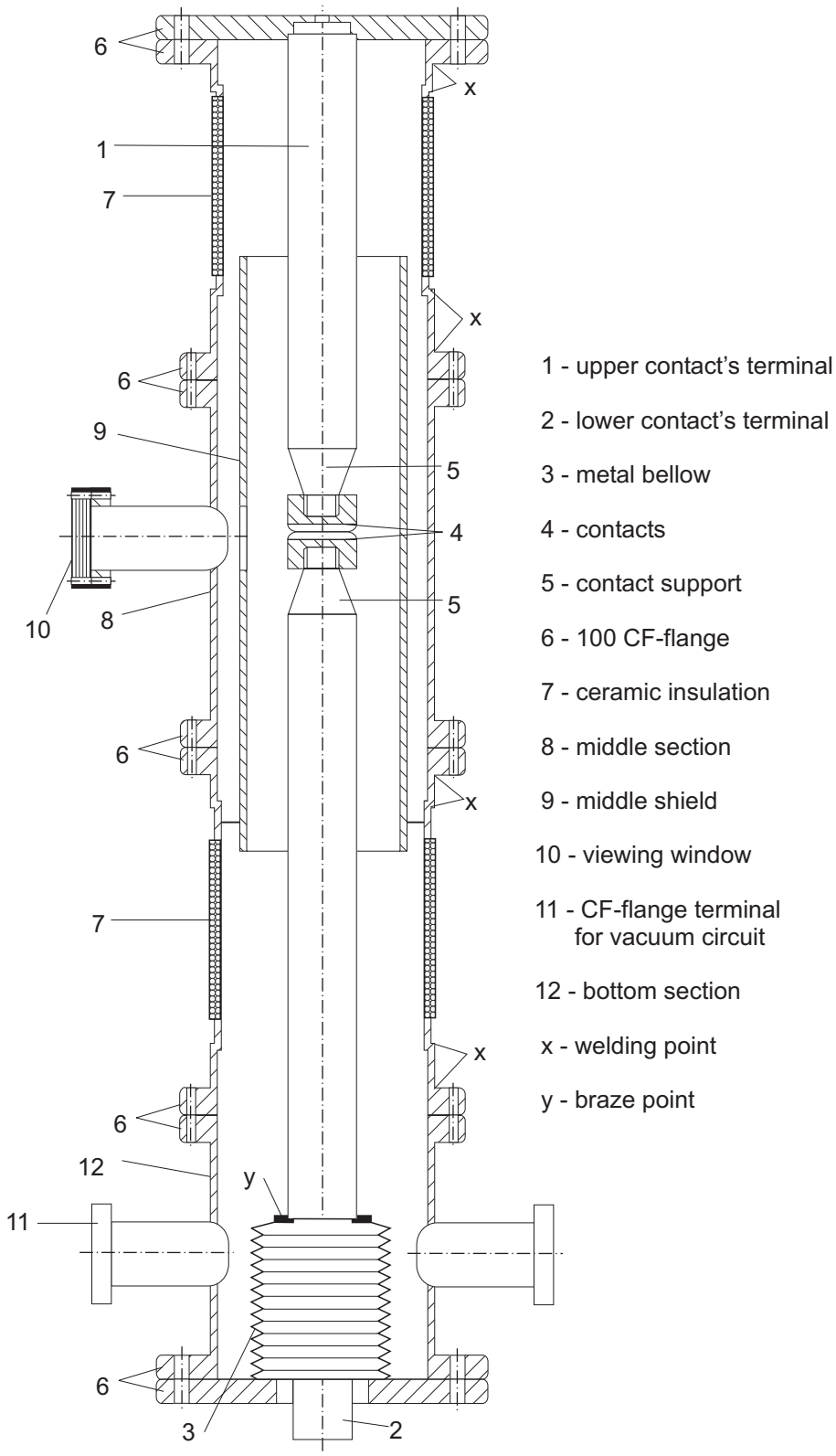

Figure 5.4: Model vacuum interrupter (MVI)

potential as the middle shield (9). A viewing window (10) is connected to the middle section of the MVI. The MVI is evacuated via a 35 mm CF-flange terminal (11), which is welded to the bottom section (12). Another 35 mm and two 16 mm CF-flange terminals are welded to the bottom section as well, which can either be used for gas inlet or be closed using blank flanges.

As in DVQ only measurements on the interrupter in open position are performed, a mechanical drive for switching operations is not required. The contact gap distance is adjustable between 0 and 20 mm using a micrometer screw. Gap measurement is carried out with the help of a linear displacement sensor ("SLS190 linear potentiometer") in the voltage divider mode. The electrical separation of the contacts is defined as the zero-point, which is found using an ohmmeter.

During the investigations, two different contact configurations are used: plate-plate and tip-plate. **Figure 5.5** shows the geometry of both of the plate and tip contacts, having the same diameter of 20 mm. The edges are rounded to avoid unwanted field enhancement. With the help of M 16 × 1.5 threads, the contacts can be directly screwed to the contact supports. Different contact materials such as CuCr and OFHC (oxygen free high conductivity copper) are investigated during this work. Before starting the investigations on each contact pairs, they are subjected to the so called "conditioning" process using ac voltage [Ball 92] to achieve stable field emission characteristic and high enough dielectric strength of the gap.

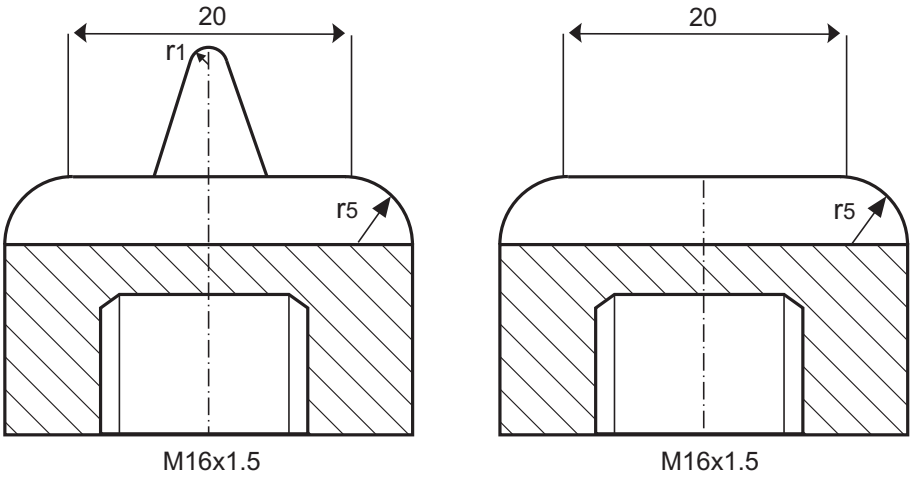

Figure 5.5: Different contacts geometries installed in the MVI

Commercial vacuum interrupters

Different commercial interrupters with increased internal pressures up to 10^{-3} mbar as well as reference interrupters with a pressure of about 10^{-7} mbar are tested. The internal pressure of each interrupter was measured directly by the manufacturer with the help of a Magnetron device. All interrupters were subjected to the conditioning process, and their withstand voltages correspond to the IEC standard requirements [IEC6 93]. A Plexiglas basin filled with Fluorinert^{3M} liquid (FC-72) can be used to avoid external flashovers at higher voltages. FC-72 has very high withstand field strength of 150 kV/cm and is very easy to handle [3M 00]. No switching operation was necessary during the measurement, and the gap distance adjustment is done in a similar way as for the MVI.

The geometry of the contacts in case of the commercial interrupters is more complex than in case of the MVI (Figure 5.5). Most of the available test samples have RMF contacts of CuCr25 (see **Figure 5.6**).

Figure 5.6: Example of the contact geometry of the commercial vacuum interrupters

5.2.2 Vacuum circuit

For the experimental investigations on the MVI a vacuum circuit is required. The vacuum circuit is shown in **Figure 5.7**. For galvanic insulation between the MVI and the vacuum circuit, ceramic spacers are used. Possible mechanical vibrations are damped using the gangway bellows. The pumping station contains a two stage rotary vane pump and a turbo molecular pump with the associated electronic drive unit. The pumping speed for nitrogen is 500 l/s. The pumping station can be disconnected from the MVI using the slide valve. With the help of a venting valve, it is possible to vent the pumping station with dry air, which opens automatically in case of a loss of power supply. The adsorption

trap prevents penetration of oil vapor into the UHV part. Gas inlet is performed using a motor-driven gas dosing valve, which can be operated from the measurement cabin and gives the possibility to vary the internal pressure and type of gas in the MVI.

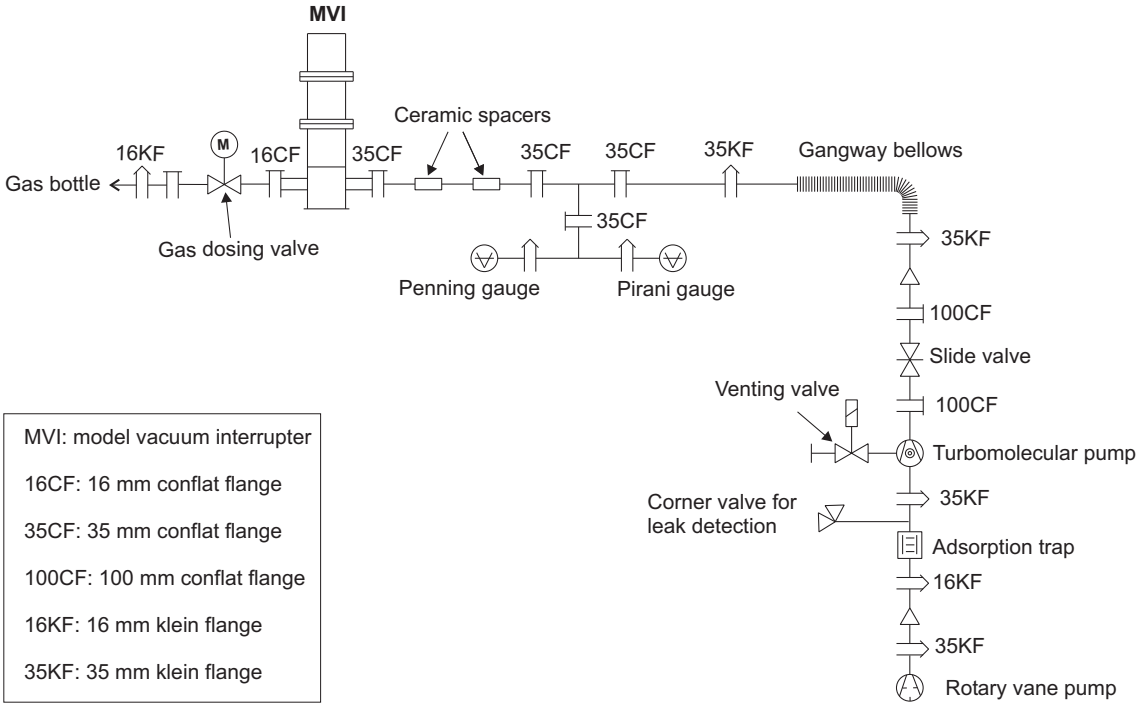

Figure 5.7: Vacuum circuit

Pressure measurement is performed using a combination of a pirani gauge and a penning gauge. The pirani gauge is a thermal conductivity gauge and is used for pressure measurements down to 10^{-3} mbar. At pressures below this value (UHV) the penning gauge is switched on, which works according to the cold cathode ionization principle. Combination of both gauges gives the possibility to measure pressures between 1 bar and 10^{-9} mbar.

5.2.3 Experimental circuit

Figure 5.8 shows the entire experimental circuit. It includes a high-voltage circuit for field emission current generation (left part) and an impulse current circuit for arc-polishing (right part). The specimen is a vacuum interrupter (VI) in open position with adjusted gap spacing.

The arc-polishing circuit is a series resonant circuit consisting of capacitor C_0, inductor L_0, triggered spark gap TG and specimen VI. After charging capacitor C_0, using transformer T_2 and diode rectifier D, the spark gap will be triggered and the HF impulse current flows

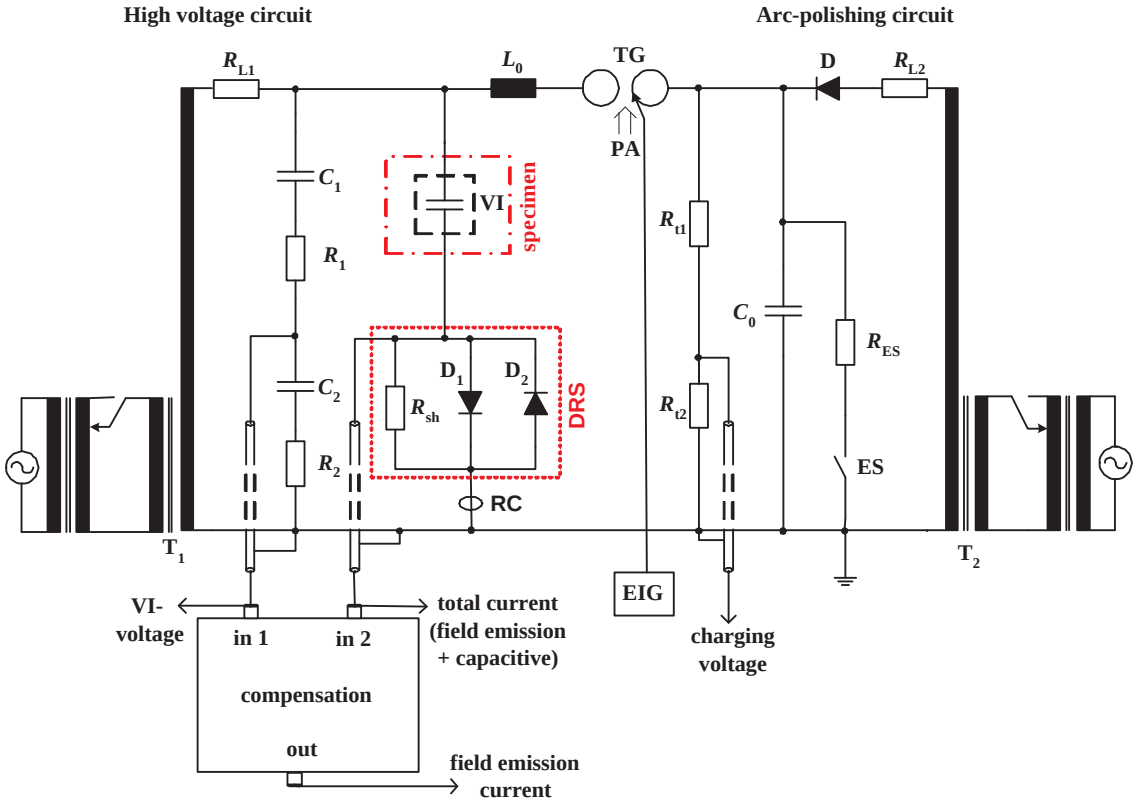

Figure 5.8: Experimental circuit for DVQ.
VI: vacuum interrupter
TG: triggered spark gap
PA: pressurized air (synchronized with trigger signal)
EIG: electronic impulse generator
RC: Rogowski coil for HF current measurement
ES: earthing switch
$R_{ES} = 100\,k\Omega$: damping resistor
T_1, T_2: Transformers
$R_{L1} = 846\,k\Omega$ and $R_{L2} = 1.3\,M\Omega$: current limiting resistors
D: diode rectifier
R_{t1}, R_{t2}: resistive voltage divider
C_1, R_1, C_2, R_2: damped capacitive voltage divider
$C_0 = 0.75\,\mu F$: capacitor of the arc-polishing circuit
$L_0 = 0.2\,mH$, $1.8\,mH$ or $25\,mH$: inductor of the arc-polishing circuit
DRS: diode-resistor-shunt
D_1, D_2: power diodes (anti-parallel)
$R_{sh} = 68\,\Omega$: shunt resistor

through the inductor, the VI and the anti-parallel bypass diodes of DRS (D_1 and D_2) to ground. The HF current flows in form of an electrical arc between the VI's contacts, and its energy input causes gas desorption from the contacts surface (arc-polishing). After arc

extinction, it is important to immediately measure the field emission current. That means re-ignition of the trigger gap must be absolutely avoided. After intense testing, this finally worked by blowing compressed air through the sphere gap, synchronized with the spark gap trigger signal. Amplitude of the HF current is variable between 100 A and 2 kA and its frequency between 1 kHz and 12 kHz. It is measured with the help of a Rogowski coil (RC) as shown in Figure 5.8. The charging voltage of capacitor C_0 is measured using an ohmic voltage divider. An earthing switch ES is used to discharge the capacitor C_0 after circuit de-energizing for safety reasons.

The high-voltage circuit consists of transformer T_1, limiting resistor R_{L1} and specimen VI. Above a certain inception voltage, measurable field emission current ($> 10\ \mu A$) will flow through the VI and the shunt resistor R_{sh}. This current is overlapped with a capacitive component due to the VI's stray capacitance, which is not of interest. To measure the pure field emission current an effective compensation of the capacitive component is performed, which is explained in detail in 5.1. The high voltage across the VI is measured using a damped capacitive voltage divider.

At the beginning of the test, the VI's gap spacing is adjusted. Using transformer T_1, the voltage is increased and at voltages below inception voltage compensation of the capacitive component is performed. The voltage is further increased, until measurable field emission current appears. Afterwards, using the arc-polishing circuit, the HF current is ignited and the arc flows through the VI and partly cleans its contacts surface. During this arcing time the high voltage circuit is short-circuited and the whole voltage drops across the limiting resistor R_{L1}. Immediately after HF current interruption, the high voltage will appear again across the VI and the field emission current can be measured using the DRS. This signal is then recorded using a digital oscilloscope for the evaluation of field emission current's changing rate and consequently the internal pressure of the VI.

5.3 Setups for part-project "ICS"

To investigate the performance of vacuum interrupters during their dielectric recovery after capacitive switching, measurement of field emission current after the interruption of capacitive loads is performed both in an experimental circuit in the high-voltage lab (setup "a") as well as in a full-power test-circuit in a power lab (setup "b"). The measurements are performed on both commercial and non-regular interrupters.

5.3.1 Test objects

In contrast to "DVQ", in part-project "ICS" the investigations are performed during mechanical operations. Three different vacuum circuit breakers (VCB1, VCB2 and VCB3) up to 36 kV rated voltage were available for this purpose. Only one pole of the breakers is used as test sample (test-pole). Commercial interrupters from different manufacturers (with rated gap spacing or reduced gap spacing) as well as non-regular interrupters (each having intentionally a certain process modification) are mounted in the test-pole of the breaker. **Tables 5.2**, **5.3**, **5.4** show overviews of the different specimens mounted in VCB1, VCB2 and VCB3.

Table 5.2: Overview of the specimens mounted in VCB1 ($V_\mathrm{r} = 17.5\,\mathrm{kV}$, $d_\mathrm{r} = 8\,\mathrm{mm}$)

Specimen	Commercial / non-regular	Modification by manufacturing	Manufacturer	Gap spacing d in mm	Quantity
A	commercial	-	M1[a]	8	2
B	commercial (same design as A)	-	M1	6 (75% of d_r)	1
C	non-regular (same design as A)	intentionally manufactured in non-clean room conditions[b]	M1	8	3
D	non-regular (same design as A)	intentionally manufactured without conditioning process	M1	8	3
E	commercial	-	M2	8	2

[a]Siemens AG
[b]Particle purity of air (particle size $\leq 0.5\mu\mathrm{m}$) in workshop: $1500000/\mathrm{m}^3$, in clean room: $35000/\mathrm{m}^3$, in laminar box: $350/\mathrm{m}^3$

Table 5.3: Overview of the specimens mounted in VCB2 ($V_\mathrm{r} = 24\,\mathrm{kV}$, $d_\mathrm{r} = 11\,\mathrm{mm}$)

Specimen	Commercial / non-regular	Modification by manufacturing	Manufacturer	Gap spacing d in mm	Quantity
F	commercial	-	M1	8 (72% of d_r)	1
G	commercial (same design as F)	-	M1	4 (36% of d_r)	1
H	non-regular (same design as F)	intentionally manufactured in non-clean room conditions	M1	8 (72% of d_r)	1

Table 5.4: Overview of the specimens mounted in VCB3 ($V_\mathrm{r} = 36\,\mathrm{kV}$, $d_\mathrm{r} = 20\,\mathrm{mm}$)

Specimen	Commercial / non-regular	Modification by manufacturing	Manufacturer	Gap spacing d in mm	Quantity
I	commercial	-	M1	20	1

5.3.2 Experimental circuit (setup "a")

Due to the huge investment necessary to build up a direct test circuit, a synthetic circuit is designed. **Figure 5.9** shows the experimental setup "a", installed in a high-voltage lab. It includes a high-voltage circuit (right part) to supply the unidirectional recovery voltage and a load-current circuit (left part) to supply the breaking current. The circuit for inrush current generation is not shown in this figure. One pole of the VCB is the test sample. The other two poles, connected in series, are used to separate the high-voltage and the load-current circuits from each other.

The load-current circuit consists of a 230 V ac source, switch s, current limiting reactor L_1, VCB and the bypass diodes of the DRS. When the test starts the VCB is in closed position. After closing switch "s" the breaking current flows for up to 80 ms through the load-current circuit, VCB and anti-parallel connected diodes. Using different current limiting reactors L_1 breaking currents of 500 A and 20 A (50 Hz) can be achieved, which is measurable with the Rogowski coil (RC). This current will be interrupted after 80 ms by VCB at current zero after contact opening.

The high-voltage circuit consists of transformer T with adjusted peak voltage of $\hat{v}_\mathrm{T}$, capacitors $C_{0,1}$ and $C_{0,2} << C_{0,1}$, the VI under test and the shunt resistor R_sh. It serves for generating a unidirectional recovery voltage of a $\{1 - \cos(\omega t)\}$ wave shape after current interruption. Before current interruption, the high-voltage circuit is in short circuit condition and the voltage drops across capacitor $C_{0,1}$. The transformer voltage of the high-voltage circuit and the source voltage of the load-current circuit are in phase, which means that at current zero crossing the transformer voltage is at its maximum and therefore the capacitor $C_{0,1}$ is charged to the transformer peak voltage. The recovery voltage across the specimen v_rec after current interruption is therefore approximately:

$$v_\mathrm{rec}(t) = v_\mathrm{T}(t) - V_{\mathrm{C}_{0,1}} = v_\mathrm{T}(t) - \hat{v}_\mathrm{T} = \pm\hat{v}_\mathrm{T}(1 - \cos(\omega t)) \tag{5.4}$$

Where, v_T is the transformer voltage and $V_{\mathrm{C}_{0,1}}$ is the capacitor charged voltage. The recovery voltage is measured using an ohmic capacitive voltage divider as shown in Figure 5.9. At high enough voltages, the field emission current can be measured using the DRS

and the compensation process (hardware or software) as explained in 5.1.

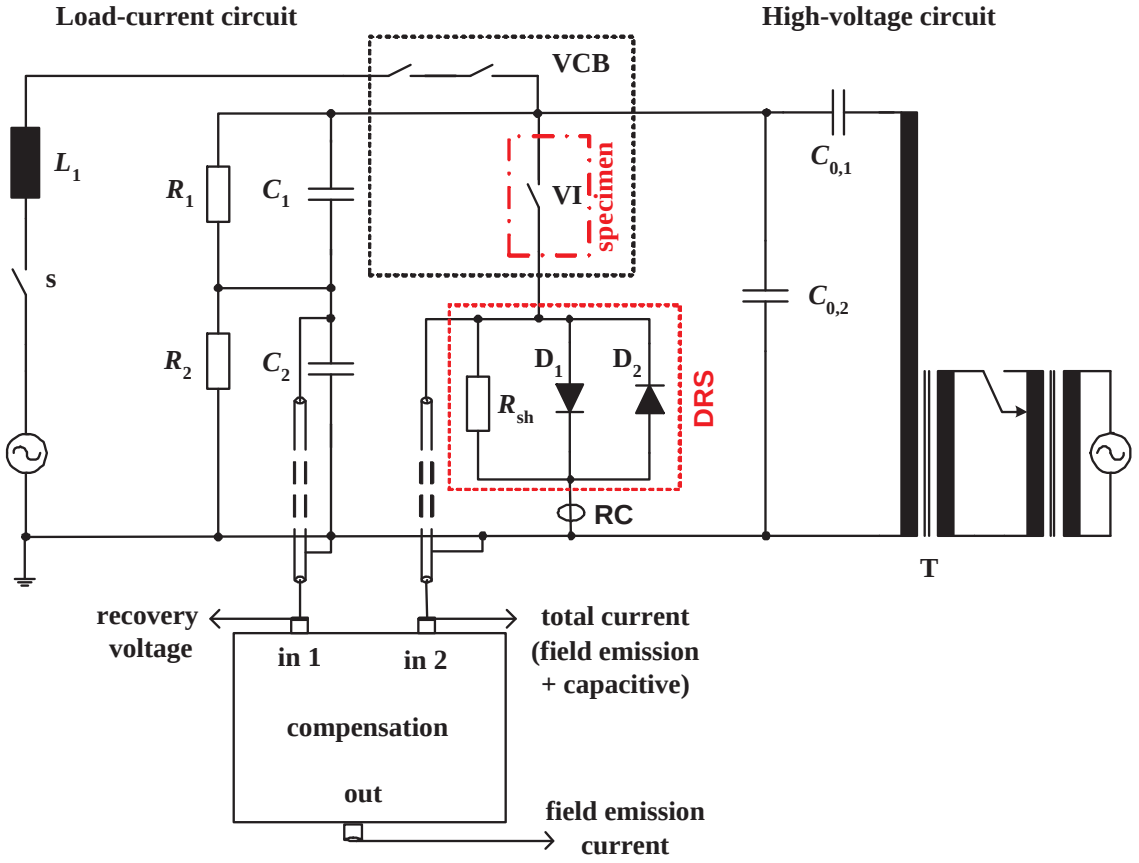

Figure 5.9: Experimental circuit for ICS (setup "a").
VCB: vacuum circuit breaker
specimen: VI (vacuum interrupter, one pole of VCB)
s: switch
RC: Rogowski coil for breaking current measurement
T: Transformer
C_1, R_1, C_2, R_2: mixed ohmic-capacitive voltage dividers
$C_{0,1} = 10\,\text{nF}$, $C_{0,2} = 2.4\,\text{nF}$: capacitors of the high-voltage circuit
$L_1 = 1.4\,\text{mH}$ or $36.6\,\text{mH}$: current limiting reactor
DRS: diode-resistor-shunt
D_1, D_2: power diodes (anti-parallel)
$R_{sh} = 500\,\Omega$: shunt resistor

Circuit for inrush current injection during contact closing

To stress the interrupter with inrush current during closing operation the circuit shown in **Figure 5.10** is built up. It is basically a series resonant circuit. The capacitor bank C_i is

firstly charged to V_{ch}. After closing the VI, the capacitor will discharge through inductor L_{i} and the VI. At a certain gap distance during closing operation, the gap pre-strikes and the inrush current starts to flow through the vacuum arc. This pre-arcing continues until contact touch and leads to contact welding. The inrush current flows further through the closed contacts, until it is damped to zero. Frequency and amplitude of the inrush current can be varied with varying capacitor C_{i}, inductor L_{i} and charging voltage V_{ch}. For an interrupter with rated voltage of $V_{\mathrm{r}} = 17.5$ kV, $C_{\mathrm{i}} = 45\,\mu$F and $L_{\mathrm{i}} = 220\,\mu$H amplitude and frequency of the inrush current are as follows:

$$V_{\mathrm{ch}} = V_{\mathrm{r}} \times \frac{\sqrt{2}}{\sqrt{3}} \tag{5.5}$$

$$\hat{i}_{\mathrm{inrush}} = 6\,\mathrm{kA};\, f = 1.6\,\mathrm{kHz} \tag{5.6}$$

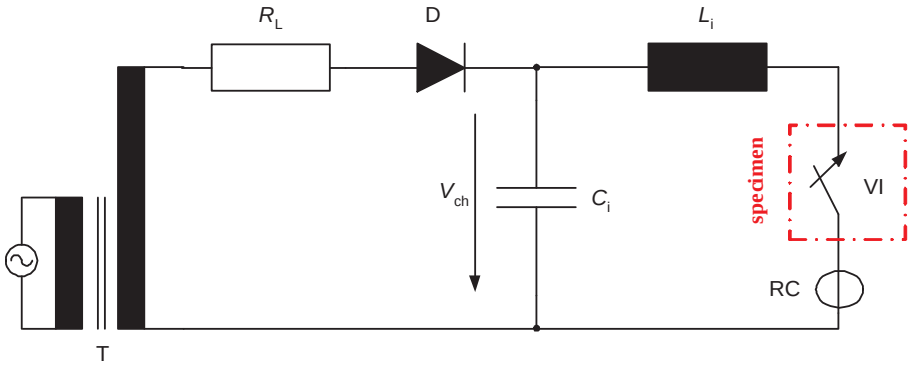

Figure 5.10: Circuit for closing the interrupter under charged capacitor bank.
specimen: VI (vacuum interrupter, one pole of VCB)
$C_{\mathrm{i}} = 45\,\mu$F: capacitor bank
$L_{\mathrm{i}} = 220\,\mu$H: impulse inductance
$R_{\mathrm{L}} = 1\,\mathrm{M}\Omega$: limiting resistance
RC: Rogowski coil
T: transformer
D: diode rectifier

5.3.3 Full-power test-circuit (setup "b")

In addition to the experimental circuit (setup "a"), full-power test-circuit (single phase capacitive circuit as well as single phase back-to-back circuit), is implemented in a power lab[1]. **Figure 5.11** shows the single phase capacitive circuit. Both load currents (break

[1]KEMA, Arnhem/Netherlands

and inrush) as well as recovery voltage are generated using one circuit consisting of source side and load side.

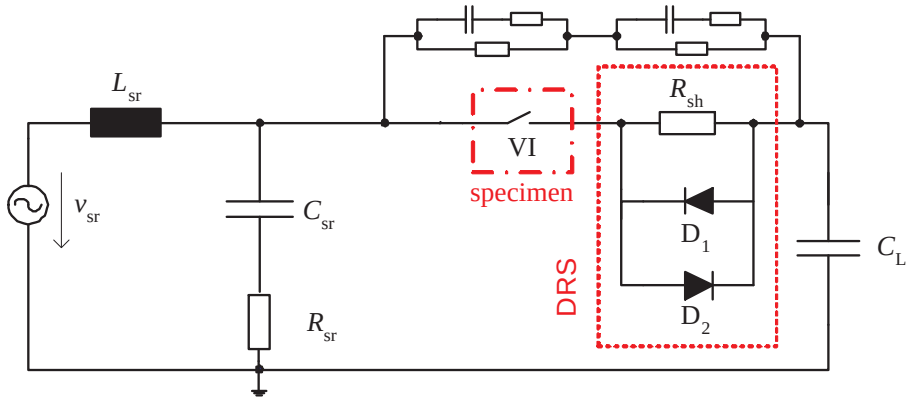

Figure 5.11: full-power test-circuit (KEMA) for ICS (setup “b”).
specimen: VI (vacuum interrupter, one pole of VCB)
C_L: load capacitance
L_{sr}, R_{sr}, C_{sr}: source side
DRS: diode-resistor-shunt
D_1, D_2: power diodes (anti-parallel)
$R_{sh} = 500\,\Omega$: shunt resistor

During making operation, inrush current up to several kiloamperes and several kilohertz may flow through the test sample. Afterwards, a capacitive current with amplitude up to several hundred amperes will flow. This current will be interrupted by the VI at a certain current zero. Due to the 90° phase difference between source voltage and breaking current, at the moment of current interruption the capacitor C_L has been charged to the peak value of the source voltage. Therefore, the recovery voltage across the VI is again the difference between the direct voltage of the load capacitance and the alternating voltage of the source side and has a $\{1 - \cos(\omega t)\}$ wave shape. This voltage is measured using a mixed damped voltage divider. The total current (field emission + capacitive) is measured with the help of the DRS. Here, because of the need to measure current and voltage signals at floating potential, 14-bit floating digitizers and digital optical data transfer are used. Due to electromagnetic compatibility issues in the actual surrounding and the floating potential of the specimen, the hardware (analogue electronic) compensation is not used in the direct vicinity of the interrupter. Thus, the compensation process is performed using software compensation[2] (offline). After each measurement the recorded data (total current and recovery voltage) are entered to the mentioned digital signal processing algorithm (realized with MATLAB tools) to calculate the pure field emission current.

[2]developed by the project partner (KEMA)

A single phase back-to-back circuit is also used to achieve inrush currents according to IEC circuit breaker standard [IEC6 08] with amplitude of 20 kA and frequency of 4.25 kHz. In this case the measurement principle is exactly the same as explained above. However, the bypass diodes of the DRS are dimensioned to withstand higher inrush currents (20 kA and 4.25 kHz).

6 Investigations on DVQ - Field emission current at high and semi vacuum range

This chapter deals with the dielectric behavior of the vacuum interrupter in high and semi vacuum range. Particularly, the influence of the internal pressure on the field emission current is of interest. In this regard, verification of the field emission current measurement according to the FNE is of great importance. The investigations are performed, applying alternating voltage on both commercial interrupters and on the MVI with gap distance adjusted in the range of a few hundred micrometers up to a few millimeters.

6.1 Verification of the field emission current measurement at alternating voltages

As is mentioned in 5.1, for the measurement of the pure field emission current under applied alternating voltage, an effective compensation of the capacitive current due to the fairly high stray capacitance of the interrupter in the range of approx. $(10 \cdots 100)$ pF is carried out. **Figure 6.1** shows a measurement example for gap spacing of $d = 1\,\text{mm}$. It includes both the total current (uncompensated signal in green) as well as the pure field emission current (compensated signal in red using hardware processing) for different voltage levels. It is observed that at lower voltages the current has basically only a capacitive component (Figure 6.1a). Increasing the voltage above the inception voltage, measurable field emission current appears (Figure 6.1b and Figure 6.1c). At higher voltages the current consists mainly of field emission current (Figure 6.1d). This is due to the exponential dependency between field emission current and voltage, whereas the capacitive component changes linearly with voltage. It is clear that at even higher voltages the capacitive component is

negligible compared to the field emission current, and the compensation process is then not necessarily required any more.

Since the supply alternating voltage is not a pure sinusoidal voltage, the capacitive component of the current contains higher harmonics of the 50 Hz power frequency. As the compensation processing is performed using the same supply voltage, the equivalent capacitive current, generated in the compensation circuit, contains also the same harmonics. Therefore, the higher harmonics will be compensated as well.

At each voltage level in Figure 6.1, at voltage peak, the value of the field emission current is equal to the measured total current. This has to be the case as the capacitive component is equal to zero whenever the voltage reaches its peak.

Figure 6.2 shows another measurement example of the pure field emission current using hardware compensation. The measurement is performed on a commercial interrupter with adjusted gap spacing of $d = 1.5\,\mathrm{mm}$. It is observed that the amplitude of the field emission currents at positive and negative polarities are different, which is due to the unequal surface condition of the contacts.

According to the FNE, explained in 2.2.2, there is an exponential dependency between the interrupter voltage and the corresponding field emission current. Therefore, ideally for pure field emission current, drawing the voltage-current-characteristic of the gap in the form of the Fowler-Nordheim-Plot (FNP), by plotting $\log(i_\mathrm{F}/v_\mathrm{vac}^2)$ against $(1/v_\mathrm{vac})$, gives a linear relationship. **Figure 6.3a** shows the current-voltage-characteristic of the gap in exponential form, and Figure 6.3b shows the FNP for the selected area in Figure 6.2, which gives a straight line. Using the slope of the line and its intersection with the y-axis, the surface parameters, i.e. field enhancement factor β and emitting area A_e, can be calculated (see 2.2.2). This analysis is performed to verify the field emission current according to the voltage-current-characteristic of the gap with the help of the FNP and to evaluate the surface parameters. For this reason, a MATLAB-program is developed that allows to perform this analysis for every measurement in a simple way.

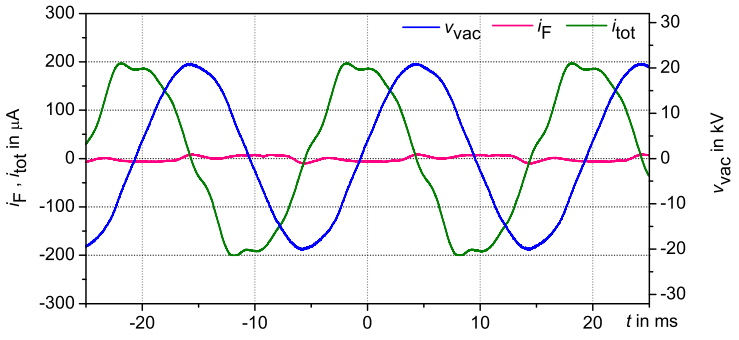

(a)

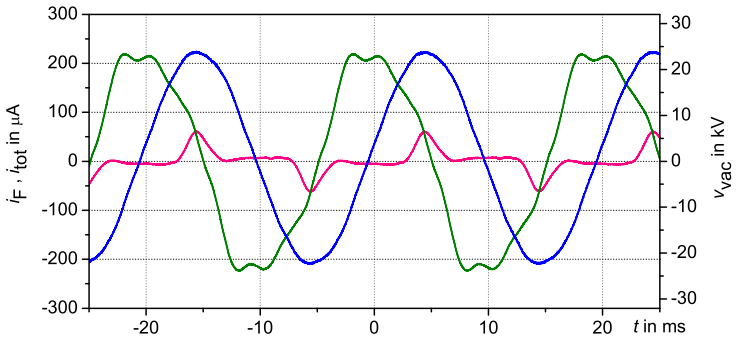

(b)

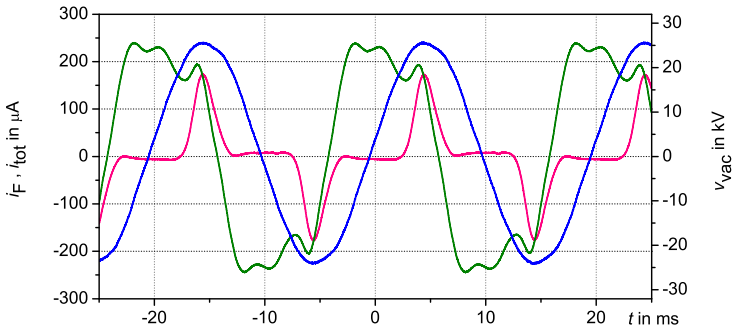

(c)

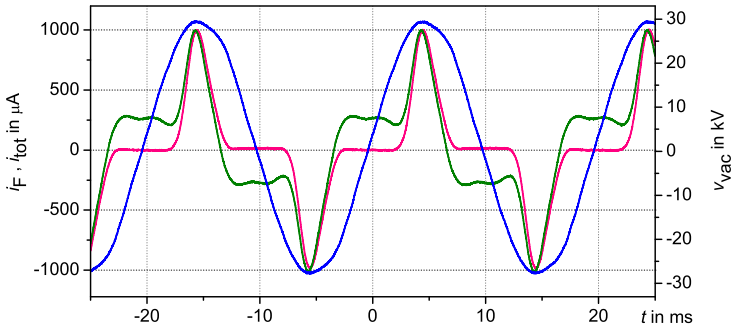

(d)

Figure 6.1: Measurement example showing waveforms of the interrupter voltage in blue, pure field emission current in red and total current in green at different voltage levels. a: $\hat{v}_{\mathrm{vac}} = 21\,\mathrm{kV}$, b: $\hat{v}_{\mathrm{vac}} = 23.5\,\mathrm{kV}$, c: $\hat{v}_{\mathrm{vac}} = 25\,\mathrm{kV}$, d: $\hat{v}_{\mathrm{vac}} = 29\,\mathrm{kV}$

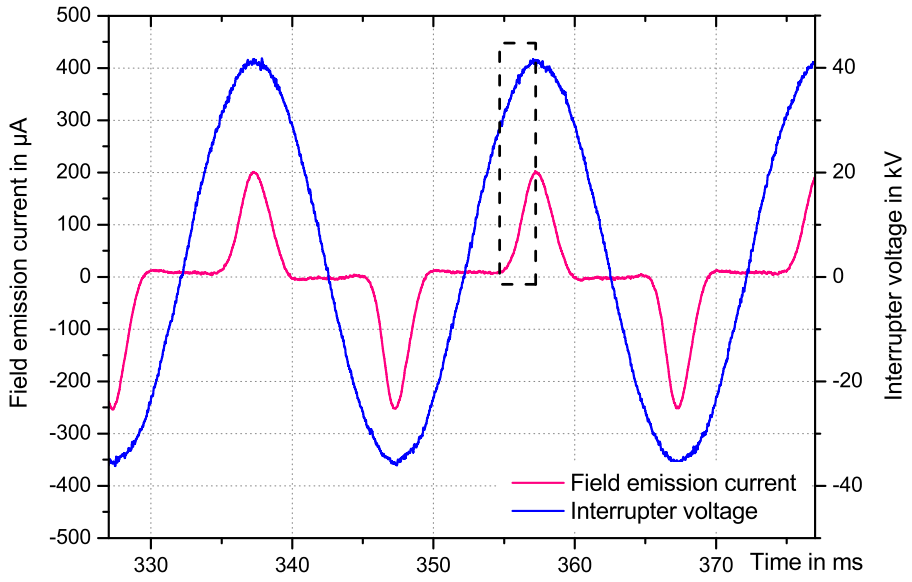

Figure 6.2: Measurement example showing waveforms of the interrupter voltage in blue and pure field emission current in red

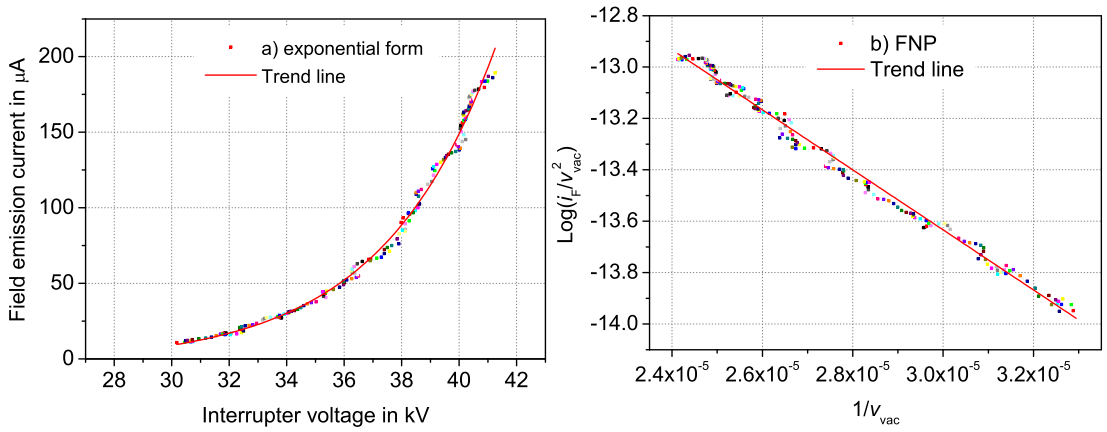

(a) (b)

Figure 6.3: Current-voltage-characteristic of the vacuum gap for the selected area shown in Figure 6.2. a: exponential form b: FNP

6.2 Influence of the internal pressure on the current-voltage characteristic of the gap

As is mentioned in the previous chapters, the field emission current depends, besides other parameters, on the electrodes' work function, which is itself dependent on the electrodes' material as well as on the gas layer covering the electrode surfaces (gas type and gas coverage ratio). Adsorption of different residual gases on different contact materials affects the surface work function and consequently the field emission current. However, the gas layer coverage ratio is itself a function of the interrupter internal pressure. Thus, the field emission current depends on the internal pressure as well. Rise of the internal pressure results in growth of the gas layers covering the contact surfaces and accordingly in changes of the field emission current.

Figure 6.4 shows current-voltage-characteristics of the gap at different internal pressures. The measurements are performed on the MVI with gap spacing of $d = 1$ mm and contact-gas system of CuCr-N_2. Before starting the experiment the internal pressure and the gap distance of the MVI is adjusted. An alternating voltage is applied across the interrupter, and the voltage is increased from $\hat{v}_{\mathrm{vac}} = 10$ kV in 5 kV steps. At each voltage level the peak value of the field emission current is recorded. This is repeated for three different pressures. It is observable that at higher pressures and constant gap voltage the field emission current is lower. This is due to the growth of the gas layer on the contact surface, when increasing the pressure. All curves can be fitted to exponential trend lines, as expected by FNE, which are plotted in dashed form.

Further measurements are performed, varying the internal pressure during one single experiment and keeping either the voltage (**Figure 6.5**) or the field emission current (**Figure 6.6**) constant. Figure 6.5 shows the dependency of the field emission current on the internal pressure. Each curve is one experiment at constant interrupter voltage. Independent from the voltage, it is observed, that the field emission current decreases with increasing internal pressure in a system of CuCr-N_2.

In Figure 6.6, during one experiment (one curve) the voltage across the interrupter is varied such that the field emission current stays constant. It is seen that with increasing the internal pressure, higher voltages are necessary to keep the field emission current constant.

It is important to note that the absolute value of the field emission current is dependent on many other parameters, such as electrode surface condition and gap history. Therefore,

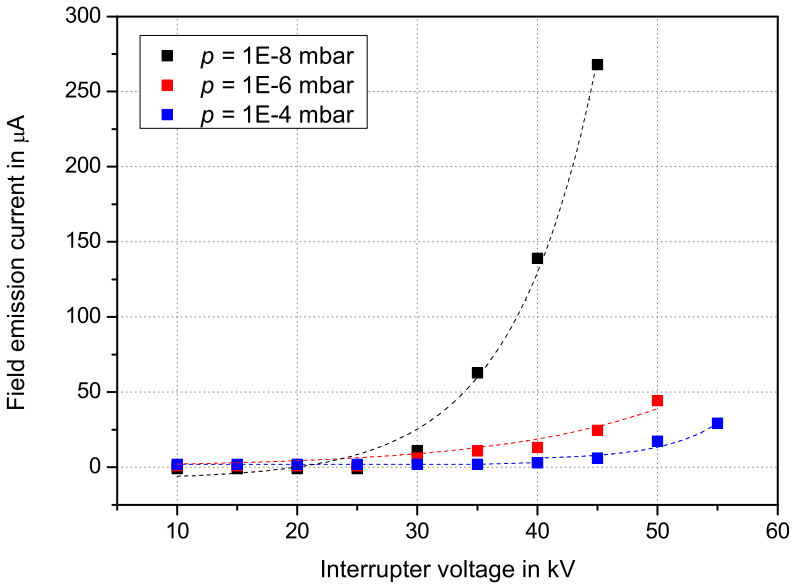

Figure 6.4: Current-voltage-characteristic of the vacuum gap (MVI) at different internal pressures. Dashed curves: exponential trend lines

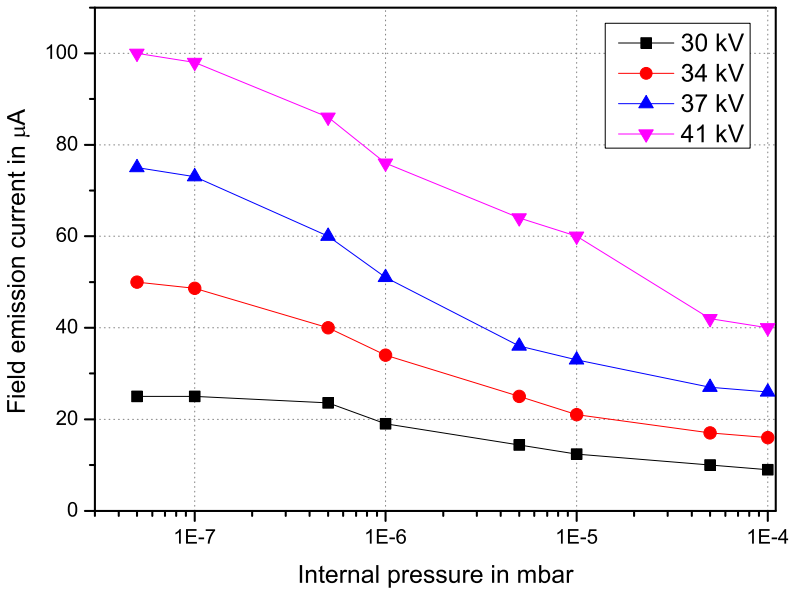

Figure 6.5: Field emission current versus internal pressure for different adjusted interrupter voltages.

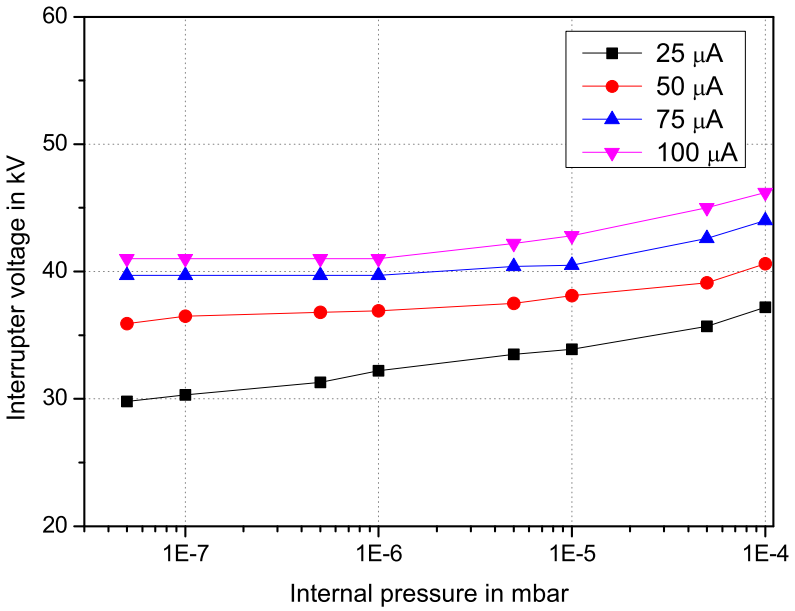

Figure 6.6: Interrupter voltage versus internal pressure for different adjusted field emission currents.

it may vary even at given gap distance, internal pressure and applied voltage. For this reason any comparison between the measurements can be done only relatively.

To find out the impact of internal pressure on field emission current for different residual gases, measurements are performed on the MVI with two different contact-gas systems: Cu-O_2 and Cu-N_2. This is shown in **Figure 6.7**. For both contact-gas systems, the internal pressure of the MVI is increased during the experiment from 10^{-7} mbar up to 5×10^{-4} mbar (curve I) at constant interrupter voltage and gap distance, and subsequently decreased back to 10^{-7} mbar (curve II).

It is seen that with increasing the internal pressure (curve I) the field emission current decreases in both contact-gas systems. The field emission current has smoother decrease at the beginning ($p < p_1$) and at the end ($p > p_2$) of curve I. Whereas, in the middle of the curve ($p_1 < p < p_2$) steeper decrease in the field emission current is observed. The value of these threshold pressures (p_1 and p_2) and the pressure range with strong impact on the field emission current are dependent on the contact-gas system, as is obvious from Figure 6.7. This effect may be due to the dependence of the contact work function on the gas type and its coverage ratio.

During reduction of the internal pressure back to 10^{-7} mbar (curve II), it is seen with both contact-gas systems that the field emission current does not return to its initial value. Smooth increase in the field emission current is observed in the Cu-N_2 system due to gas

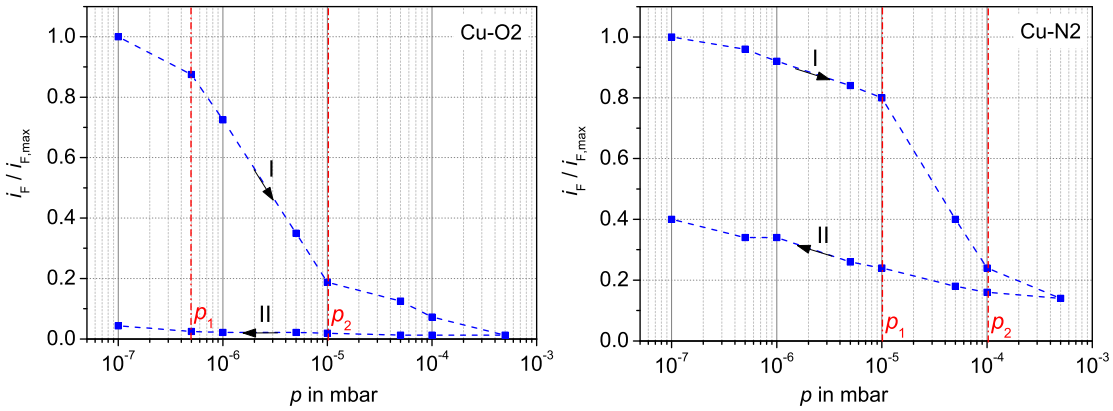

Figure 6.7: Dependency of the field emission current on the internal pressure for different contact-gas systems. a: Cu-O_2 b: Cu-N_2

desorption process. Whereas, in the Cu-O_2 system, the field emission current remains nearly constant as the pressure falls. The interaction energy of the gas molecules with the electrode surface depends on the contact-gas system. In Cu-O_2 system with higher interaction energy, the gas desorption process is slower than in Cu-N_2 system. More energy input or time is required for desorption of O_2 molecules from the Cu electrode to return to the initial condition at 10^{-7} mbar.

The electrode surface condition, especially in the Cu-N_2 system, also plays an important role regarding the adsorption process and the changes of the surface work function. **Figure 6.8** shows an example for the Cu-N_2 system, where the field emission current initially increases with increasing the internal pressure.

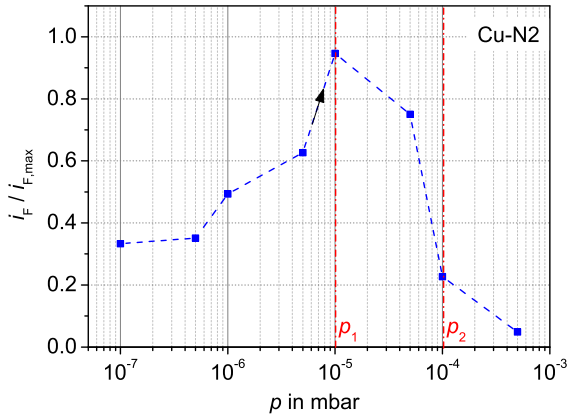

Figure 6.8: An example showing the influence of the internal pressure on the field emission current in Cu-N_2 system

From these investigations it can be concluded that there is a lack of correlation between the absolute value of the field emission current and the internal pressure. This is on one hand due to the time dependent characteristic of the field emission current as well as its strong dependency on different parameters (e.g. electrode surface condition, electrode temperature, electrode material and residual gas type), and on the other hand because of the influence of the contact-gas system on the threshold pressures p_1 and p_2. Therefore, it is not adequate to estimate the internal pressure only with the help of the absolute value of the field emission current. In the next chapter, the FEA method, which is based on the changing rate of the field emission current, and not only on its absolute value, is investigated.

7 Investigations on DVQ - Verification of the FEA method in semi-vacuum range

As was shown in the previous chapter, the absolute value of the field emission current has no simple dependence on the internal pressure, and it is not sufficient for the estimation of the interrupter vacuum quality. Therefore, the FEA method, based on the changing rate of the field emission current after arc-polishing of the contacts [Fron 93a], as a possible method for DVQ, is investigated in this chapter.

The principle of the FEA method is explained in 3.2. The former experimental findings by [Fron 93a] show that the duration of the adsorption of a gas layer on a metal surface distinctly depends on the internal pressure. Basically, it is shorter for higher internal pressures. According to this finding, the gas layer could be removed from parts of the contact surface with the help of arc-polishing (by spark-over of the electrodes and a subsequent defined current flow), and afterwards the time response of the re-adsorption of the gas layer could be observed by measuring the field emission current over time. It must be noted that these findings are based only on investigations on a MVI with a certain contact geometry, contact material (CuCr) and residual gas (air).

However, it is necessary to make this method work also properly in the complex regime of commercial vacuum interrupters, with complicated contact geometries (for instance see Figure 5.6) and unknown type of the residual gas. Therefore, more investigations are required for the verification of applicability of the method on commercial interrupters, which are presented in this chapter. For this reason, the method is applied on the self-made MVI as well as on various commercial interrupters with increased internal pressure to verify if the method is applicable "on-site" or not. The results are finally compared and discussed.

In this respect, different parameters are considered:

- Electric field stress is varied in order to adjust the amplitude of field emission currents.
- Arc-polishing current parameters are varied in order to have influence on the arc energy.
- Contact geometry, material as well as the sort of residual gas and the internal pressure are varied by using the MVI.

The method is applied at an adjusted fix contact gap, and no mechanical operation is performed during the experiments.

7.1 Adjustment of the field emission current

The amplitude of the field emission current before arc-polishing is set by adjusting the applied electrical field (applied alternating voltage and gap distance). However, dependent on the gap condition, unequal field emission current may be achieved at constant applied electric field. Therefore, it is required to set the amplitude of the field emission current for each measurement separately. In this regard, it is important that no breakdown during the whole measurement periods occurs, even after arc-polishing, where the field emission current is basically higher than before at constant applied voltage.

For this reason, measurements are performed to find out the breakdown voltage at different gap spacings. **Figure 7.1** shows one example of such measurements. At each gap distance between 0.2 to 0.6 mm, alternating voltage is applied across the interrupter. The voltage is increased until internal breakdown occurs. The amplitude of the voltages at defined field emission currents as well as the breakdown voltage are recorded for each gap spacing.

Small gap distances are preferred for two reasons. Firstly, at small distances, same field emission current can be achieved at lower applied voltage. Secondly, there is almost a linear dependency between the breakdown voltage and the gap spacing at small gap distances, whereas at larger distances, the breakdown voltage is not linearly dependent on the gap spacing and it may happen that a breakdown occurs even without prior measurable field emission current (known as particle effect in the literature).

The applied electrical field is in most cases adjusted such that measurable field emission current before arc-polishing is in the range of ten to hundred microamperes. The investigations show that the adjusted amplitude of the field emission current has no significant impact on the measurement results (assuming no internal breakdown occurs).

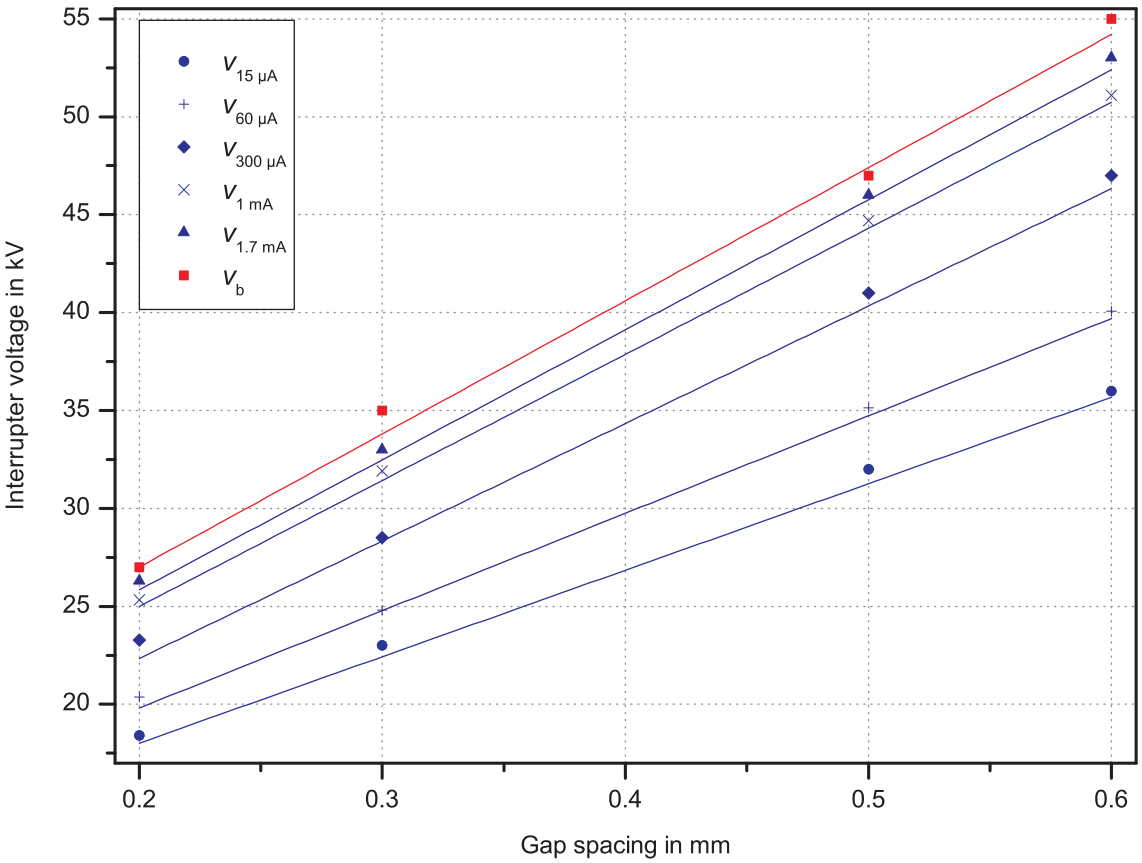

Figure 7.1: Dependency of the interrupter breakdown voltage v_b and voltages at defined field emission currents (from 15 µA to 1.7 mA) on the gap spacing

7.2 Arc-polishing parameters

Arc-polishing of the electrodes surface is performed by spark-over of the electrodes and a subsequent HF oscillating current flow. The HF current flows in the form of an electrical arc between the electrodes, and the arc energy input leads to gas desorption from the contact surfaces. The amplitude of the HF current is varied between 100 A and 2 kA and its frequency between 1 kHz and 12 kHz. **Figure 7.2** shows typical waveforms of the HF current during arc-polishing of the contacts for different interrupter internal pressures and HF current frequencies. The measurement is performed at gap spacing of 0.5 mm.

It is observed that even at higher frequencies the interrupter is able to interrupt the current after a few cycles at pressures below the threshold value of 10^{-4} mbar (Figure 7.2a and b). Only, at higher pressures (above 10^{-3} mbar), the interrupter loses its current switching capability, and a damped oscillation without current interruption is observed (Figure 7.2c).

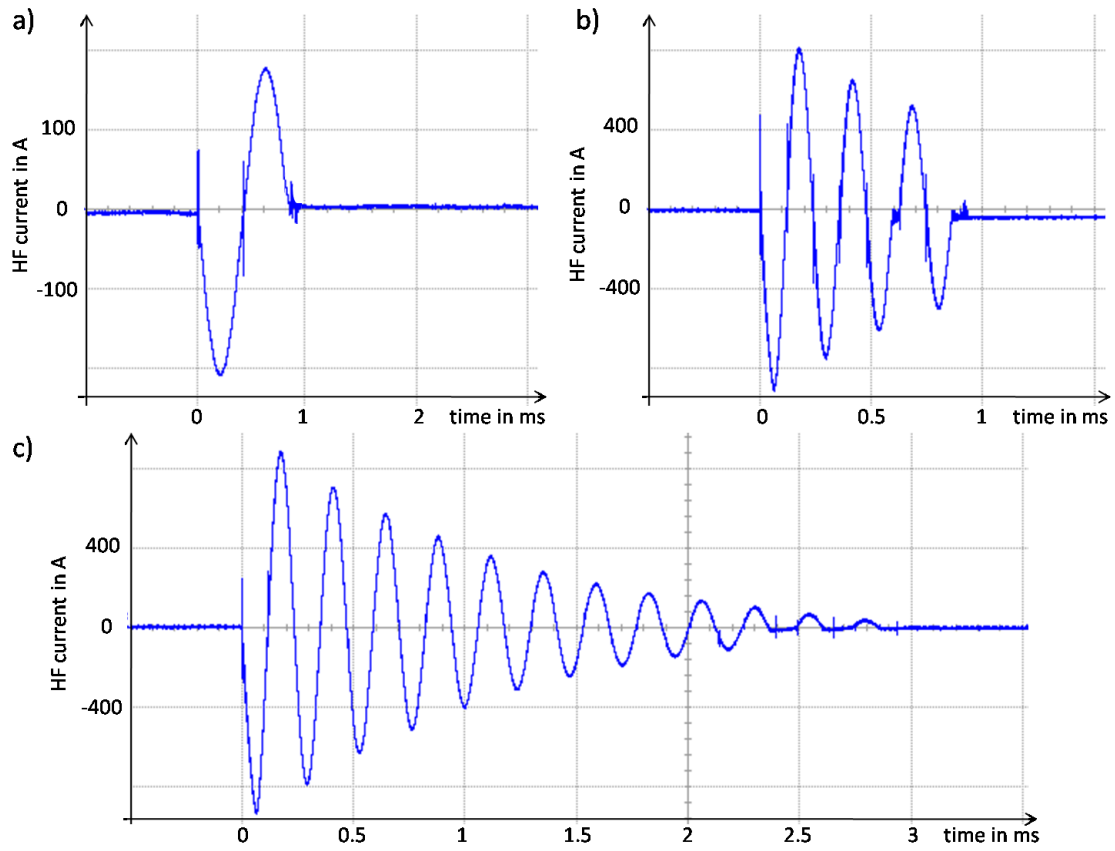

Figure 7.2: Typical waveforms of the HF current during arc-polishing of the contacts with gap spacing of 0.5 mm. a: $p = 10^{-7}$ mbar, $f = 1.2$ kHz b: $p = 10^{-7}$ mbar, $f = 4.3$ kHz c: $p = 10^{-3}$ mbar, $f = 4.3$ kHz

During the experiments, it is shown that the arc-polishing is more effective at HF currents of lower amplitudes (a few hundred amperes) with frequencies between 1 kHz and 5 kHz. Higher current amplitudes may change the electrode surface from the microscopic point of view, which is not desirable. Since the field emission current is strongly dependent on the microscopic condition of the surface, the arc-polishing should only affect the gas coverage layer but not the surface condition. Therefore, to obtain reproducible measurement results, the arc-polishing is performed in the above mentioned HF current range.

7.3 Measurement results on the MVI

In the following, some measurement examples are presented for the MVI. Thereafter, the results are evaluated and the dependency between the decay time of the field emission

current and the internal pressure for the tip-plate contact configuration is studied. Finally, the reproducibility of the measurements according to the contacts configuration is discussed.

Figure 7.3 shows one measurement for the MVI with internal pressure of 5×10^{-5} mbar, contact-gas system Cu-N_2, tip-plate configuration of 1 mm radius of the tip (see Figure 5.5) and gap spacing of $d = 0.25$ mm. Before performing the experiment, the MVI was baked out at up to 300 °C. When starting the measurement the ac voltage is adjusted such that measurable field emission current appears. The plate electrode is connected to high ac voltage, whereas the tip electrode is always grounded. Therefore, at positive polarity of the ac voltage, the tip electrode is the cathode and is decisive for the field emission current. At time instant $t = 0$, the arc-polishing circuit is triggered and the HF impulse current flows through the MVI and cleans mainly the tip area of the cathode surface. With the tip-plate configuration, the arc-polishing occurs around a small area on the cathode, where the highest electric field stress will also be present later during high voltage application, i.e. directly on the tip. Thus, the possibility that the HF current during arc-polishing and the field emission current after arc extinction flow from the same cathode area, is high. And, it is more likely that the field emission current originates from the cleaned cathode surface immediately after arc-polishing. **Figure 7.4** shows a photo from the HF arc between the cathode tip area and the anode during arc-polishing.

From Figure 7.3 it is seen that the measured field emission current immediately after arc-polishing is much higher than before. However, the current decays slowly with time as the removed gas molecules re-adsorb on the cathode surface and increase surface work function. The applied voltage across the interrupters remains constant during the measurement.

Figure 7.5 shows another measurement example for the MVI under the same conditions. It is observed that, for the same applied electric field, the field emission current before arc-polishing is much higher than in Figure 7.3. Furthermore, it is seen that the field emission current immediately after arc-polishing is lower than before arc-polishing. The electrode surface condition plays an important role in regard to the changes of the field emission current concerning the sorption process. Applying the HF impulse current to the interrupter on one hand changes the micro-structure of the contact's surface and on the other hand removes the gas layer from the surface and consequently changes its work function. Therefore, it may be possible, that the field emission current immediately after arc-polishing either increases (in 90% of cases) or decreases (observed in only 10% of cases) (compare Figures 7.3 and 7.5).

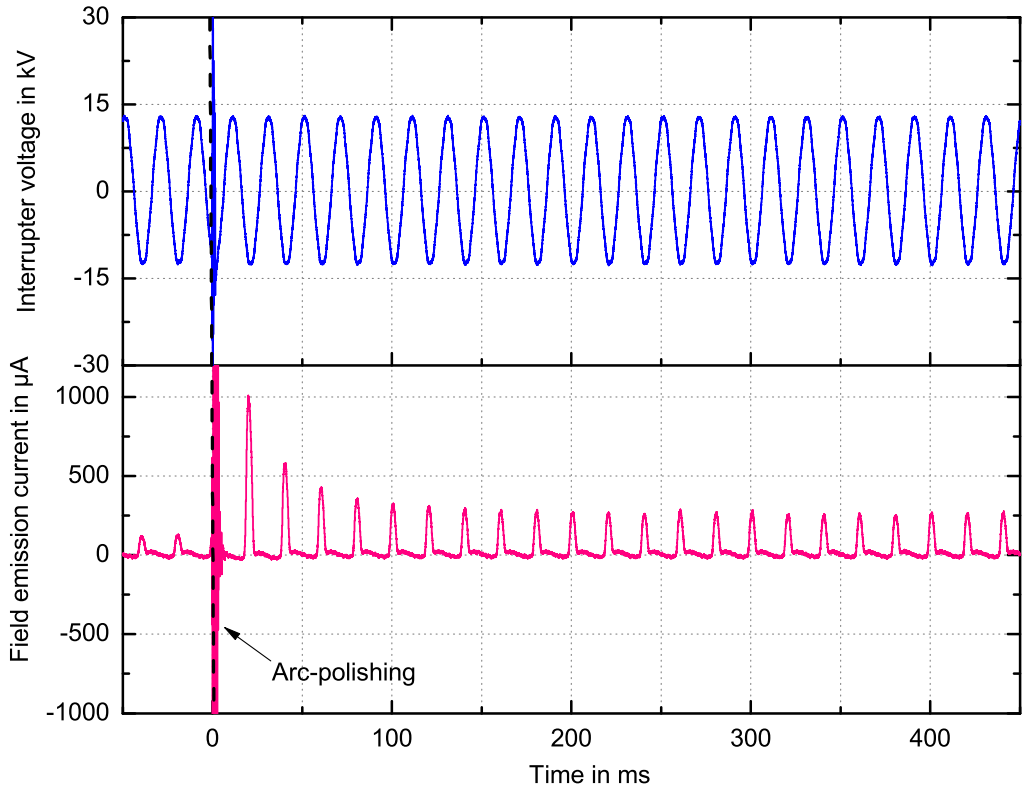

Figure 7.3: Typical waveform of the interrupter voltage (blue curve) and the field emission current (red curve) for the MVI with tip-plate configuration at increased internal pressure of $p = 5 \times 10^{-5}$ mbar

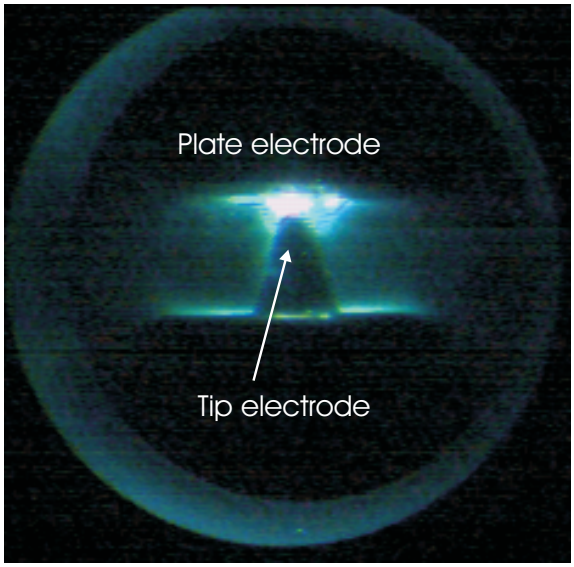

Figure 7.4: HF arc between the cathode tip area and the anode during arc-polishing

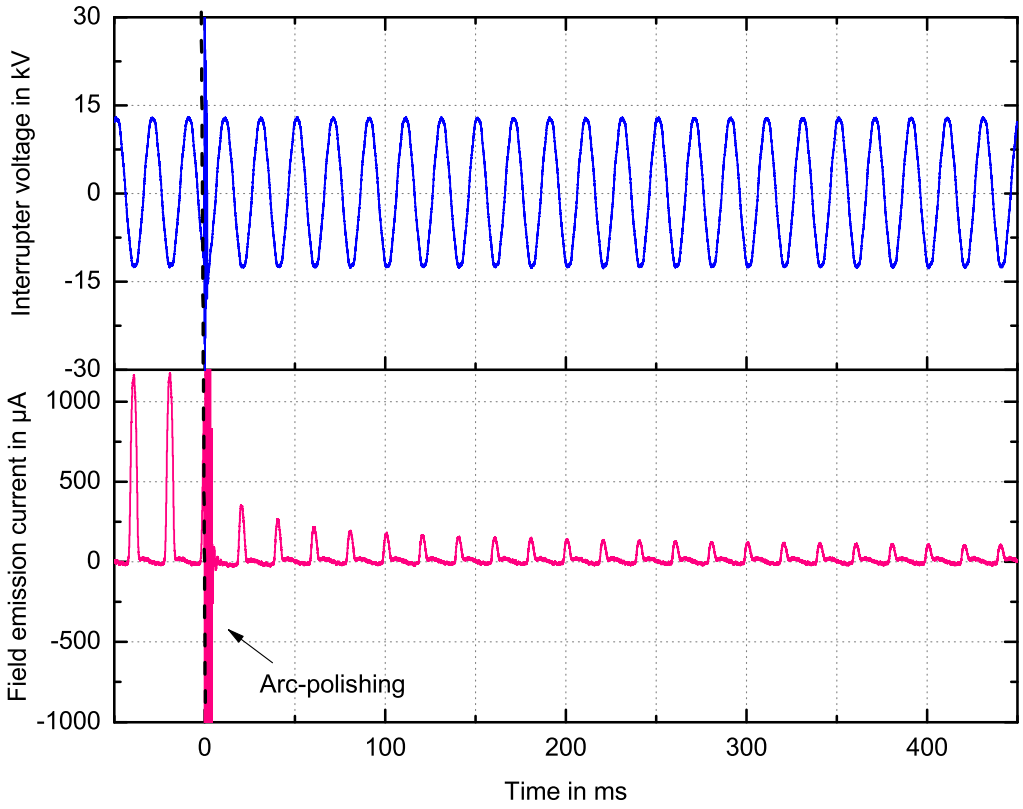

Figure 7.5: Waveform of the interrupter voltage (blue curve) and the field emission current (red curve) for the MVI with tip-plate configuration, where lower field emission current immediately after arc-polishing is observed.

7.3.1 Evaluation of the decay function of the field emission current after arc-polishing

To assess the internal pressure of the interrupter, proper evaluation of the decay function of the field emission current after arc-polishing is necessary. For quantitative analysis of the dependency between internal pressure and the decay of the field emission current, two different methods, each giving two quantities, are applied: decay time constants τ_1 and τ_2 named as "method 1" and time parameters $t_{0.5}$ and $t_{1.2}$ named as "method 2", which follows the proposal by Frontzek and König.

The first method is based on the modeling of the decay function by an exponential trend line. In general, for all measurements, without any exception, it was not possible to model the decay of the field emission current by only one exponential trend line; instead, the decay obviously includes more than one time constant. It is observed that the decay function matched well to double exponential decay function with certain offset. In the second

method, two different time parameters are defined and evaluated. All measurements are analyzed using both methods. The measurement duration was chosen as four seconds for proper evaluation of the decay time.

In the following, both methods are described on the basis of one measurement example for the MVI with internal pressure of 10^{-5} mbar, contact-gas system Cu-N_2, tip-plate configuration of 1 mm radius of the tip and gap spacing of $d = 0.5$ mm. **Figure 7.6a** shows this measurement example and Figure 7.6b shows the zoom area. **Figures 7.7** and **7.8** show the principle of both methods for this measurement example. The peak value of the field emission current at each cycle after arc-polishing is recorded and plotted versus time in these depictions (red measurement points).

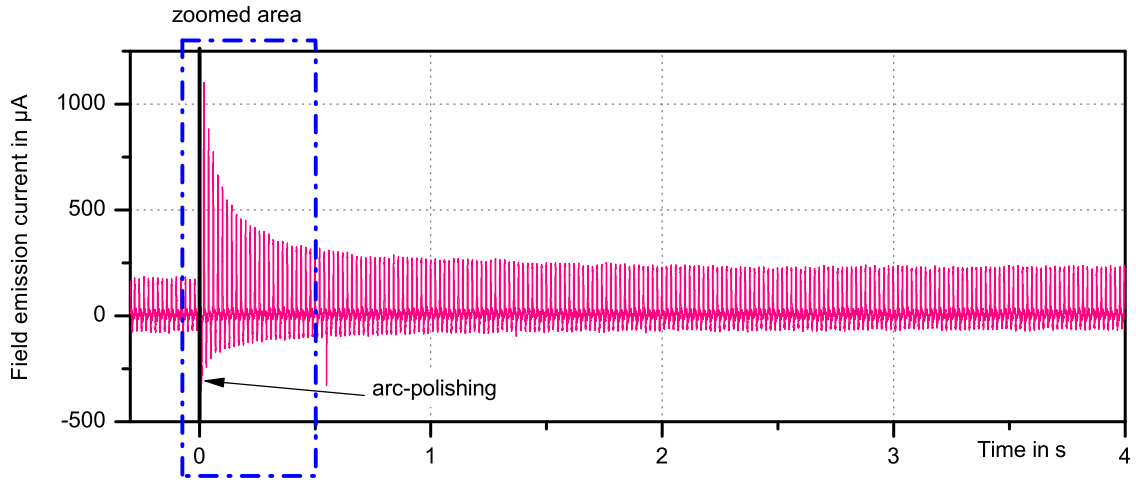

(a)

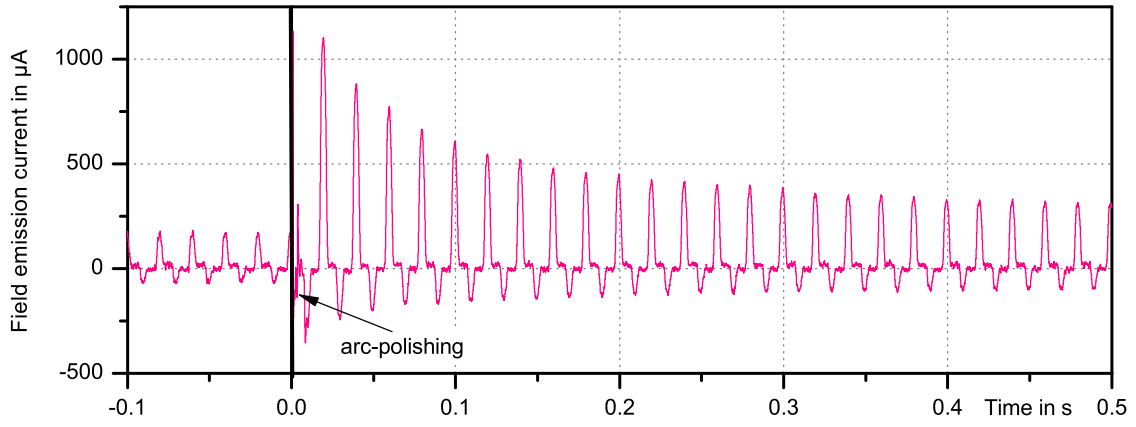

(b)

Figure 7.6: Measurement example for the evaluations of the decay time constants. a) whole measurement b) zoomed area

In the first method, shown in Figure 7.7, the measurement points (red points) are matched to trend line y (green curve), which is a double exponential decay function with offset. The formula of this trend line is shown below:

$$y = y_0 + \text{exp1} + \text{exp2} \tag{7.1}$$

$$\text{exp1} = A_1 \cdot \mathrm{e}^{-t/\tau_1} \tag{7.2}$$

$$\text{exp2} = A_2 \cdot \mathrm{e}^{-t/\tau_2} \tag{7.3}$$

where y_0 is the offset of the function shown in blue (stabilized value of the field emission current), exp1 is the fast exponential function (lilac curve) with time constant τ_1 and amplitude of A_1 and exp2 is the slow exponential function (brown curve) with time constant of τ_2 and amplitude of A_2. These values are calculated for the measurement example of Figure 7.6, and the resulting trend line is given as:

$$y = 0.24 + 0.80 \cdot \mathrm{e}^{-t/55.6\text{ms}} + 0.23 \cdot \mathrm{e}^{-t/272.7\text{ms}} \tag{7.4}$$

The two time constants τ_1 and τ_2 of this double exponential decay function are evaluated for each measurement for further analysis (see 7.3.2).

In the second method, shown in Figure 7.8, two time parameters $t_{0.5}$ and $t_{1.2}$ for the evaluation of the decay function of the field emission current are defined as proposed by Frontzek and König. The red points show again the measurement points (peak value of the field emission current at each cycle). The time parameter $t_{0.5}$ is defined as the time interval between the end of arc-polishing and the moment, when the field emission current has decayed to 50% of its initial value ($i_{\mathrm{F},50\%}$). Time parameter $t_{1.2}$ is defined as the time interval between the end of arc-polishing and the moment, when the field emission current has decayed to a value that equals factor 1.2 multiplied by the stabilized value of field emission current ($1.2 \times i_{\mathrm{F,\,stab}}$). These time parameters $t_{0.5}$ and $t_{1.2}$ as well as decay time constants τ_1 and τ_2 are calculated for different internal pressures in semi vacuum range for every measurement.

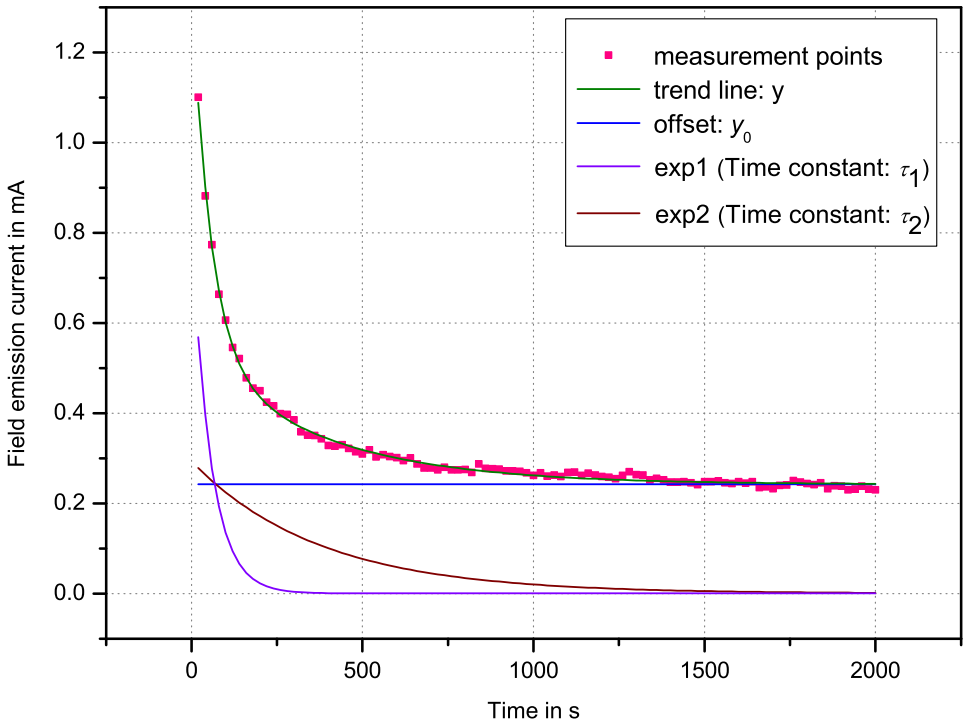

Figure 7.7: Decay time constants τ_1 and τ_2 according to the trend line with double exponential decay function

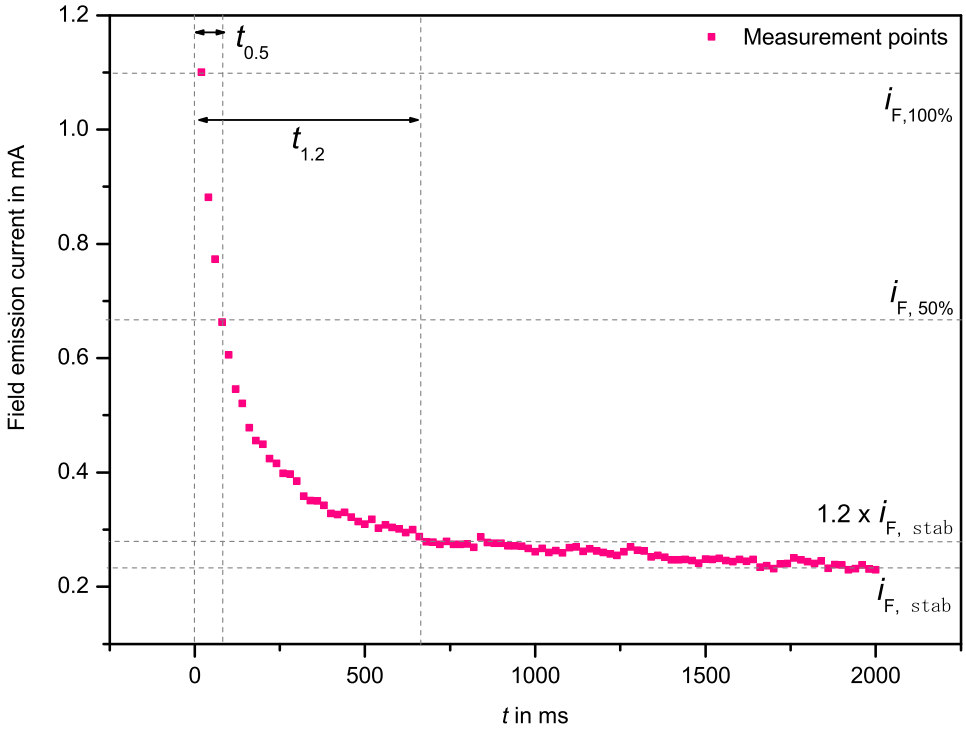

Figure 7.8: Definition of time parameters $t_{0.5}$ and $t_{1.2}$

7.3.2 Impact of the interrupter internal pressure on the decay function of the field emission current

For statistical analysis, twenty measurements according to FEA method are performed on the MVI with tip-plate configuration at each pressure level: 10^{-5} mbar, 5×10^{-5} mbar and 10^{-4} mbar. During the measurements, other parameters (contact material, gas type, gap distance, arc-polishing parameters, electric field stress) are kept constant. Thereafter, time parameters $t_{0.5}$ and $t_{1.2}$ as well as decay time constants τ_1 and τ_2 are calculated and compared. **Figures 7.9** and **7.10** show the calculated mean value of these quantities and their maximum and minimum values from twenty measurements at each pressure level.

Each Figure (7.9, 7.10) also includes the calculated formation time of a mono molecular air layer on a metal surface at approximately room temperatures $T \approx 300\,\mathrm{K}$ (dashed line) according to [Wutz 00]. This formation time t_{mono} is inversely proportional to the pressure:

$$t_{mono}/\mathrm{s} \approx \frac{3.6 \times 10^{-6}}{p/\mathrm{mbar}} \tag{7.5}$$

Comparing the results of Figures 7.9 and 7.10 with the formation time t_{mono}, the decay time constant τ_2 is considered more representative for the re-adsorption process. It is seen, that increase of internal pressure results in smaller τ_2. At higher pressures, the gas molecules are faster re-adsorbed on the metal surface, causing a faster change of the field emission current and consequently a smaller time constant. The deviation from the mean values is nevertheless rather high, which even results in overlapping of the measured values for different pressures.

Figure 7.11 shows measured values of the decay time constant τ_2 (twenty measurements at each pressure level). It is seen that at certain pressure level the time constant τ_2 changes arbitrarily. Therefore, performing a single measurement is not enough to evaluate the internal pressure. Twenty or even more measurements would be necessary. Change of the electrode's surface from the microscopic point of view during field emission current flow after arc-polishing may be the reason for this large stray.

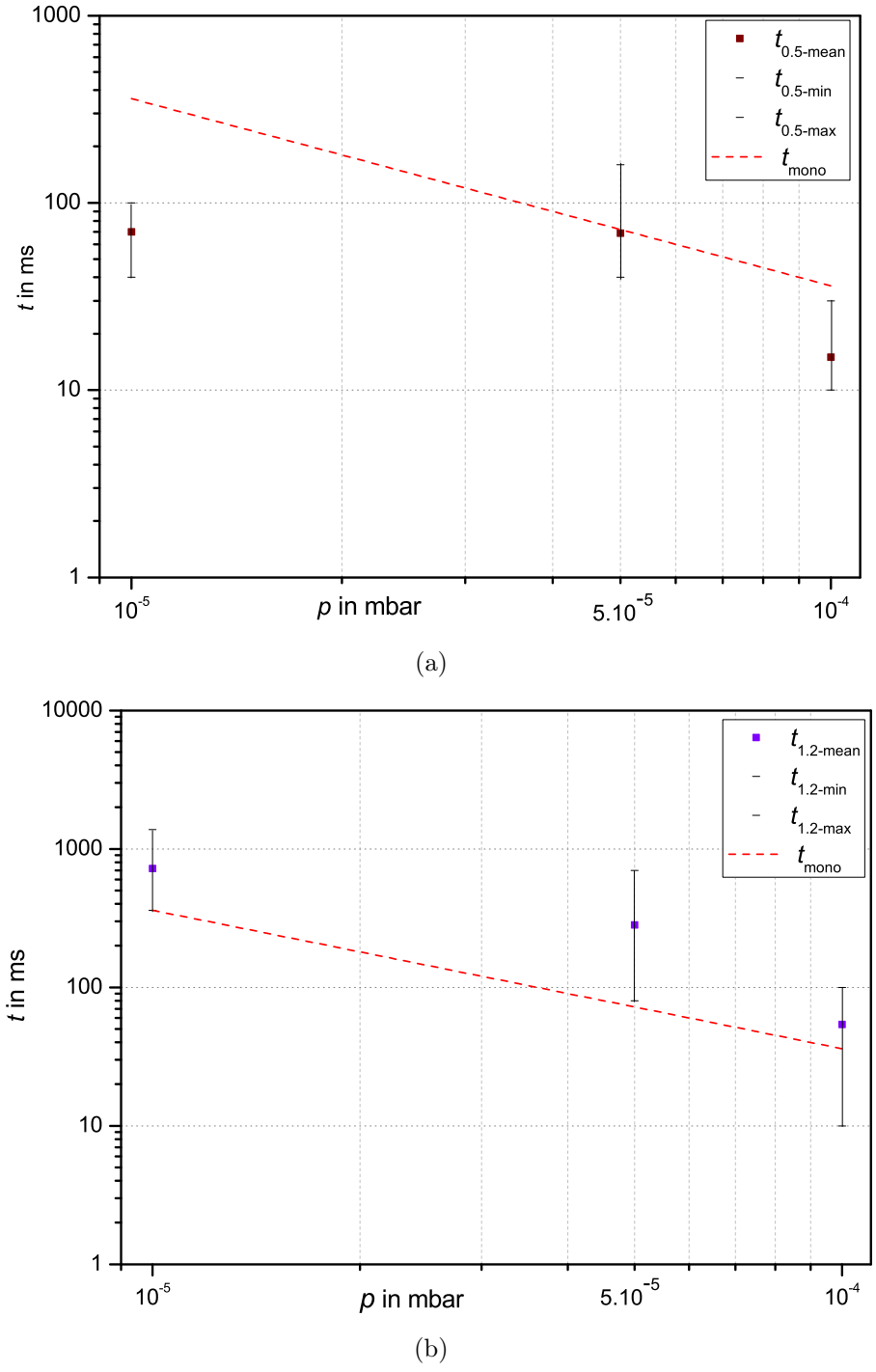

Figure 7.9: Mean value, maximum and minimum of the decay time parameters according to method 2 for the measurements on MVI (Tip-plate configuration, Cu-N_2). a) $t_{0.5}$ b) $t_{1.2}$

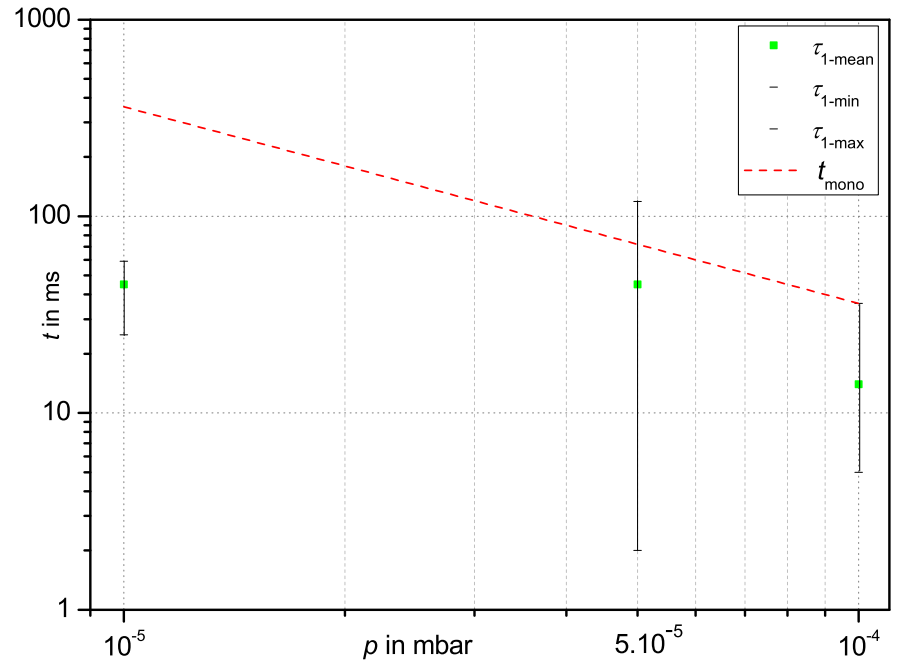

(a)

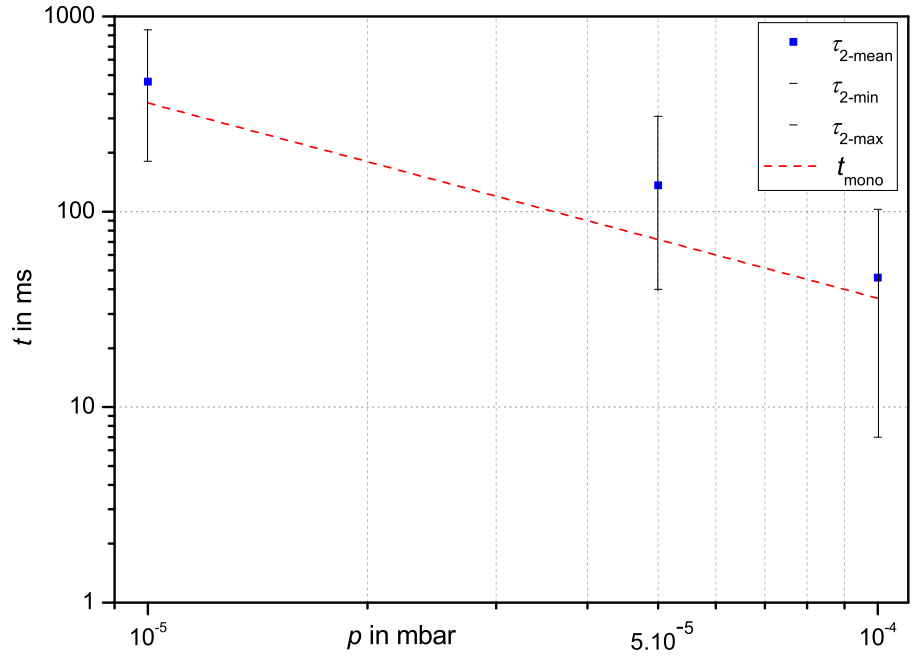

(b)

Figure 7.10: Mean value, maximum and minimum of the decay time constants according to method 1 for the measurements on MVI (Tip-plate configuration, Cu-N_2). a) τ_1 b) τ_2

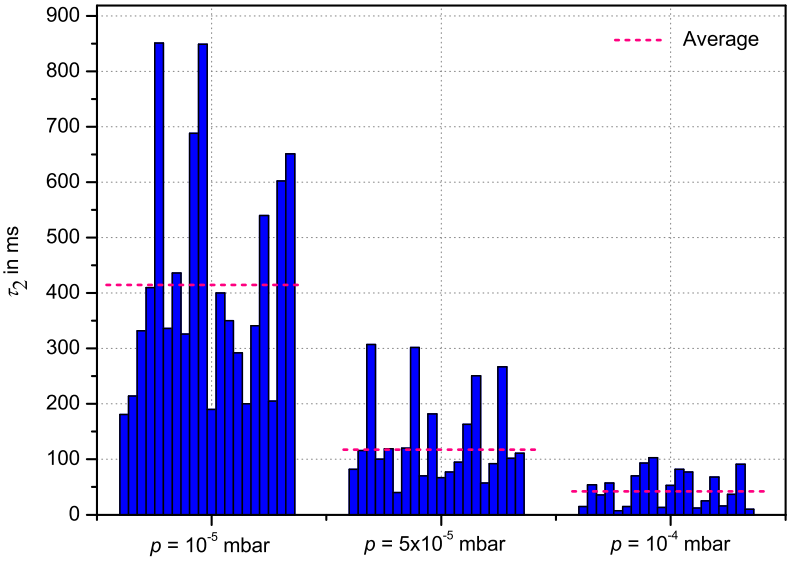

Figure 7.11: Measured values of the decay time constant τ_2 for three different pressure levels between 10^{-5}mbar and 10^{-4}mbar (twenty measurements at each level). Red dashed line: average of twenty measurements, Tip-plate configuration, Cu-N_2 system

7.3.3 Measurement reproducibility

From the discussions above, it is concluded, that the FEA method is applicable for internal pressure evaluation of the MVI with tip-plate configuration in semi-vacuum range. The measurements are performed for Cu-N_2 and Cu-O_2 systems, where for both systems an inverse dependency between the decay time constant τ_2 and the internal pressure is found. Nevertheless, an adequate number of measurements (at least twenty) must be performed for correct evaluation of the internal pressure.

It is important to mention that the decay of the field emission current is not observed in every measurement. Thus, more measurements have to be carried out to obtain at least twenty results, where the decay is clearly visible (reproducible measurements). High reproducibility of the measurements is of great importance, otherwise a large number of measurements is required.

For the tip-plate configuration, in 85% of all cases the field emission current decays with time (85% reproducibility), otherwise the current stays constant or a breakdown inside the interrupter after arc-polishing occurs, which changes the surface condition (micro-structure and gas layer).

The decay of the field emission current is observable only when the field emission current

originates from a micro-emitter, which has been cleaned during arc-polishing. For the tip-plate configuration with tip radius of 1 mm, it is nearly assured that this condition is fulfilled. Therefore the high reproducibility (85%) is obtained.

In order to complement the validation measurements, further investigations with the MVI but plate-plate configuration, which is closer to the configuration of a commercial interrupter, are performed. In this regard four different contact-gas systems are investigated:

- Cu-N_2
- Cu-O_2
- CuCr-N_2
- CuCr-O_2

The yield in terms of visible decays of field emission current after arc-polishing is much lower than in case of the tip-plate configuration: in only about 5% of all cases the effect could be observed. This is obviously independent from the type of gas or contact material. For the plate-plate configuration the probability to have the arc and field emission flow from the same position on the electrode surface is lower and therefore the reproducibility is too low. For this configuration in most cases, the measured current stays constant for several hundred milliseconds after arc-polishing. This indicates that the field emission current after arc-polishing originates from an unpolished cathode area, so that no re-adsorption process takes place on its surface. Therefore, work function of the emitting area and consequently the field emission current remains constant.

With such a low measurement reproducibility, it is obvious that an extremely high number of measurements must be carried out (about 400 measurements) in order to be able to evaluate the internal pressure, which is totally unrealistic for commercial application of the FEA method. Moreover, with such a high number of measurements, there is a risk of changing the cathode surface condition, which may again interfere the results.

7.4 Measurement results on the commercial interrupters

Different commercial interrupters of different types with increased internal pressures up to 10^{-3} mbar as well as reference interrupters with a pressure of about 10^{-7} mbar are investigated. **Figure 7.12** shows, as an example representative for many other measurements on

a bigger lot of interrupters, different measurements on a commercial vacuum interrupter with an intentionally increased internal pressure of 10^{-5} mbar. Arc-polishing is performed by HF impulse currents as explained earlier. It takes place at time $t = 0$. A decay of the field emission current after extinction of the arc, as can be seen in Figure 7.12a, occurs in only 3% of all cases. In other cases, some instabilities in the interrupter (breakdowns or micro-discharges) can be observed (Figure 7.12c) or the current stays constant after arc-polishing (Figure 7.12b).

From Figure 7.12 it is observed, that in contrast to MVI with tip-plate configuration the field emission current flows in both directions. However, the field emission current is still asymmetric due to the unequal contact surface conditions from the microscopic point of view.

The instabilities observed during the measurements (Figure 7.12c) are referred to the arc energy input, which may disturb the contact surface condition or generate micro-particles and consequently result in a micro-discharge or even a full breakdown. This event is less observed on the MVI with tip-plate configuration, as for this interrupter low energy arcs (see 7.2) are sufficient for an effective arc-polishing effect and reproducible measurement results. For commercial interrupters, low energy arcs result in constant field emission current (Figure 7.12b) in most cases, whereas higher energy arcs mostly result in instabilities in the interrupter (Figure 7.12c)

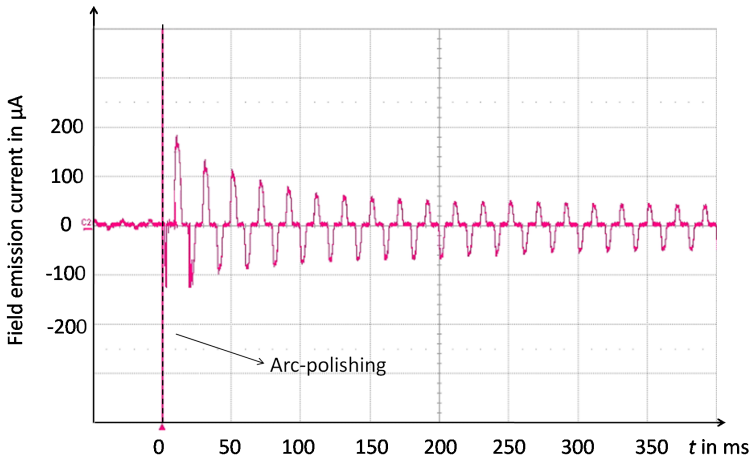

(a)

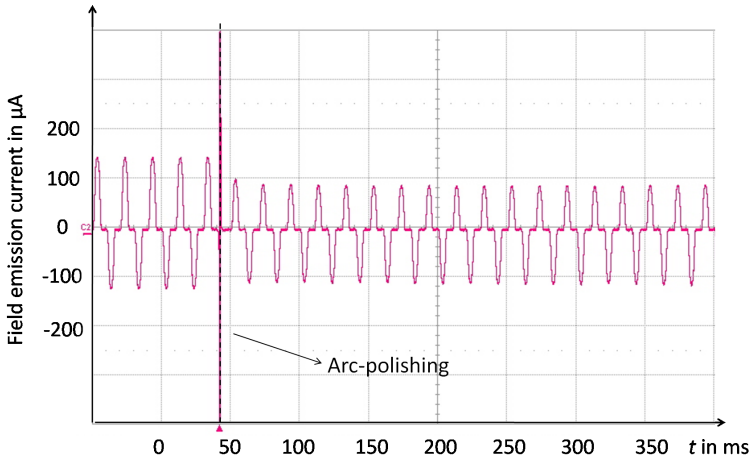

(b)

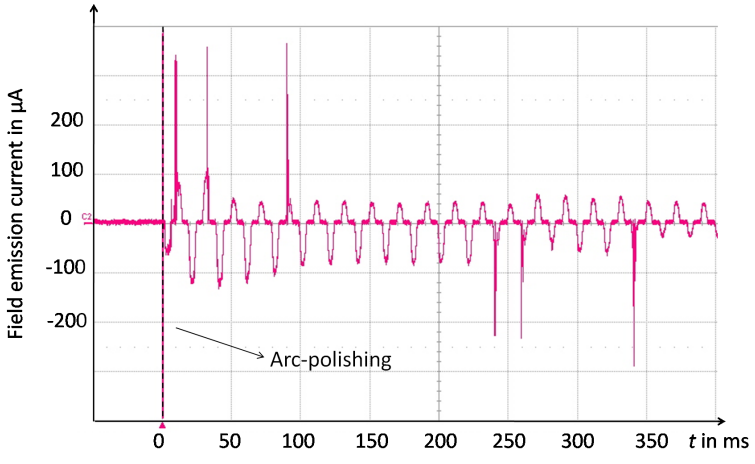

(c)

Figure 7.12: Typical waveforms of the field emission current before and after arc-polishing for commercial interrupters at increased internal pressure

7.4.1 Measurement reproducibility

Because of the low reproducibility (only 3%) of the current decay after arc-polishing, it is not possible to evaluate the results and derive the internal pressure from the decay time constant. Following explanation of this finding is suggested: The arc that appears between the contacts should have enough energy to desorb the gas molecules from the surface on one hand; on the other hand, it should not destroy the contact surface. Therefore, it is rather difficult to determine a general, optimum arc-polishing current which, in combination with the applied alternating voltage, will not result in electrical discharges during the re-adsorption period of the gas layer. It is also necessary that the arc-polishing (removing of the gas molecules from the contact surface) takes place on the same area, where later on the field emission current flows. Otherwise, field emission current would flow from an unpolished cathode area, and thus no change in the emission current will be observable. This, in consequence, means that on a plate electrode surface it will be just a matter of statistics if the effect of interest can be observed or not. As vacuum interrupters do have plate-like electrode surfaces this would basically disqualify the investigated method for the intended purpose of an on-site diagnostic tool.

7.5 Conclusion

It can be summarized that for commercially available vacuum interrupters it is not possible to define a test method or any test parameter configuration in the chosen method, respectively, which would reproducibly cause a decay of the field emission current after arc-polishing. In only 3% (commercial interrupters) and 5% (MVI with plate-plate electrodes) of all cases the effect of the decay of field emission current could be observed. This also supports that no other parameters (special electrode geometries of the investigated industrial interrupterss; differences between AMF and RMF contacts) might have been the reason for the missing effect on commercial interrupters.

It is recognized that the yield is much higher for inhomogeneous electrode configurations where the locations of arc-polishing and the origin of the subsequent field emission current are more likely the same. But even in the investigated extreme case of a tip-plate electrode, the effect would occur in only 85% of all cases. For this special configuration, evaluation of the internal pressure with regard to the decay time constant of the field emission current τ_2 in semi vacuum range is statistically applicable. Regarding further that due to the wide stray of the decisive decay time constant τ_2 at least twenty successful measurements are required for a statistically reliable evaluation (meaning that on a commercial interrupter

700 trials would be necessary which is a totally unacceptable value), the investigated method has quite obviously no practical meaning for monitoring purposes. Though the effects that were published earlier are basically present, the reproducibility is too low, in a degree that the method cannot be used as an on-site diagnostic tool.

8 Investigations on ICS - Determination of field emission current after capacitive switching

For more detailed information on the behavior of vacuum interrupters during their dielectric recovery, measurement of field emission current after interruption of capacitive loads is performed both in an experimental circuit in the high-voltage lab (setup "a") and in a full-power test-circuit in a power lab (setup "b"). For these measurements, a special measurement system (DRS) comprising a low-inductive shunt resistor protected by gas-discharge arresters and anti-parallel power diodes as explained in 5.1 is developed. As the current through the interrupter during recovery voltage application contains a capacitive component due to the interrupter's stray capacitance, this component must be compensated. Different online and offline compensation methods for different applications are developed[1]. In the following the measured pure field emission current is validated according to the FNE. Furthermore, the two compensation methods (hardware and software processing) are compared with each other.

8.1 Measurements correlation with FNE

Figure 8.1 shows a measurement example using experimental circuit setup "a". The measurement is performed on a commercial vacuum interrupter of $V_\mathrm{r} = 17.5\,\mathrm{kV}$ rated voltage and a rated gap spacing of $d_\mathrm{r} = 8\,\mathrm{mm}$. Compensation of the capacitive component is done here using the hardware processing. The contacts start to separate at time point t_0. The breaking current flows further through the arc until current zero crossing (t_1).

[1]Software compensation is developed by the project partner (KEMA)

After current interruption, recovery voltage appears immediately across the interrupter and increases slowly in form of a $\{1 - \cos(\omega t)\}$ function ($\omega = 2\pi \cdot 50$ Hz). The field emission current can be measured correlated to the recovery voltage. The voltage drop across the shunt resistor (red curve) before zero crossing is equal to the limiting voltages of the diodes and is of no interest here.

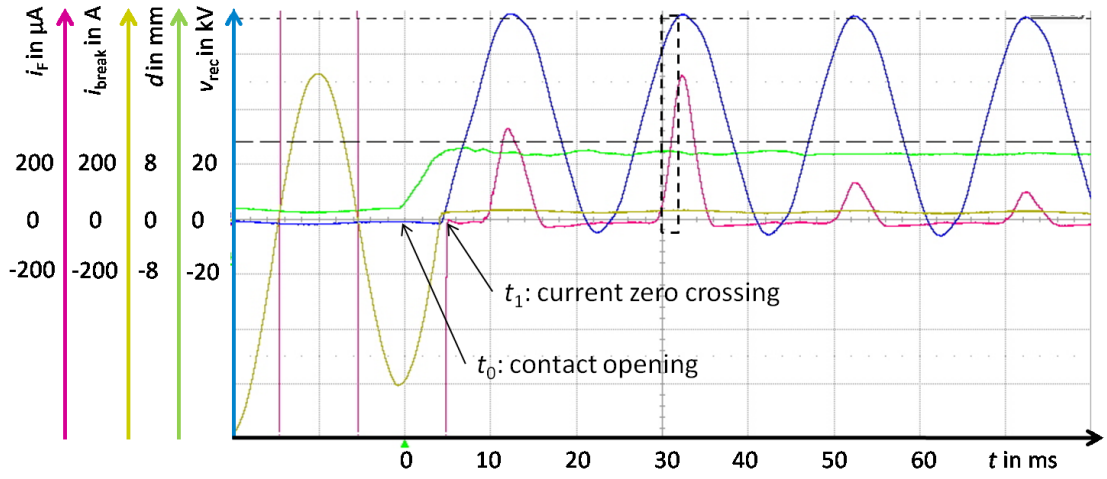

Figure 8.1: Measurement example of experimental setup "a" with hardware compensation. Recovery voltage v_{rec} in blue, field emission current i_{F} in red, 50 Hz breaking current i_{break} in yellow and gap spacing d in green

As explained in 6.1, there is an exponential dependency between the gap voltage and the corresponding field emission current. Therefore, drawing the voltage-current-characteristic of the gap in the form of the FNP gives a linear relationship. **Figure 8.2a** shows the current-voltage-characteristic of the gap in exponential form, and Figure 8.2b shows the FNP for the selected area in Figure 8.1 as a representative example. As is observed, the FNP gives a straight line. Using the slope of the line and its intersection with the y-axis (constant surface work function is assumed), the surface parameters are calculated as:

- field enhancement factor $\beta = 684$
- emitting area $A_{\text{e}} = 2 \times 10^{-15}$ m^2

This analysis is performed, after every measurement for each cycle of the recovery voltage, to check the voltage-current-characteristic of the gap according to the FNE and to evaluate the surface parameters.

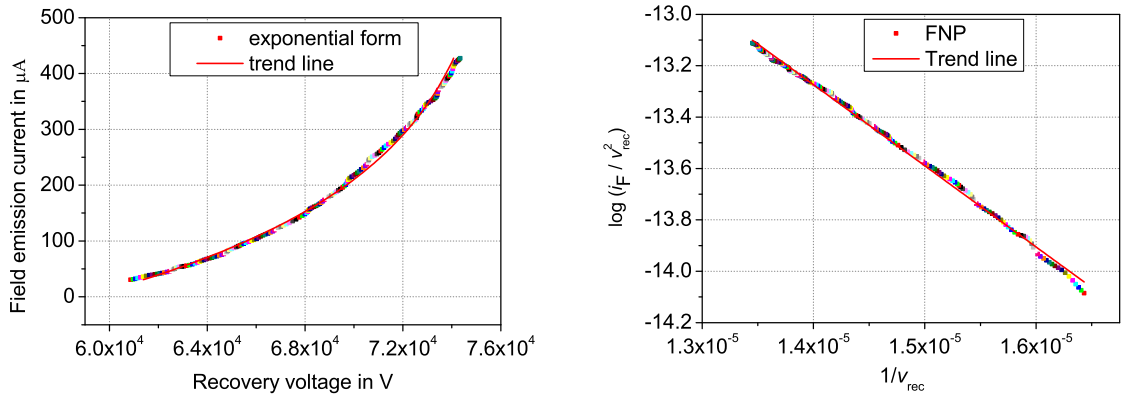

(a) (b)

Figure 8.2: Current-voltage-characteristic of the vacuum gap for the selected area shown in Figure 8.1 during dielectric recovery of the interrupter. a: exponential form b: FNP

8.2 Comparison of the software and the hardware compensation methods

Due to electromagnetic compatibility issues in the actual surrounding of the interrupter and due to the fact that the interrupter is on floating potential, for some applications it is advisable to use the software compensation processing. The software compensation is an offline compensation contrary to the hardware compensation. The principle of both compensation methods are explained in detail in 5.1.1. Here, a comparison of the outcomes of both methods based on a same measurement example is given.

To compare hardware and software compensation, measurements are performed using setup "a". For this purpose, field emission current is measured directly with hardware compensation (electronic), and the total current (sum of field emission and capacitive current) is also recorded and compensated later by the software tool. **Figure 8.3** shows an oscillogram of such measurements. Amplitude of the applied recovery voltage is 90 kV, and the contact gap spacing is 4 mm. It is seen that at every peak of the recovery voltage the value of the field emission current is equal to the measured total current. This has to be the case as the capacitive current component is zero whenever the voltage reaches its peak.

With the help of the software method, the capacitive component of the total current is compensated. **Figure 8.4** compares the results of hardware and software processing for this measurement. It is seen that both curves match perfectly in regions where field emission current is expected to flow. In regions where field emission current is expectedly

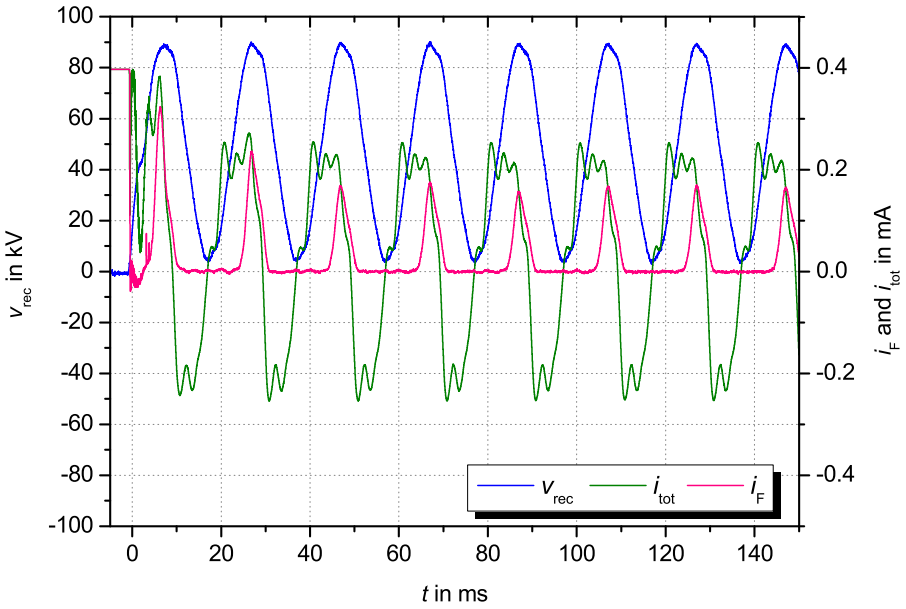

Figure 8.3: Wave shapes of the recovery voltage (blue curve), field emission current (hardware compensated, red curve) and total current (green curve), used for the comparison of hardware and software compensation methods

zero (due to low electrical field) the software compensated signal is superimposed by some noise (few microamperes). This noise is not disturbing, since the evaluation of surface parameters (β and A_e) according to the FNE can only be performed at sufficient high field emission current. For both methods, the surface parameters at each rise and fall of the field emission current during recovery phase is calculated. As an example, **Figure 8.5** shows the FNP for the selected area in Figure 8.4. Each plot contains 4 kilo-samples. The surface parameters for this example are calculated as:

- By hardware compensation:
  - Field enhancement factor $\beta = 308$
  - Emitting area $A_e = 5.33 \times 10^{-16}\ \mathrm{m}^2$
- By software compensation:
  - Field enhancement factor $\beta = 299$
  - Emitting area $A_e = 5.65 \times 10^{-16}\ \mathrm{m}^2$

It is observed that the FNPs for hardware and software processing are in very close agreement. The surface parameters β and A_e for the two methods are also nearly the same and

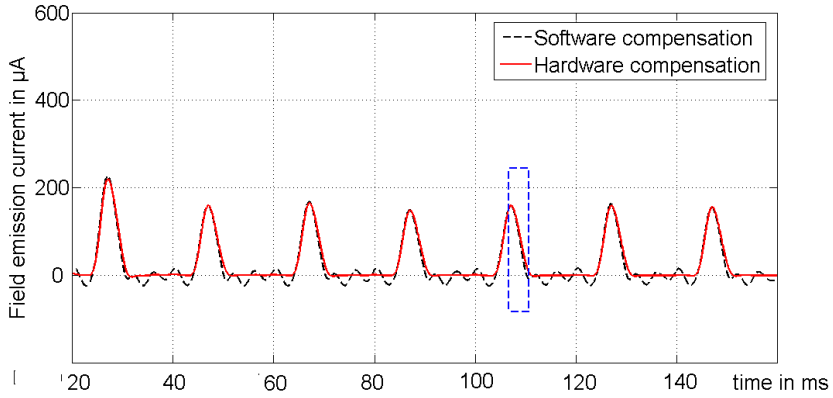

Figure 8.4: Comparison of the results of hardware and software methods for measurement example shown in Figure 8.3. FNP for the selected area (dashed blue line) is shown in Figure 8.5.

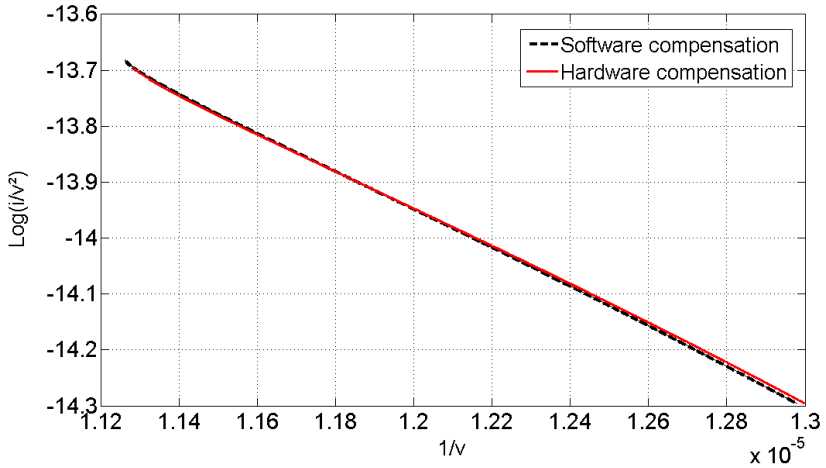

Figure 8.5: FNP for the selected area in Figure 8.4

differ by only 3% and 6%, respectively. It is thus possible and appropriate to use the software tool rather than the hardware compensation in surroundings of high electromagnetic interferences like in a power lab.

9 Investigations on ICS - Dielectric behavior of vacuum interrupters after capacitive switching

To understand the relation between field emission current and dielectric breakdowns during recovery phase, field emission current measurements are performed immediately after current interruption. In this context, various commercial interrupters as well as non-regular interrupters, each having a certain process modification (as introduced in 5.3.1), are investigated. The effect of the power-frequency arc, particularly its amplitude and duration (arcing time), on the field emission characteristic of the interrupter after current interruption is studied. Furthermore, the impact of pre-arcing, the number of making operations and the amplitude of the inrush current on the contact surface condition is investigated. In the following, the testing procedures are introduced, and finally the results of the investigations are presented.

9.1 Testing procedures

During the investigations, three different testing procedures are applied. In each procedure, field emission current as well as dielectric breakdowns during the recovery phase are recorded.

Procedure 1

This procedure is applied in the full-power test-circuit (setup "b"). It consists of three phases:

1. Energizing of the capacitive load: making operation under HF inrush current with amplitude of several kiloamperes to a few ten kiloamperes and frequency of a few kilohertz (pre-arcing during contact closing)

2. Interruption of the capacitive load: subsequent contact opening during power-frequency breaking current with amplitude of a few hundred amperes (arcing during contact opening)

3. Dielectric recovery: immediate application of the power-frequency recovery voltage with $\{1-\cos(\omega t)\}$ function after current zero. The amplitude of the recovery voltage in most cases is $\hat{v}_{\mathrm{rec}} = 82\,\mathrm{kV}$ (standard value for 36 kV breaker [IEC6 08]), whereas in some cases a higher recovery voltage of up to 115 kV is also applied. The duration of recovery voltage application is 300 ms.

Figure 9.1 shows the principle of this testing procedure.

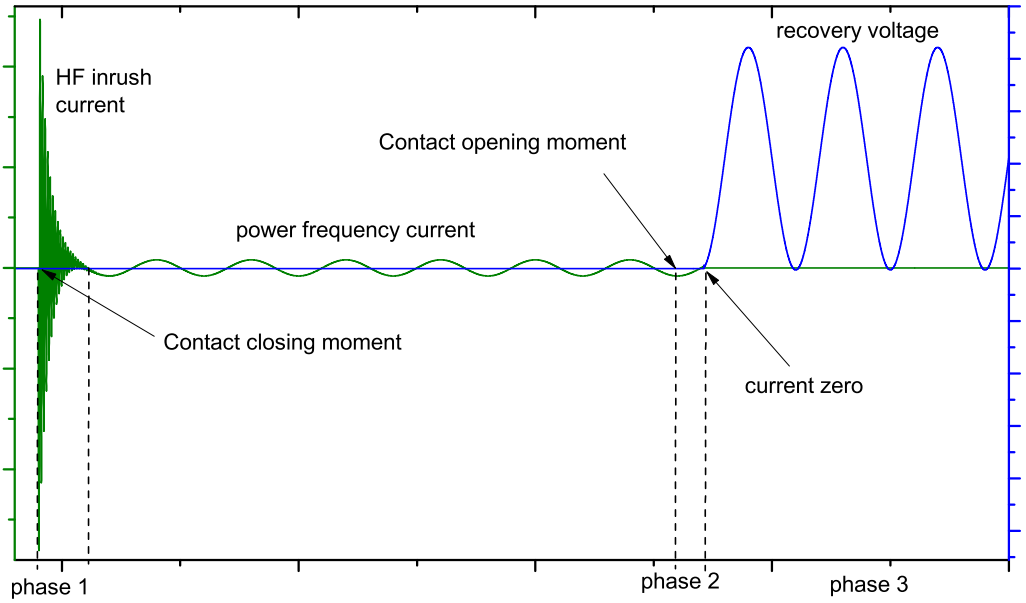

Figure 9.1: Testing procedure 1. Phase 1: inrush current flow, phase 2: power-frequency breaking current flow, phase 3: recovery voltage application

Procedure 2

This procedure is applied in the experimental circuit setup "a". It consists of thirty capacitive current interruptions without pre-arcing (closing at no load). The power-frequency breaking current is in the range of a few ten amperes to several hundred amperes with the duration of 80 ms.

With this testing procedure (as well as testing procedure 3) different interrupters, mounted in two VCBs with rated voltages of 17.5 kV and 24 kV, are investigated. As during tests with recovery voltage standard value, no dielectric breakdown is observed for any of the test samples, it was decided to test with an increased recovery voltage of $\hat{v}_{\mathrm{rec}} = (70 \cdots 90)$ kV. Further increase in voltage was not possible due to the limited external dielectric strength of the interrupters.

Procedure 3: (10×10)-measurement

This procedure is also applied in the experimental circuit setup "a". It includes ten test series, where each test series consists of ten capacitive current interruptions without pre-arcing. Before each test series, the interrupter is subjected to making operations under HF inrush current.

The number of making operations applied before each test series is varied between one, three and six operations. The amplitude of the inrush current is in the range of several kiloamperes and its frequency is in the range of a few kilohertz. Power-frequency breaking current and applied recovery voltage are the same as in procedure 2.

Figure 9.2 shows an example of the (10×10)-measurement result on interrupter type "A". Each curve represents one test series including one making operation at 6 kA, 1.5 kHz inrush current and subsequently ten capacitive current interruptions (20 A) with closing at no load. The peak of recovery voltage in all 100 measurements is $\hat{v}_{\mathrm{rec}} = 75$ kV. Each point in the curves shows the maximum of field emission current measured during recovery after one single interruption. Among 100 measurements, no dielectric breakdown is observed on this commercial vacuum interrupter.

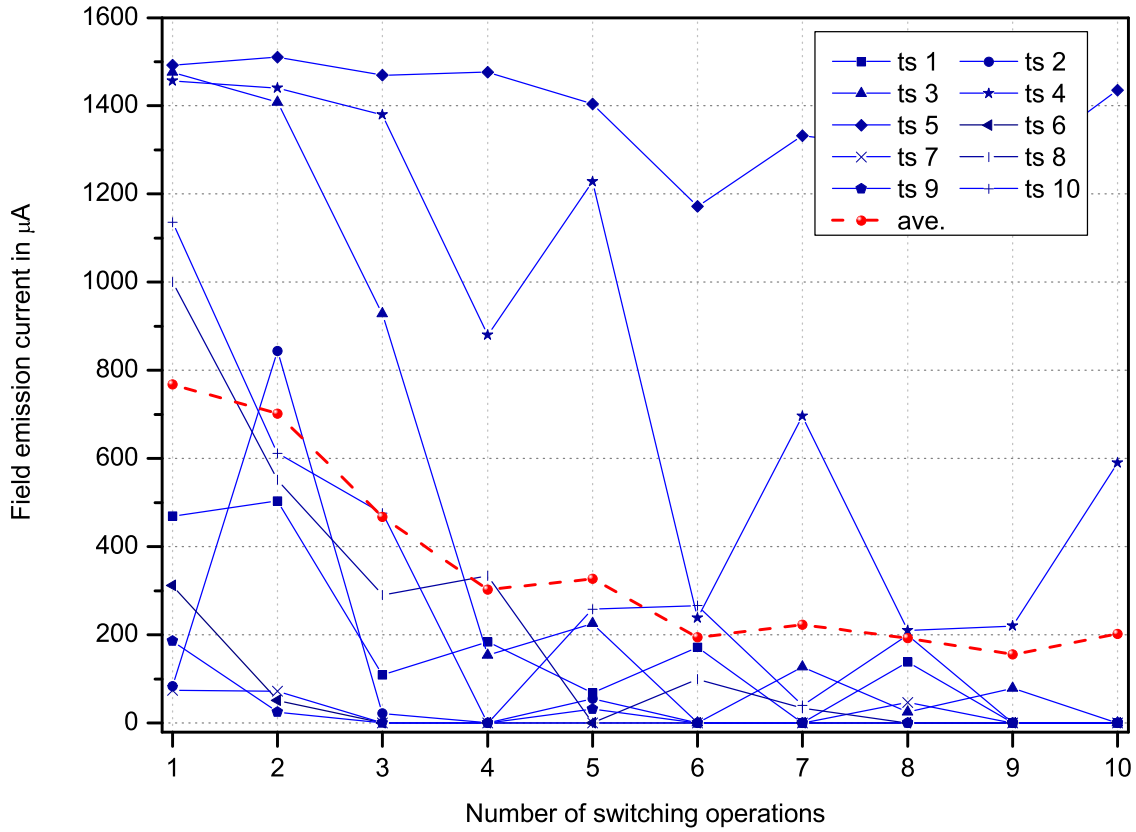

Figure 9.2: Example of a (10 × 10)-measurement (procedure 3) on interrupter type "A". Each blue curve represents one test series (ts). The red, dashed curve is the average of all ten curves.

9.2 Impact of inrush current on field emission characteristics after current interruption

As is discussed in 4.2, during making operation by closing the contacts, the electric field stress between the contacts rises. At a certain gap spacing, the gap can no longer withstand the electrical stress and a pre-strike between the contacts occurs. From this moment on until the first contacts touch, the inrush current flows in the form of pre-arcing. Due to the arc's energy input to the contacts, the contact surfaces melt locally. This may lead to contact welding after closing. These welds will be broken during the next contact opening and result in new micro-protrusions on the contact surfaces, which may locally cause a higher field enhancement, worse dielectric performance and higher field emission current.

At substantially high inrush current frequency, it is possible that pre-arcing takes several

current cycles until the first contacts touch. Here, at each zero crossing, the current will be interrupted and shortly afterwards the contacts pre-strike again. Depending on the instantaneous value of the gap spacing at each current zero, either immediate pre-strikes or a current-free interval in the beginning may occur. These two cases are shown in **Figure 9.3** (case b and a, respectively).

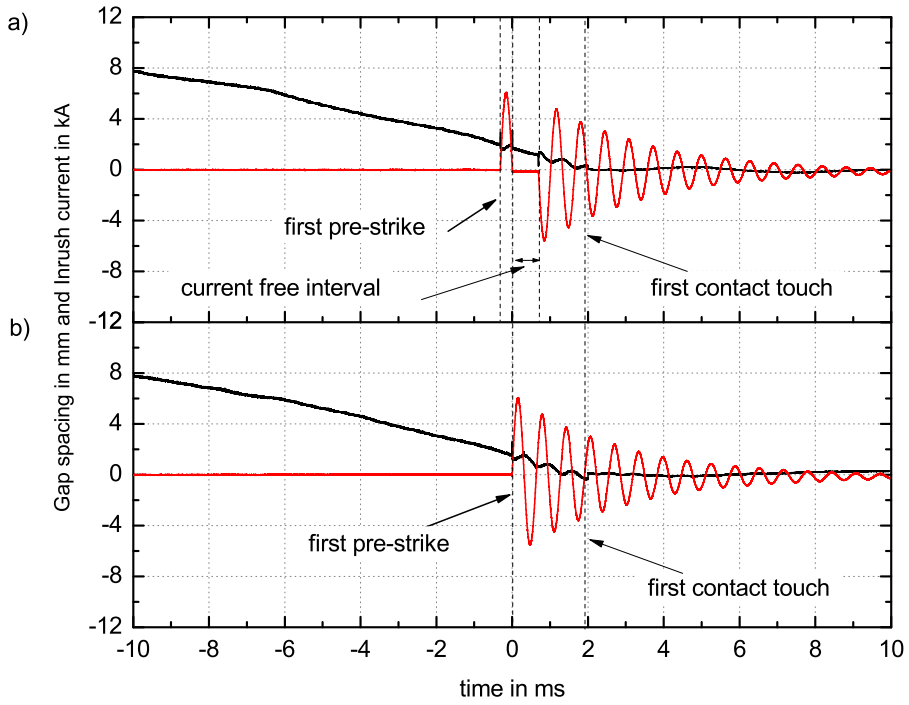

Figure 9.3: Typical waveforms of the inrush current (red curve) and contact gap spacing (black curve) during contact closing. a) with current-free interval, b)without current-free interval

In case a, the first pre-strike occurs at a field stress of $E_{\mathrm{hom}} = 7.5$ kV/mm and a gap spacing of $d_0 = 2$ mm. One half cycle later, the current is interrupted and a current-free interval of 0.8 ms is observed. This interval lasts until a new breakdown occurs (second pre-strike) at smaller gap spacings ($d = 1$ mm in this example). In case b, the first pre-strike occurs at a field stress of $E_{\mathrm{hom}} = 9.4$ kV/mm and a gap spacing of $d_0 = 1.6$ mm. The pre-arcing duration is about $t_{\mathrm{p\text{-}a}} = 1.9$ ms without any current-free interval. Amplitude of the inrush current in both cases is $\hat{i}_{\mathrm{inrush}} = 6$ kA in the first cycle.

During the measurements, it is observed that a current-free interval occurs especially after several closings under inrush current and no-load openings. This is because of higher contact roughness after a no-load opening, which results in pre-strike at larger gap spacings. After a short duration of pre-arcing (surface smoothing), the gap dielectric strength may

increase and the pre-arcing may be interrupted (current free interval). However, at shorter gap distances, the gap breaks down again and the current continues to flow.

Figure 9.4 is an example showing the impact of the inrush current on the field emission characteristic of the interrupter in open position. The closing operation is performed one times under inrush current of $\hat{i}_{\text{inrush}} = 6$ kA and a second times currentless, whereas in both cases the opening operation is carried out at no load condition. It is seen that applying an ac voltage of $\hat{v}_{\text{vac}} = 40\,\text{kV}$ across the interrupter in open position ($d = 8\,\text{mm}$) results in field emission current of a few ten microamperes after closing operation under $\hat{i}_{\text{inrush}} = 6\text{kA}$ (red curve). For the other case (no load closing), no measurable field emission current is observed (green curve). This shows that contact welding at no load closing is less pronounced.

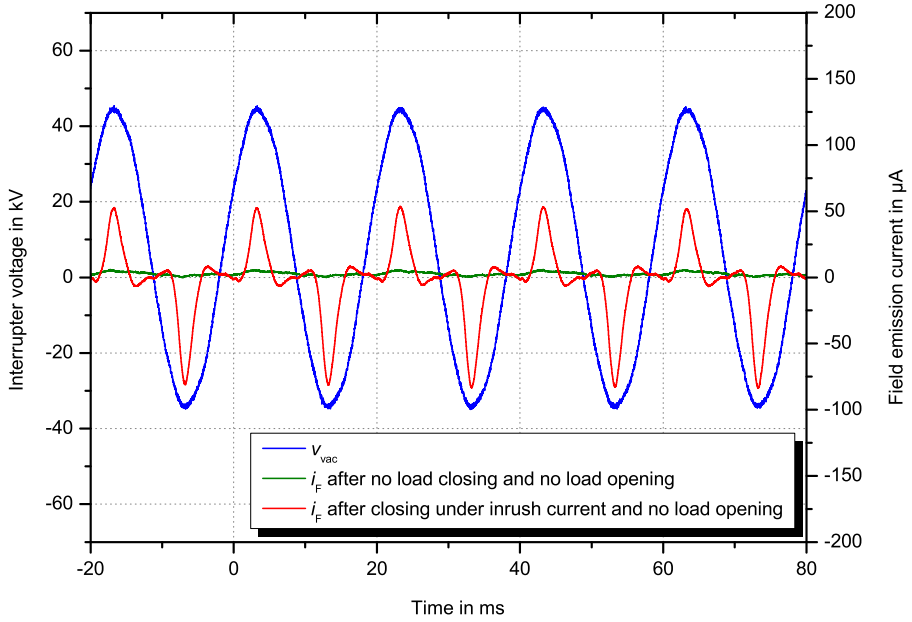

Figure 9.4: Example showing the impact of pre-arcing on the field emission characteristic. Interrupter voltage in blue, field emission current after inrush current of $\hat{i}_{\text{inrush}} = 6\,\text{kA}$ in red, field emission current after no load closing in green

To study the impact of pre-arcing on the field emission current during recovery and consequently on the contact surface parameters (β and A_{e}), amplitude of the inrush currents as well as the number of making operations are varied, and for each condition the (10×10)-measurement is performed. These investigations are performed on one interrupter of type "A".

Amplitude of the recovery voltage is 75 kV, and the breaking current is 20 A. **Figure 9.5** shows the field emission current average curves of (10×10)-measurements, and **Figure 9.6**

shows the average values of field emission current for the following making operations:

- A: $\hat{i}_{\text{inrush}} = 6\,\text{kA}$; 1 making operation
- B: $\hat{i}_{\text{inrush}} = 6\,\text{kA}$; 3 making operations
- C: $\hat{i}_{\text{inrush}} = 8\,\text{kA}$; 1 making operation
- D: $\hat{i}_{\text{inrush}} = 11\,\text{kA}$; 1 making operation

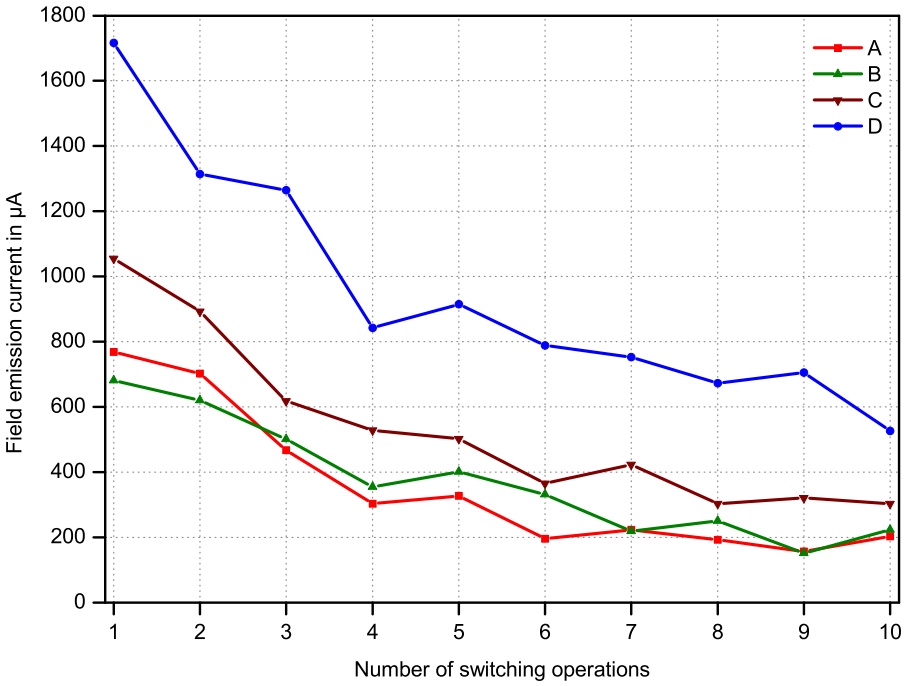

Figure 9.5: Average curves of field emission current from the (10×10)-measurements for conditions A, B, C and D

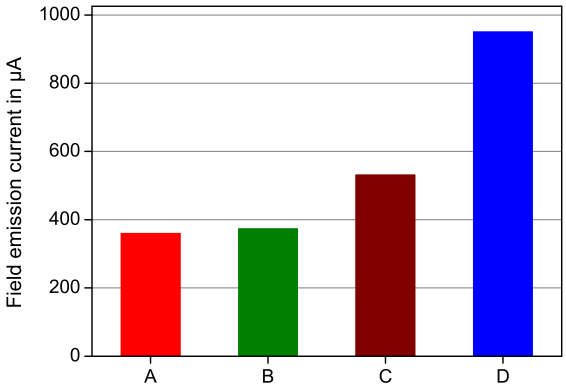

Figure 9.6: Average values of field emission currents for conditions A, B, C and D

From these figures, it is observed that by different numbers of making operations (1 or 3 times) the field emission currents do not significantly differ (conditions A and B). Further increase in the number of making operations (6 times) shows also the same result. But, increasing the amplitude of the inrush current results in higher field emission current (compare conditions A, C, D). This is especially more pronounced when increasing the inrush current to 11 kA. Here, an increase of a factor of approximately three can be seen (compare conditions A and D).

Figures 9.7 and **9.8** show the average calculated surface parameters β and A_e for the same conditions as of Figure 9.5. The same tendency is also obvious in the surface parameters. It can therefore be concluded, that for higher inrush current amplitudes the contacts surface condition after opening is dielectrically less favorable, and consequently, the field emission current is higher. It is important to note that the surface parameters are calculated assuming constant contact work function, which might not always be the case. However, their absolute values are not of interest here but only their tendencies.

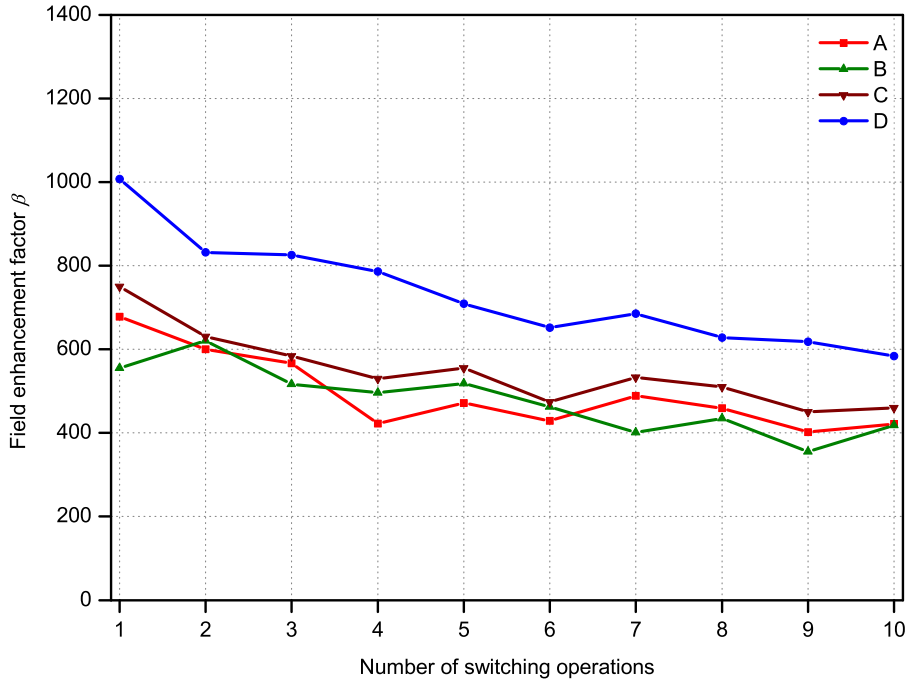

Figure 9.7: Average calculated field enhancement factors β from the (10 × 10)-measurements for conditions A, B, C and D

The impact of the inrush current is also studied using the full-power test-circuit. The measurements are performed on interrupter type "I". Amplitude of the applied recovery voltage is about 80 kV, and the breaking current is 400 A. Here, two different inrush currents are compared:

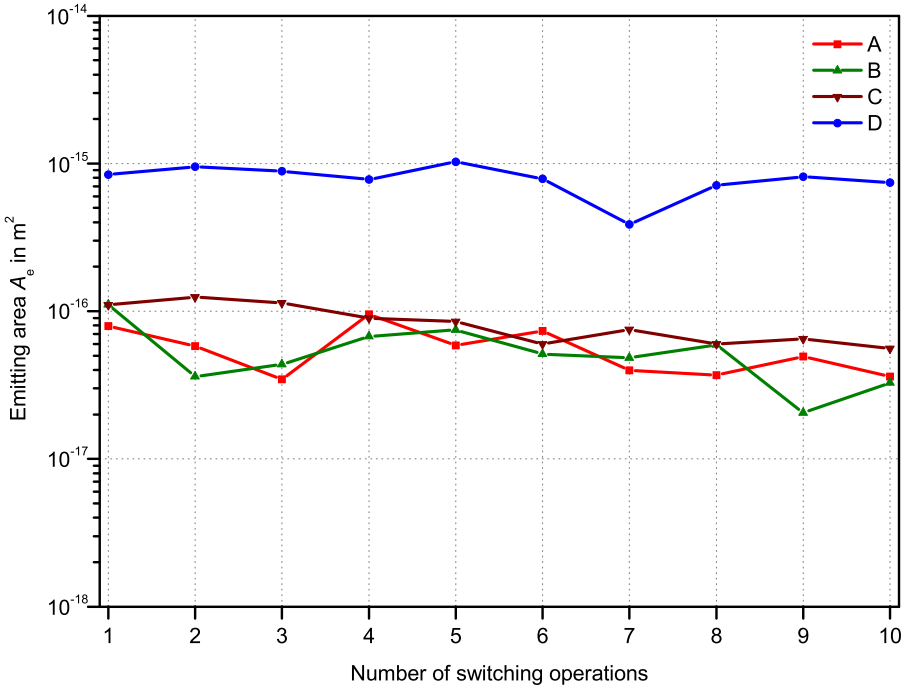

Figure 9.8: Average calculated emitting areas A_e from the (10×10)-measurements for conditions A, B, C and D

- E: $\hat{i}_{\text{inrush}} = 530\,\text{A};\ f = 280\,\text{Hz}$
- F: $\hat{i}_{\text{inrush}} = 20\,\text{kA};\ f = 4.25\,\text{kHz}$

The results show that in case "E" the field emission current after capacitive interruption is very low (a few microamperes). Whereas, in case "F" it even reaches several hundred microamperes although the gap distance is 20 mm. In this context amplitude and duration of the breaking current have significant influence on field emission current. It has a positive conditioning effect on the surface condition. This will be discussed in more detail in 9.3.

9.3 Effect of the breaking current on the field emission characteristics after current interruption

The worsening effect of the inrush current on the dielectric properties of vacuum interrupters (de-conditioning) is more significant, when the produced broken welds are not burned out by sufficient arcing activity during contact opening. The most critical case

is currentless opening, where the broken welds cannot be eliminated. Also, by capacitive switching, the conditioning effect of the arc might also not be enough due to the relatively low breaking current or low arcing time, which leads to high field enhancement during recovery. In the following the influence of the breaking current depending on its amplitude and arcing duration is shown.

In this regard, measurements are performed on one interrupter type "A" using experimental setup "a". The making operation before one test series (ten interruptions after no-load closings) is set to one closing under $\hat{i}_{\mathrm{inrush}} = 6\,\mathrm{kA}$ and $f_{\mathrm{inrush}} = 1.5\,\mathrm{kHz}$. From the measurements it is observed that the conditioning effect of 500 A breaking current is higher than that of 20 A. Due to the arc energy input during arcing time, micro-protrusions and broken welds may be removed from the contact surface, or they may be smoothened. Both effects would result in lower field enhancement and consequently lower field emission current. This positive conditioning effect is more pronounced at higher breaking currents.

Figure 9.9 is one representative example showing the recovery voltage (blue curve) and field emission current (red curve) immediately after first capacitive interruption of $i_{\mathrm{break}} =$ 500 A. It is seen that after just one single interruption the field emission current falls down to a few ten microamperes and less. This effect is probably related to the much larger number of cathode spots that are active on the surface at 500 A. In spite of the deconditioning effect of the making operation the broken welds are eliminated during opening due to sufficient energy input of the 500 A arc. This results in a very low field emission current after opening (positive conditioning effect of the breaking arc).

Figure 9.10 shows another representative example for breaking current of 20 A. The red curve shows the field emission current after first interruption (beginning of the test series). In this case, relatively high field emission current in the range of several hundred microamperes is measured. Just after several interruptions (five to ten) the amplitude of the field emission current decreases to a few ten microamperes. This is seen from the green curve, which shows the field emission current after tenth interruption (end of the test series). The amplitude of the field emission current is still a bit higher than after the first interruption under 500 A breaking current.

This effect is obvious from each of the (10×10)-measurements. For example, from Figure 9.2, it is seen that each test series shows a different behavior, but they all follow the same trend which is a decrease of the field emission current (conditioning effect) with increasing number of interruptions at 20 A. This means, each subsequent interruption results in a lower field emission current during recovery phase. In most of the test series, after ten

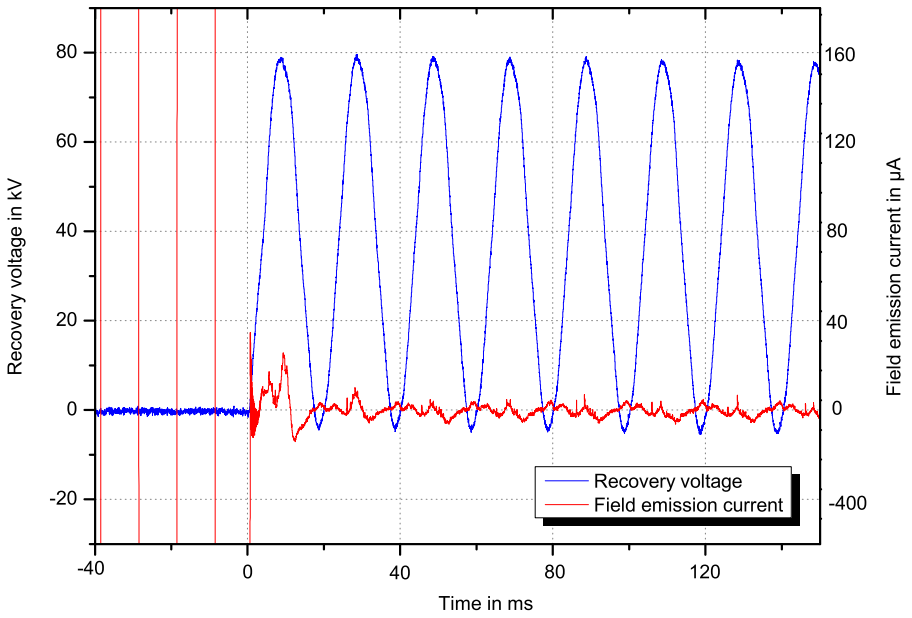

Figure 9.9: Example showing field emission current after first interruption (red curve). Breaking current: 500 A, inrush current: 6 kA, 1.5 kHz

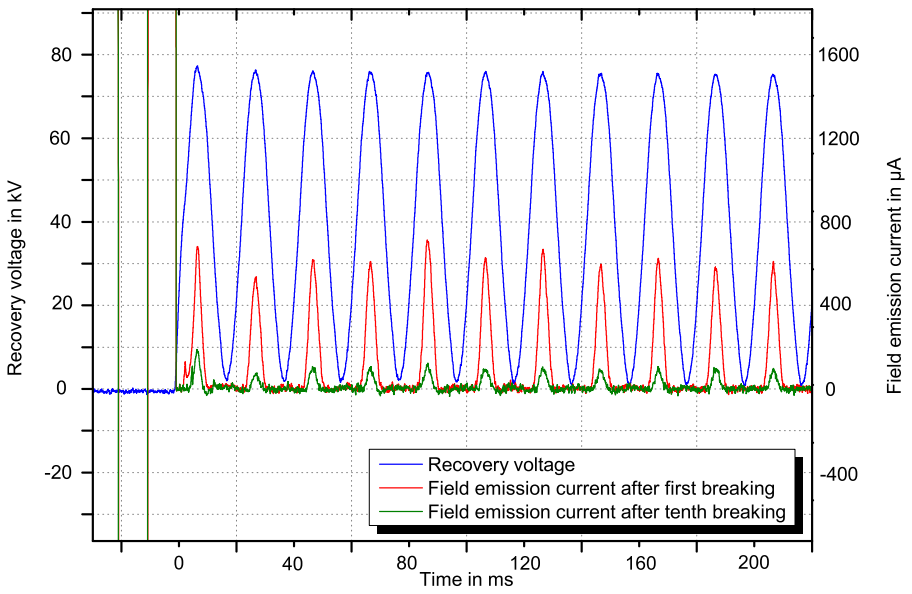

Figure 9.10: Example of one test series showing field emission current after first interruption (red curve) and after tenth interruption (green curve). Breaking current: 20 A, currentless closing during the test series, inrush current before the test series: 6 kA, 1.5 kHz, interrupter type “A” (see 9.4.1)

interruptions the value of the field emission current decreases from milliamperes to several ten microamperes.

Another point is that the breaking current in a capacitive circuit is much lower than the interrupter's breaking capability. Therefore, the current can be interrupted easily even at low arcing times, which results in low arc energies for burning out the welds and for contact conditioning.

Figure 9.11 shows a measurement example carried out using the full-power test-circuit setup "b" for two different arcing times. The measurements are performed on interrupter type "I" according to procedure 1 with recovery voltage of $\hat{v}_{\mathrm{rec}} = 85\,\mathrm{kV}$. The making operation was according to the IEC circuit breaker standard [IEC6 08] in a back-to-back switching case of 20 kA, 4.25 kHz inrush current. The capacitive breaking current was 410 A, 50 Hz with two different arcing times of 2.7 ms and 11.6 ms.

After current zero ($t = 0$) the recovery voltage appears across the contacts and field emission current is measured using software compensation. It is seen that in case of 11.6 ms arc duration the amplitude of the field emission current is much lower ($< 10\,\mu\mathrm{A}$, green curve) than after shorter arcing time of 2.7 ms (about 100 µA, red curve). In case of 2.7 ms arcing time, the reach of the cathode spots covering the contact surface is too small, making it less probable for the critical field-emitters to be removed from the contact's surface. In this measurement, it is also observed that the field emission current during the first cycle is much higher than during the other cycles. Due to very short arcing time (2.7 ms) the gap spacing does not reach its nominal value (20 mm) within 10 ms after current interruption, and consequently the field emission current is higher during the first cycle of recovery voltage.

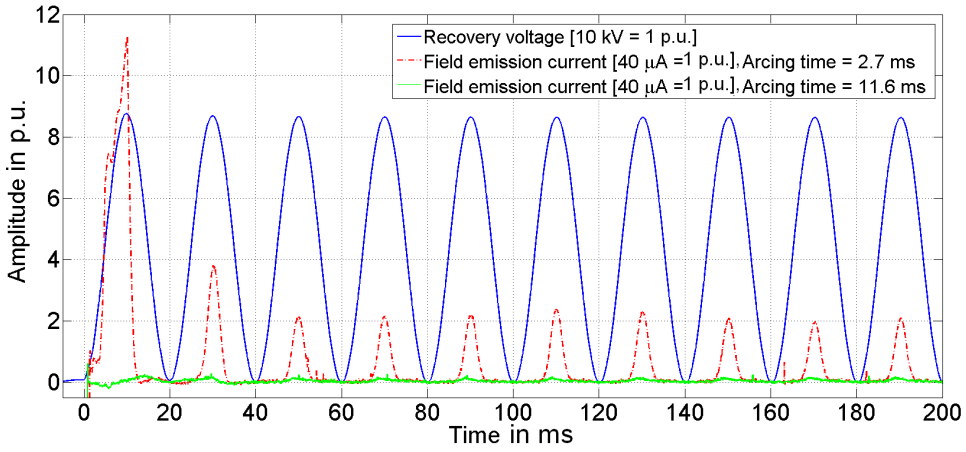

Figure 9.11: Influence of the arc duration on the field emission characteristic after capacitive switching

Despite the relatively large gap spacing of 20 mm, amplitude of the field emission current

after stabilizing is about 100 µA in case of 2.7 ms arcing time. This high value of the field emission current is on one hand caused by the short arcing time (weak conditioning) and on the other hand by the high inrush current (strong de-conditioning).

9.4 Dielectric breakdowns and field emission current during recovery phase

To understand the origin of dielectric breakdowns, investigations on different specimens, as described in 5.3.1, are performed. In this regard, the effect of the manufacturing process (intentionally modified interrupters by manufacturing process as well as commercial interrupters from different manufacturers) and also the influence of the contact gap spacing on the dielectric behavior of the interrupter during recovery are studied. The focus of these investigations is on the number and on the time for breakdowns as well as on their relation with field emission current.

The investigations are performed using experimental setup "A". Test procedure 2 with breaking current of $i_{\mathrm{break}} = 20$ A and recovery voltage of $v_{\mathrm{rec}} = 75$ kV as well as test procedure 3 with inrush current of $\hat{i}_{\mathrm{inrush}} = 6$ kA, $f_{\mathrm{inrush}} = 1.5$ kHz and same breaking current and recovery voltage as by procedure 2 are applied.

9.4.1 Influence of manufacturing process

Procedures 2 and 3 are applied on different specimens to investigate the effect of the manufacturing process:

- A (commercial, manufacturer: M1)
- C (manufactured in non-clean room condition, manufacturer: M1)
- D (manufactured without conditioning process, manufacturer: M1)
- E (commercial, manufacturer: M2)

In the following, at first some representative measurement examples for different test samples are shown, and finally the results are compared.

Measurement examples for different test samples

Figure 9.10 (chapter 9.3) showed one representative measurement result for interrupter type "A". As is seen, the amplitude of the field emission current was in the range of a few hundred microamperes, and no dielectric breakdown was observed in this measurement. Furthermore, for this type of interrupters, no breakdown during the complete measurement set (procedure 3: (10×10)-measurement) was observed (see Figure 9.2).

Figures 9.12, **9.14**, **9.15** show three representative examples for one interrupter of type "C". These interrupters have exactly the same design as interrupters of type "A", but they are intentionally manufactured under non-clean room conditions. For these interrupters, fifteen to twenty dielectric breakdowns during each complete measurement set (10×10) are observed. During the measurements, it is seen that the field emission current has high fluctuations after current interruption for about $(200 \cdots 300)$ ms time duration, and thereafter it remains almost constant or decays slowly, corresponding to the decay of the recovery voltage (see **Figure 9.20**). This is also reflected in the calculated surface parameters with the help of the FNE (**Figures 9.13** and **9.21**). Such fluctuations in the field emission current are mostly observed in the interrupters of type "C". Measurements on the commercial interrupters (type "A") show a far more stable emission current (compare Figures 9.12 and 9.10). It is assumed that this effect results from the particles which are more likely present inside the interrupters of type "C" even having larger size. Further details in this regard are provided later.

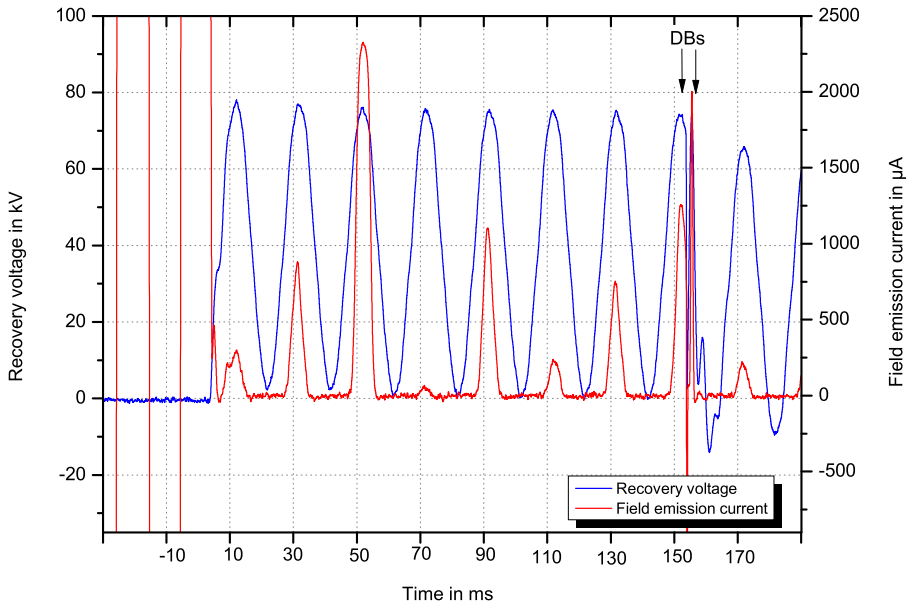

Figure 9.12: Example 1, interrupter type "C" (DB: dielectric breakdown)

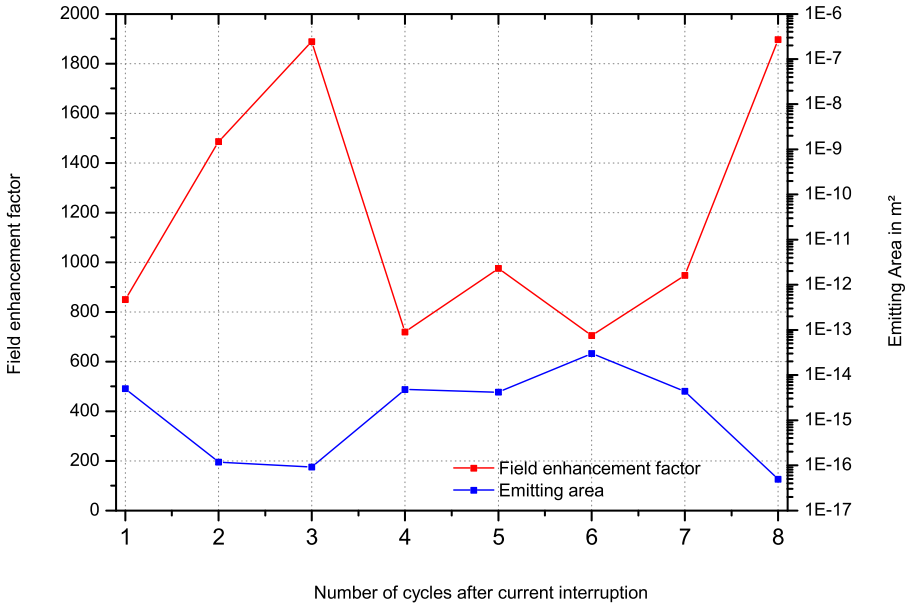

Figure 9.13: Calculated surface parameters for each cycle from current interruption to breakdown's moment (example 1, interrupter type "C")

In example 1 (Figure 9.12) two dielectric breakdowns are observed in the eighth voltage cycle. Amplitude of the field emission current at this cycle is $i_F = 1250\,\mu A$, which is not the highest value during this measurement. However, with regard to the calculated emitting areas A_e (see Figure 9.13), the field emission current density has the highest value in the eighth cycle ($j_F \approx 3 \times 10^{13} A/m^2$). It must also be noted that for a breakdown to occur not only adequate number of electrons but also sufficient metal vapor (source of positive ions) are required. During each field emission current cycle, the electron beams, originating from the cathode, impact with the anode and heat its surface. Furthermore, according to the impact energy, the electrons may penetrate into the anode's sub-surface volume and heat it. At a certain threshold temperature, this heated anode region will evaporate explosively and may initialize the breakdown [Slad 08]. Therefore, just high electron emission may not necessarily lead to a breakdown (e.g. in the third cycle with $i_F = 2300\,\mu A$ no breakdown is observed). Another source of metal vapor are the electron emitters on the cathode surface. Here, the size of the emitter is important for supplying enough metal vapor to initiate the breakdown (see 2.2.3 for more information).

During the measurements, it is observed that the amplitude of the recovery voltage becomes less after a breakdown (e.g. compare the amplitudes of the recovery voltage in the eight and ninth cycle of Figure 9.12). As the breakdown current flows in the circuit, the dc voltage component decreases due to the discharge of capacitor $C_{0,1}$ (see 5.3.2). This results in lower recovery voltage amplitudes in the next cycles. However, this fact is not disturbing as the

focus is basically on the time duration between the current zero and the first dielectric breakdown.

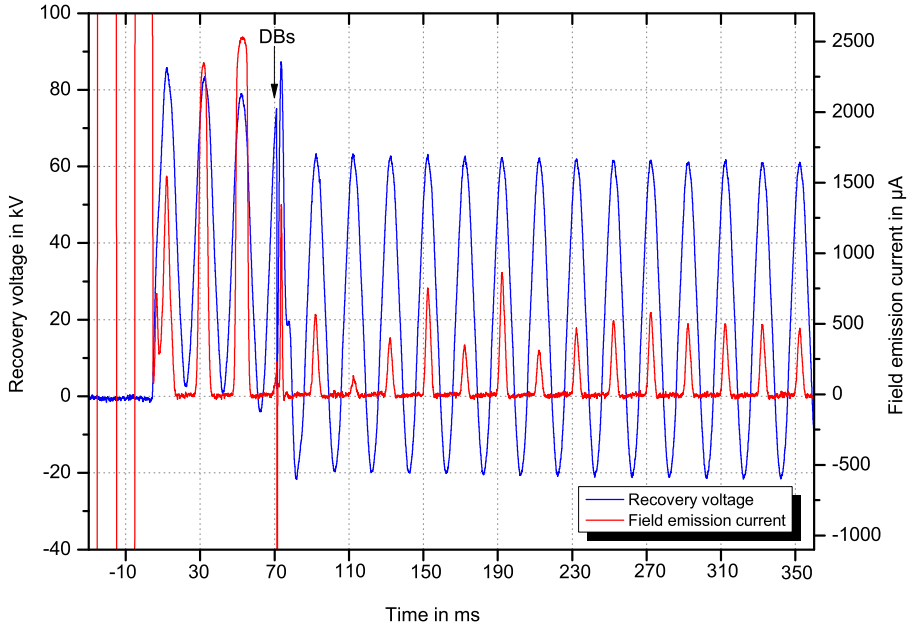

Figure 9.14: Example 2, interrupter type "C" (DB: dielectric breakdown)

Figure 9.14 shows another example. Here, it is seen that the field emission current increases continuously up to a breakdown in the fourth cycle. These kinds of dielectric breakdowns, as shown in examples 1 and 2, seem to be correlated with field emission current. However, there are also few breakdowns even at low field emission currents. In example 3 (Figure 9.15) multiple breakdowns are observed in the ninth and twenty eighth cycle after current interruption. Here, amplitude of the field emission current is $i_F \leq 100\ \mu A$.

In this regard, particles have an important influence. On one hand, they may affect the contact surface condition due to their impact with the contact (certain impact velocity is required), and thus determine the field emission current (particle induced field emission current) as well as the dielectric behavior of the interrupter. On the other hand, if particles evaporation occurs, this may result in a direct breakdown without any preceding increase in field emission current. In 2.2.2 the theory of both phenomena is described in detail.

Figures 9.16, **9.17** show two representative examples for one interrupter of type "D". These interrupters have also exactly the same design as interrupters type "A", but they are intentionally manufactured without conditioning process. The results of each complete measurement set (10×10) shows only five to ten breakdowns in this case. Figure 9.16 shows one measurement example (4), where no breakdown occurs. More stable fluctuations

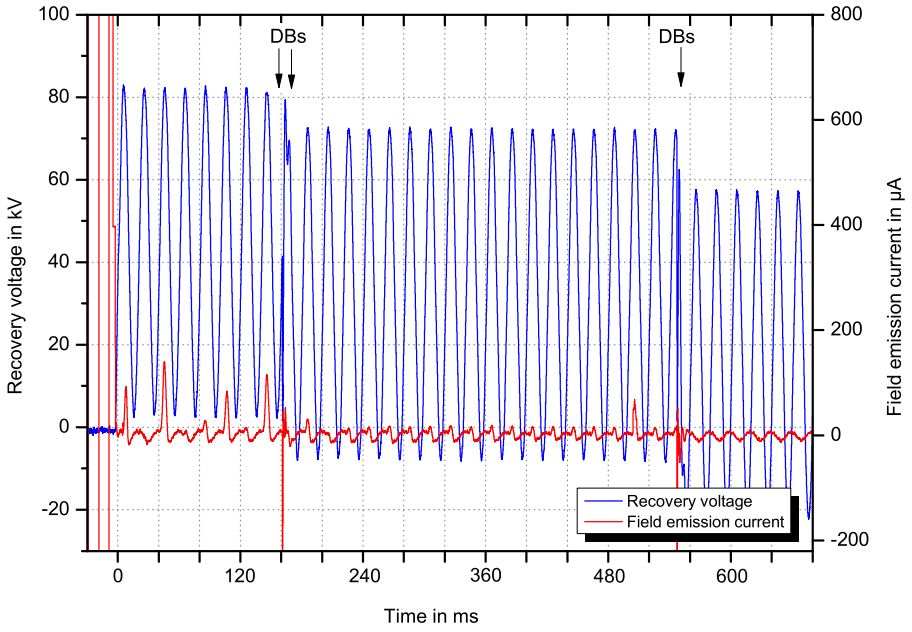

Figure 9.15: Example 3, interrupter type "C" (DB: dielectric breakdown)

(comparable with type "A") for almost 200 ms time duration after interruption is observed. Figure 9.17 shows another example of this case (example 5). A dielectric breakdown in the second cycle is here observable. It is important to note that for this variant of interrupter mostly early breakdowns (breakdowns in the first or second cycle) are the case, which indicates, that the breakdowns occur due to the high electrical field stress.

Figures 9.18, **9.19** show two representative examples for one interrupter of type "E". These interrupters are from manufacturer M2. However, they have a geometry comparable to type "A". They exhibit sixteen to twenty two breakdowns during each complete measurement set (10×10). In example 6 (Figure 9.18), multiple breakdowns in the second and seventh cycle are observed, whereas in example 7 (Figure 9.19), one breakdown in the tenth cycle is observed. Fluctuations in the field emission current are also observed for this type of interrupter, which are a bit smoother than the fluctuations in interrupters of type "C".

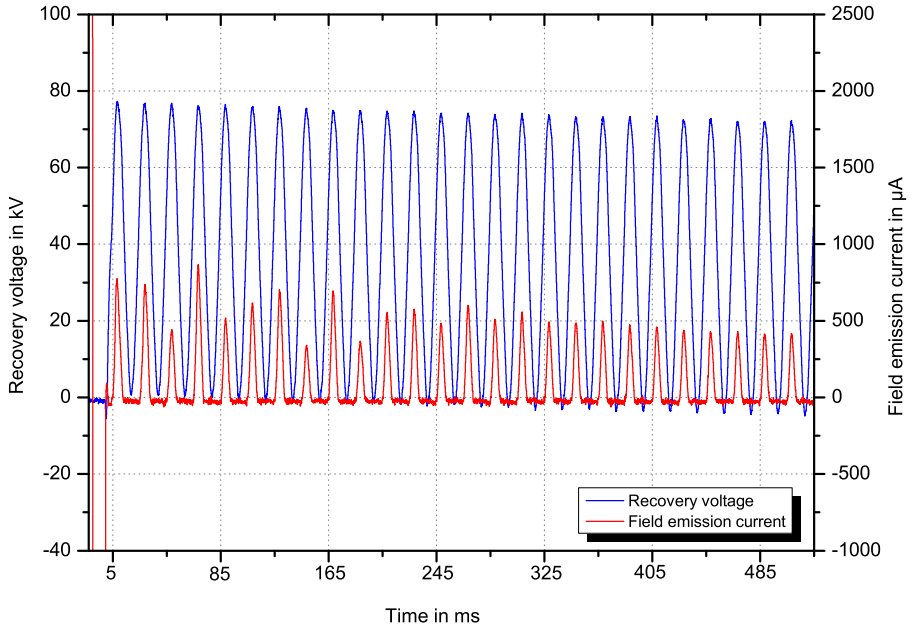

Figure 9.16: Example 4, interrupter type "D"

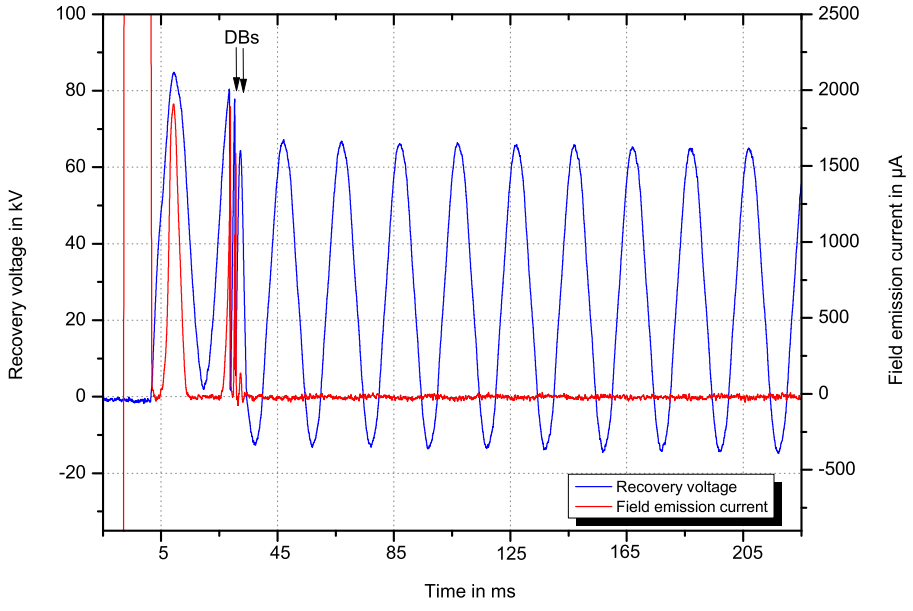

Figure 9.17: Example 5, interrupter type "D" (DB: dielectric breakdown)

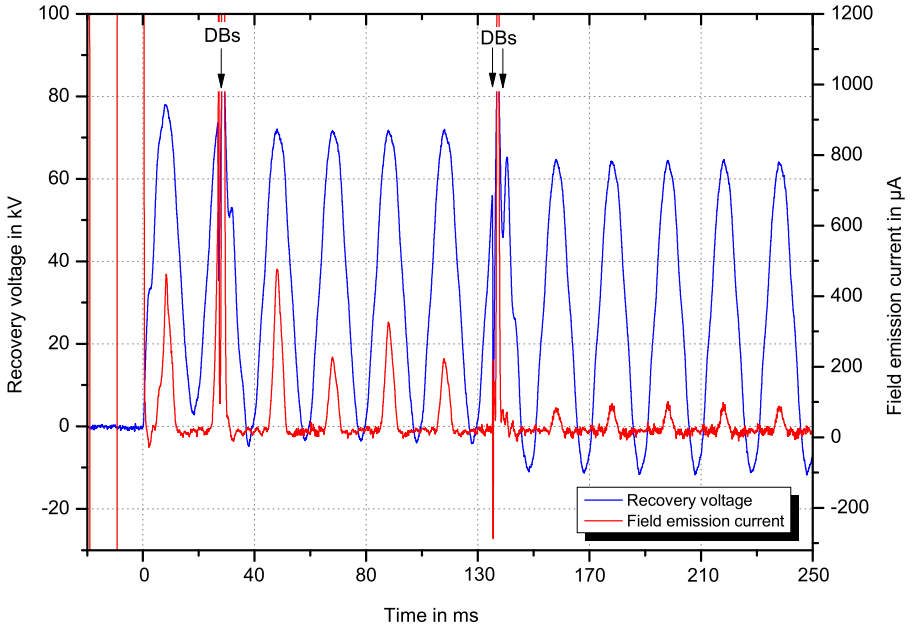

Figure 9.18: Example 6, interrupter type "E" (DB: dielectric breakdown)

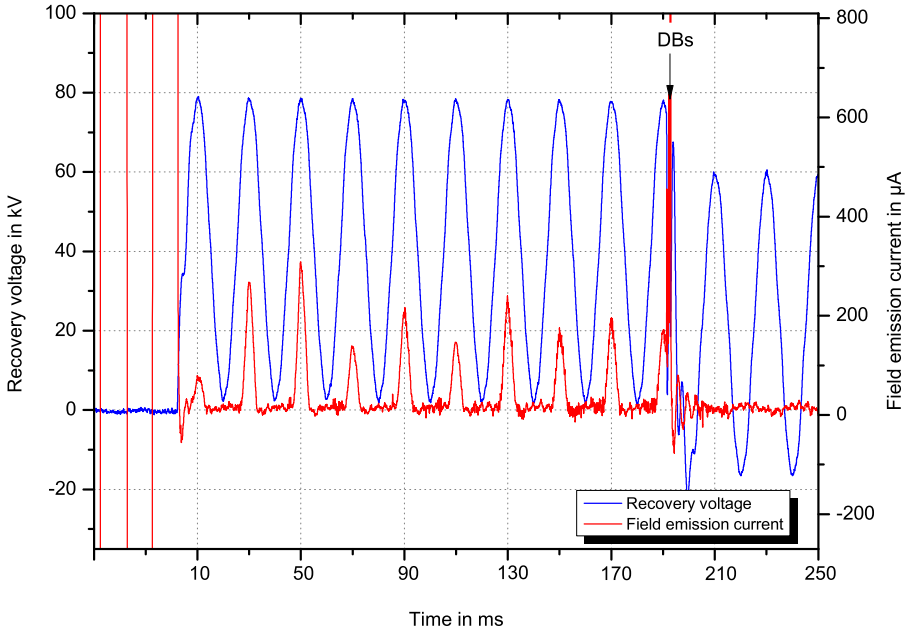

Figure 9.19: Example 7, interrupter type "E" (DB: dielectric breakdown)

Fluctuation in the field emission current

From the examples shown in the previous section, a phenomenon "fluctuation in the field emission current" is observed. Table 9.1 gives an overview of the fluctuation factors for different interrupter types.The fluctuation factor "k_f" is defined here as:

$$k_\mathrm{f} = \frac{i_\mathrm{F,max}}{i_\mathrm{F,min}} \tag{9.1}$$

where $i_\mathrm{F,max}$ is the maximum field emission current and $i_\mathrm{F,min}$ is the minimum field emission current at constant recovery voltage in the "considered" fluctuation interval (e.g. interval I in **Figure 9.20**).

Table 9.1: Fluctuation factor k_f for different types of interrupters

Interrupter type	k_f
"A"	$1 \cdots 3.5$
"C"	$5 \cdots 30$
"D"	$1.5 \cdots 5$
"E"	$2 \cdots 10$

From table 9.1, it is seen that interrupters "A" and "D" have the lowest fluctuation factors. Interrupter "E" has a middle-rate and interrupter "C" has the highest factor. It is assumed, that this phenomena is due to particles which are more likely present inside the interrupters, manufactured in non-clean room condition, even having larger size[1].

Figure 9.20 shows again example 1 for interrupter "C", however, now for the whole period of the measurement. **Figure 9.21** shows the calculated field enhancement factors for this example. The field emission current fluctuates for about 200 ms time duration after interruption and remains later on almost constant. Similar fluctuations are also observed in the field enhancement factor.

It is very important to note that such fluctuations are observed only after mechanical operations. Just applying alternating voltage across the open contacts of an interrupter (even in case of interrupter type "C") results in an approximately constant amplitude of the field emission current during the time interval of voltage application as it is known from the literature. Due to mechanical vibrations after contact opening, particles especially present in the interrupters manufactured intentionally in non-clean room conditions as

[1] Assumedly, interrupters of type "E" are not manufactured under perfect clean room conditions

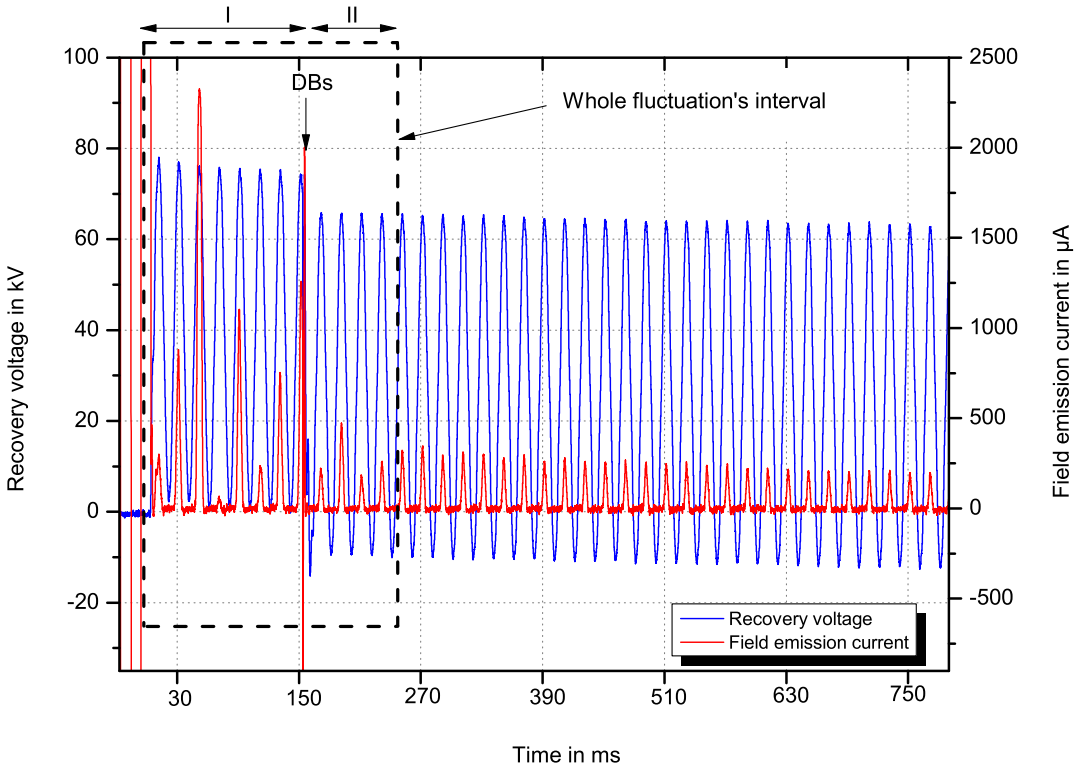

Figure 9.20: Whole measurement period of example 1, interrupter type "C" (DB: dielectric breakdown)

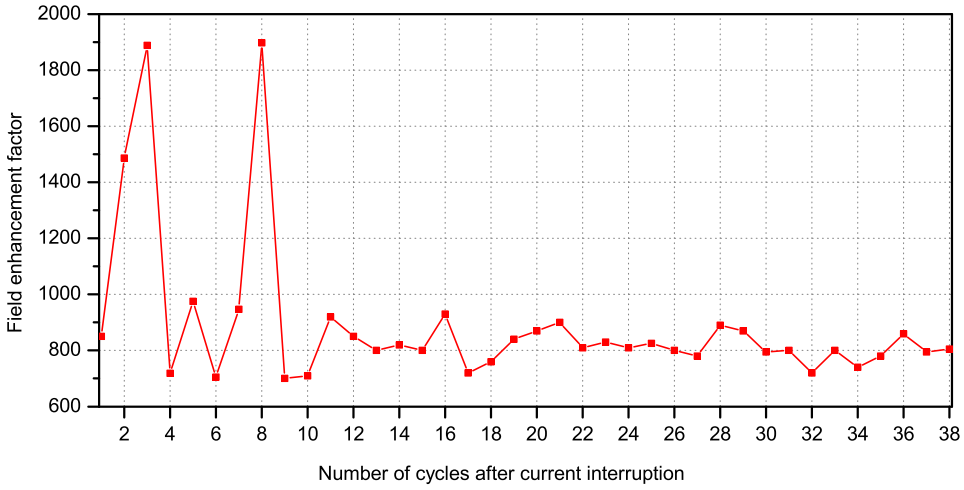

Figure 9.21: Field enhancement factor for the whole measurement period of example 1, interrupter type "C"

well as those manufactured assumedly under non-prefect clean room condition, may move in the gap, impact with metallic surfaces and thus affect the field emission characteristic of the gap.

After description of the fluctuation phenomenon, different hypotheses of its origin are presented in the following. A combination of two or three of them may explain the fluctuation phenomenon. More investigations are necessary in the future for deeper understanding.

- **Impact of particles with the cathode surface:**

  As is explained in 2.2.2, at intermediate impact velocities ($v_{cr} < v_i < 5v_{cr}$, where v_{cr} is the critical impact velocity depending on the material of the colliding surfaces) generation of a crater or a micro-protrusion on the electrode surface is possible. This effect results in an enhanced local field enhancement factor β if the impact occurs on the cathode. This indirect role of particles on the dielectric behavior of the interrupter is repeatedly described in the literature [Laff 80], [Lath 72], [Slad 08]. For example, in a microscopic study of cathode surfaces that had been subjected to high voltages, Little and Smith [Laff 80] found craters having splash rim protrusions. They conclude that the craters resulted from the particle impact.

  Non-metallic particles have an important influence on the field emission characteristic of the surface as well. For example, in [Laff 80], investigations are reported for alumina added to copper. The authors found that the field emission current occurs from the immediate vicinity of the insulating particles (insulating-metal-vacuum triple junction).

  The impact velocity of a micro-particle colliding with the cathode, assuming a spherical micro-particle with radius of r_p, is given in *equation* 2.14. Using this equation, the radius of a particle necessary to result in intermediate impact velocities ($v_{cr} < v_i < 5v_{cr}$) can be calculated. Here, following assumptions are made:

  - colliding surface: copper ($v_{cr} = 200\,\mathrm{m/s}$)
  - $v_{vac} = 75\,\mathrm{kV}$
  - $\beta = 800$
  - $d = 8\,\mathrm{mm}$

  It is seen that particle radii in the range of $5.5\,\mu\mathrm{m} \leq r_p \leq 137\,\mu\mathrm{m}$, after impacting with the cathode, may result in intermediate impact velocities, where crater and rim formation may occur. The upper limit seems a bit high for particles existing in commercial vacuum interrupters according to values give in literature [Slad 08], nevertheless, particles with radii of a few ten micrometers are likely to exist.

- **Thermal instability of the field emitter:**

  This phenomenon may occur in all types of interrupters (commercial or modified ones). Due to the field emission current flow and consequent heating of the protrusion, its shape may be changed, smoothened or even completely eliminated. In 2.2.3, different energy exchange processes in the field emitter during field emission current flow is briefly explained.

- **Space charge effect:**

  When positively charged micro-particle approaches the cathode surface, it will change the electrical field distribution at a certain distance and consequently increase the field enhancement and the field emission current. The enhancement may be as much as ten times. This phenomenon also happens during multiple transitions of the particles between the contacts, where at each reversal the particle accumulates more energy [Laff 80], [Lath 72], [Slad 08].

  Now, a cloud of particles in the intercontact gap (for interrupters manufactured in non-clean room conditions), during mechanical shocks interval shall be assumed. This may affect the field distribution on the cathode surface significantly. Therefore, without any change in the physical geometry of the micro-protrusions on the cathode surface, it may be possible that the field enhancement factor and consequently the field emission current varies with time due to the space charge of the particle cloud. This phenomenon is more probable for low speed particles, and thus larger ones.

- **Interaction of particles with the middle shield:**

  The potential of the middle shield has significant influence on the electrical field distribution around the cathode edge. The middle shield is at floating potential, because it is capacitively coupled to the contacts. Impacting of particles with enough acquired charge with the middle shield may change its potential. The potential change varies the field distribution around the cathode edge and affects the macroscopic field enhancement factor and consequently the field emission current.

  For better understanding the influence of the middle shield potential on the field emission characteristic of the cathode, calculations are performed using an analytic equation. The results are shown in **Figure 9.22**. The calculation is performed for three voltage cycles. In all three cycles, parameters such as field enhancement factor, emitting area, gap spacing, contact and gap geometry, surface work function and applied voltage are kept constant. The only parameter that varies from one cycle to the other, is the middle shield potential $v_{\mathrm{ms}} = \alpha \times v_{\mathrm{vac}}$, with α being the middle

shield potential factor. For this factor α, different values have just been assumed for each cycle in order to demonstrate possible effects on the field emission current.

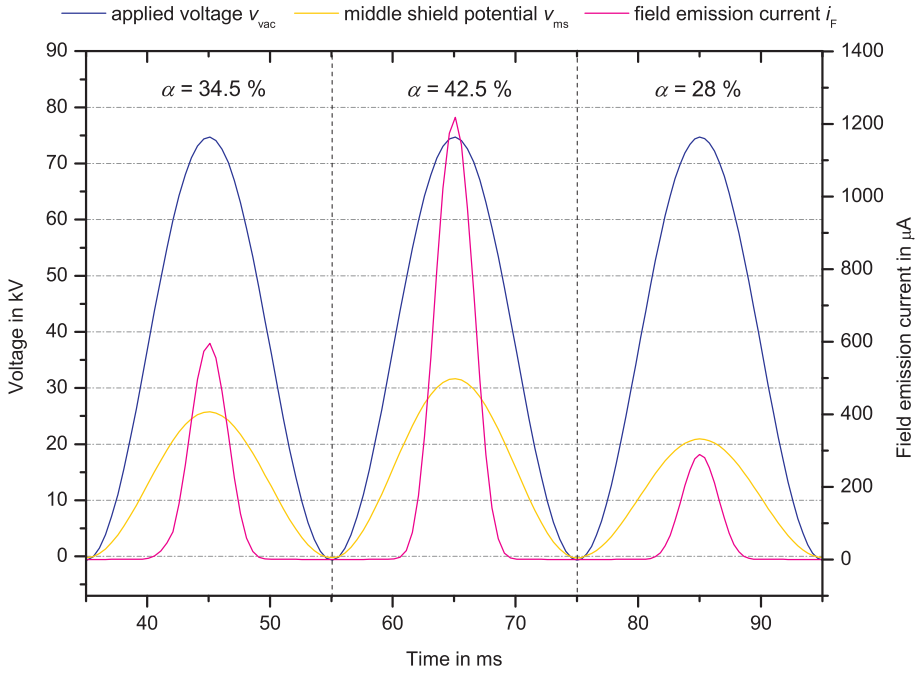

Figure 9.22: Analytical calculation showing the effect of the middle shield potential on the field emission characteristic, assuming constant $\beta = 800$, $A_e = 10^{-16}\,\mathrm{m}^2$, $\phi = 4.5\,\mathrm{eV}$, $d = 8\,\mathrm{mm}$, radius of contacts edge $r_k = 2\,\mathrm{mm}$, contact to shield spacing $d_w = 8\,\mathrm{mm}$. α: middle shield potential factor

From Figure 9.22, it is obvious that in order to double the field emission current (from cycle 1 to cycle 2), an increase of approximately 6 kV in the middle shield potential is necessary, assuming all the other parameters to be constant. The question here is if it is possible that due to the impact of particles with the shield, its potential increases by $\Delta v_{ms} = 6\,\mathrm{kV}$. For this reason, the required acquired charge as well as the required particle radius are calculated:

$$Q_p = C_{ms} \times \Delta v_{ms} = 33\,\mathrm{nC} \tag{9.2}$$

where a capacitance of the middle shield to ground $C_{ms} = 25\,\mathrm{pF}$ is assumed. This assumption is supported through measurements with the help of an impedance analyzer.

In order to acquire a charge of $Q = 33$ nC under the surface field stress of $E_m = \frac{\beta v_{vac}}{d} = \frac{800 \times 75\,\mathrm{kV}}{8\,\mathrm{mm}} = 75 \times 10^8\,\mathrm{V/m}$, the required particle radius is calculated according to *equation* 2.11, resulting in $r_p = 154\,\mu\mathrm{m}$. Therefore, either particles of such large

radii or several particles simultaneously must impact with the shield in order to cause this variation in the middle shield potential and consequently fluctuation in the field emission current.

To verify this effect, the potential of the middle shield is measured during experiments on interrupter type "H" (also manufactured in non-clean room condition). The goal is to observe if its potential varies in the range of several kilovolts during the fluctuation interval of field emission current. The measurement is performed using a charge amplifier connected through a coupling capacitor of $C_{\mathrm{cou}} = 4\,\mathrm{pF}$ to the shield (more details are provided in Appendix C). **Figure 9.23** shows one representative measurement example. It is seen that though the field emission current fluctuates with time (like for interrupters of type "C"), the middle shield potential remains almost constant. From these measurements it is concluded that it is unlikely that the fluctuation in field emission current originates from the impact of particles with the middle shield. It must be noted, however, that the measurement system has itself an influence on the measurement results. In Appendix C, the measurement uncertainty is approximately estimated.

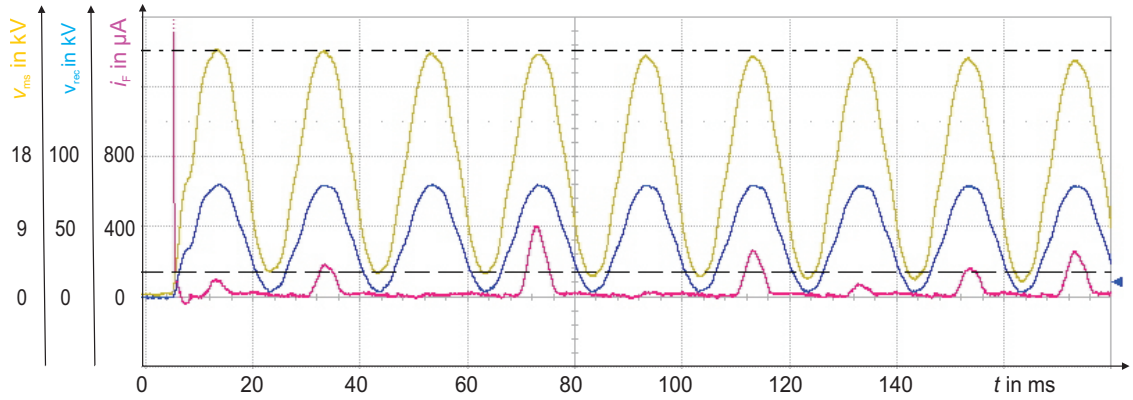

Figure 9.23: Measurement example (interrupter type "H") showing middle shield potential in yellow, field emission current in red and recovery voltage in blue

Characteristics of dielectric breakdowns during recovery

To assess the dielectric behavior of the vacuum interrupter after capacitive switching, different measurement sets (procedures 2 and 3) for different interrupters are evaluated. Within these measurement sets, a maximum of twenty two breakdowns are observed during hundred interruptions. In some of the measurement sets even no breakdowns are observed. This relative low number of breakdowns during each measurement set shows that a single measurement is not adequate, and a statistical evaluation is necessary.

Figures 9.24 and **9.25** show the cumulated number of dielectric breakdowns for one interrupter of each type during measurement sets according to procedures 2 and 3, respectively. For evaluation of the number of breakdowns, only the first breakdown after each interruption is considered. For commercial interrupter "A" no breakdown is observed during the hole measurement sets of both procedures. Whereas on the contrary, commercial interrupter "E" shows the highest number of breakdowns i.e. eighteen breakdowns at procedure 2 and twenty one breakdowns at procedure 3. Interrupters "C" and "D" show an intermediate number of breakdowns, where at the beginning of the measurement sets more breakdowns are observed for interrupter "D", and towards the end interrupter "C" shows more breakdowns. For interrupter "D" (manufactured without conditioning process), due to the conditioning effect of each interruption and breakdown event, a lower number of breakdowns are detected at the end of the measurement sets.

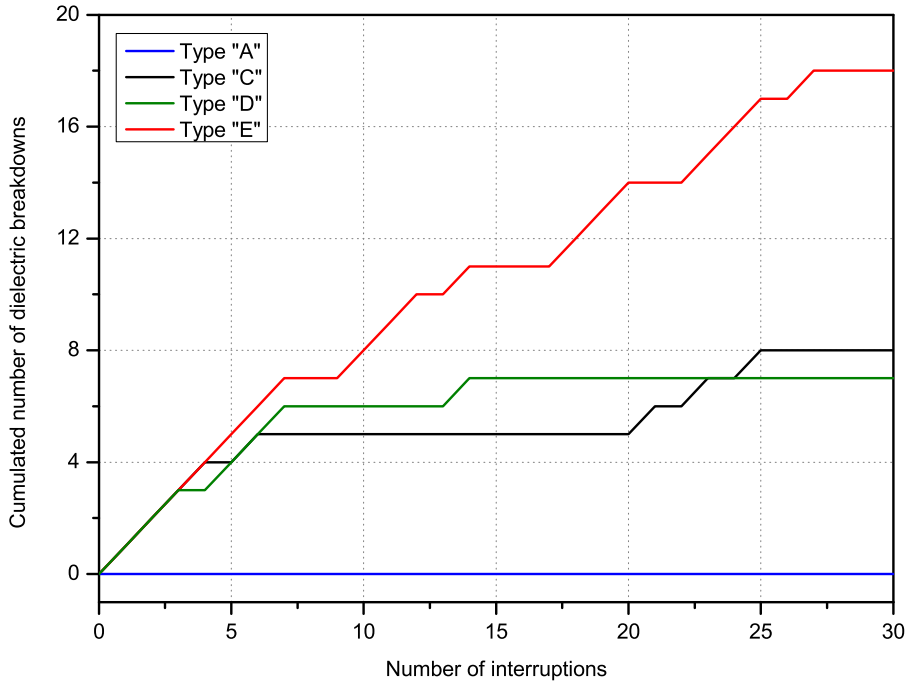

Figure 9.24: Cumulated number of dielectric breakdowns for one interrupter of each type "A", "C", "D", "E" tested acc. to procedure 2

It is observed that even during one measurement set the breakdown moment (the time interval between the current zero and first dielectric breakdown, respectively) varies considerably. Some breakdowns are observed at the first recovery voltage rise, whereas other breakdowns occur even after more than one hundred milliseconds. Furthermore, single and multiple breakdowns are observed during different measurements (compare examples 1 to 7). **Figure 9.26** shows the breakdown moments for one interrupter of each type.

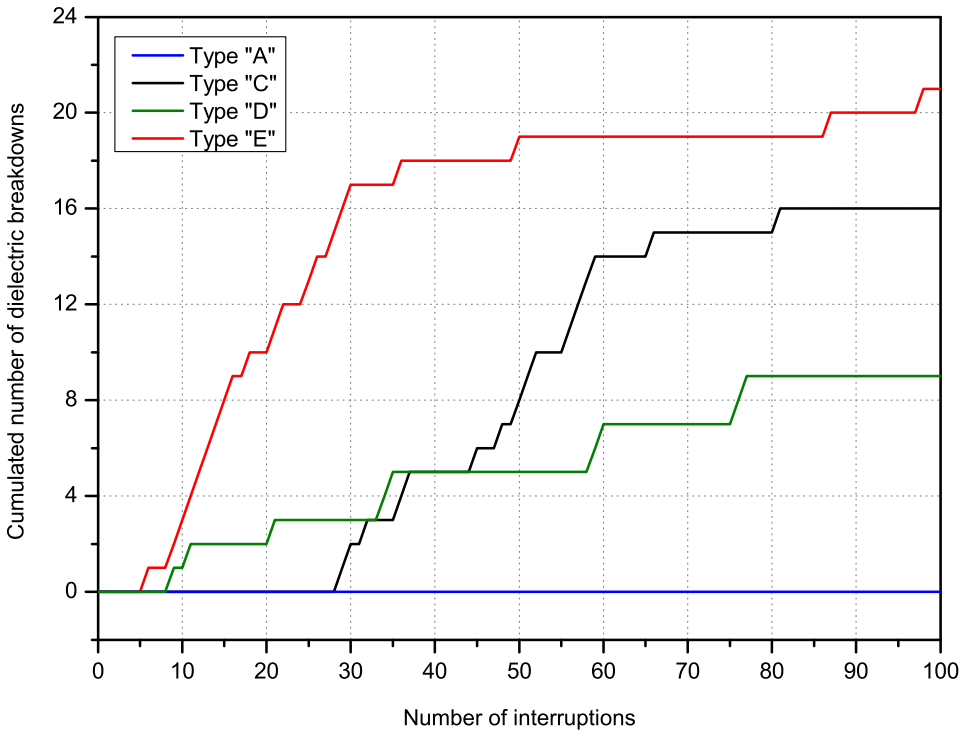

Figure 9.25: Cumulated number of dielectric breakdowns for one interrupter of each type "A", "C", "D", "E" tested acc. to procedure 3

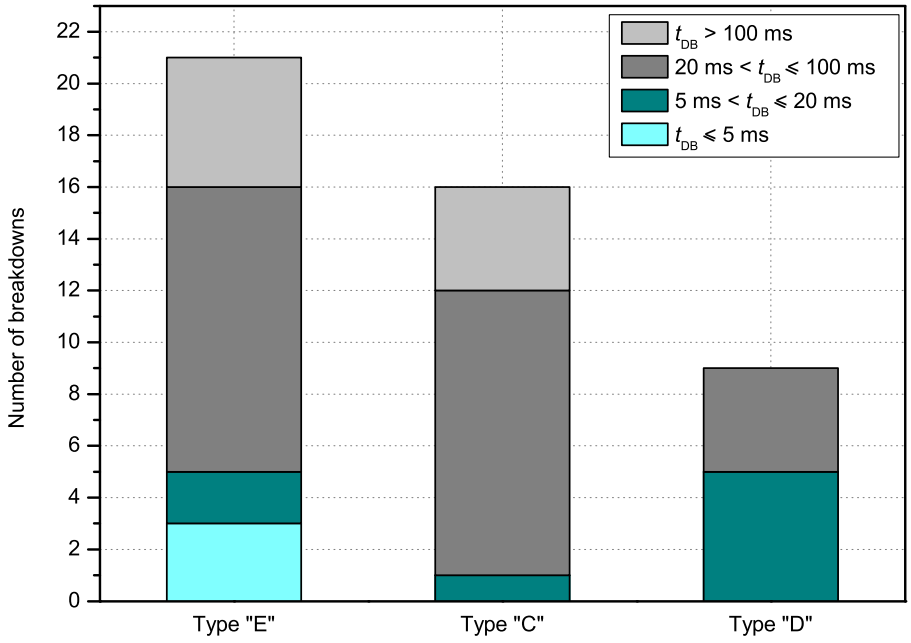

Figure 9.26: Breakdown moments for one interrupter of each type "C", "D", "E" tested acc. to procedure 3, t_{DB}: moment of dielectric breakdown

For interrupter types “E” and “C”, the breakdowns occurs most frequently after twenty to one hundred milliseconds. Some breakdowns are observed even one hundred milliseconds after current interruption. For interrupter “D”, breakdowns are observed either in the first or in the second voltage cycle. The dielectric breakdowns for this type of interrupter seem to be a kind of “conditioning breakdowns”.

Relation between dielectric breakdowns and field emission current

As the field emission current depends on many parameters and has a statistical behavior, just a single measurement is not sufficient to assess the dielectric behavior of the interrupter and the likelihood of breakdown. For this reason, the applied (10 × 10)-measurement (procedure 3) for different interrupter types (“A”, “C”, “E”) is statistically evaluated. For this evaluation, only breakdowns from the second recovery cycle are taken into account, where the field emission current flows at least for one cycle before a breakdowns occurs. Due to the low number of breakdowns observed for interrupter type “D”, this interrupter is not considered here. **Figure 9.27** shows the average field emission current amplitudes from the (10 × 10)-measurements for these interrupters. It is seen that the average field emission currents are at lowest for interrupter “A”, where also no breakdowns are observed during one hundred measurements. For interrupters “C” and “E”, higher average field emission currents and also higher number of breakdowns, fifteen and sixteen breakdowns respectively (from the second recovery cycle), are observed. For interrupters, which were manufactured in non-clean room conditions, this effect may result from particles which are more likely to be present inside such interrupters.

The frequency of occurrence of different ranges of field emission current amplitudes within one hundred measurements is compared in **Figure 9.28** for interrupters “A”, “C” and “E”. In this diagram, the number of interruptions after which a certain range of field emission current has flown, is depicted. Field emission currents of $i_F < 100\,\mu A$ are observed most frequently for interrupter “A” (55 times out of one hundred interruptions). At higher field emission currents, interrupters “C” and “E” are more dominant. Current ranges of $100\,\mu A < i_F < 500\,\mu A$ and $500\,\mu A < i_F < 1000\,\mu A$ are recorded most often for interrupter “E”, and currents of $i_F > 1000\,\mu A$ are measured mostly for interrupter “C”.

Figures 9.29 and **9.30** show the relative frequency of breakdowns at certain ranges of the field emission current for interrupters “C” and “E” respectively, according to the following formula:

$$Relative frequency = \frac{n_{DB}(i_F)}{n_{total}(i_F)} \tag{9.3}$$

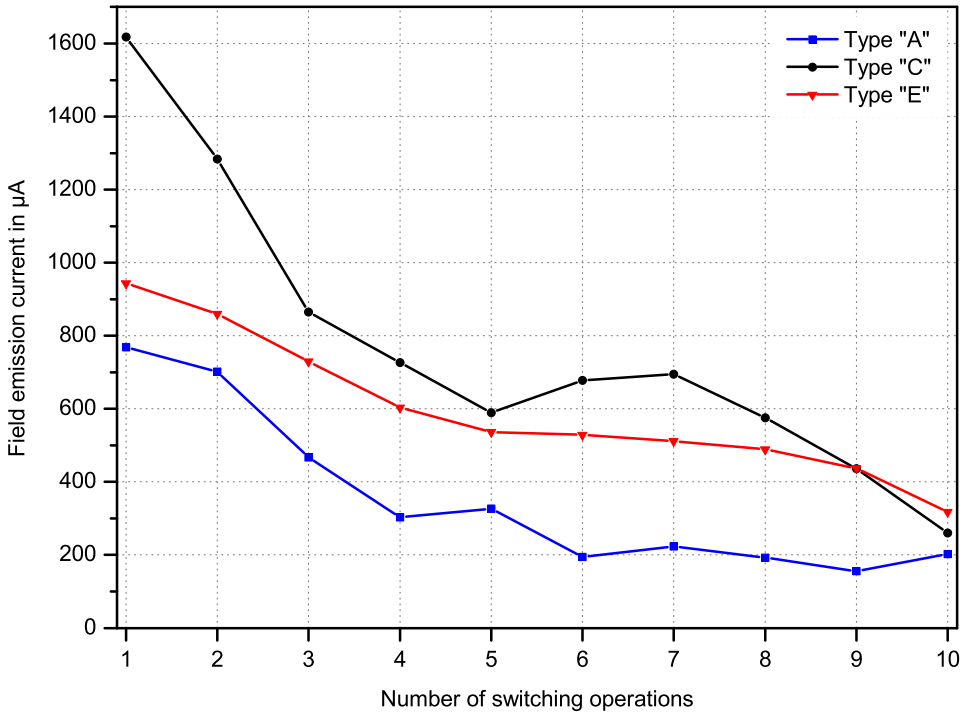

Figure 9.27: Average field emission current amplitudes during (10×10)-measurements for interrupters type "A", "C", "E".

where, $n_{\mathrm{DB}}(i_{\mathrm{F}})$ is the number of breakdowns at which a certain range of field emission current has flown before the breakdown occurs, and $n_{\mathrm{total}}(i_{\mathrm{F}})$ is the total number of measurements out of one hundred for the same range of field emission current. Different ranges of the field emission current are shown on the abscissa in Figures 9.29 and 9.30.

From Figure 9.29, it is seen that the breakdown probability is higher for field emission currents above 500 µA but without showing a clear trend. These kinds of breakdown seem to be correlated to field emission current. But, there are also several breakdowns even at low field emission currents. Such breakdowns might have other origins than field emission current (e.g. micro-particles or micro-discharges). It must be noted, that even in the same interrupter, different breakdowns may have different origins. Despite the lack of this one by one correlation between the field emission current and dielectric breakdowns, the average field emission current measured for one interrupter is a good indicator for the interrupter's instabilities and its likelihood of breakdown (compare the average field emission current amplitudes (Figure 9.27) and the number of breakdowns for interrupters "A" and "C").

For interrupter "E" more breakdowns are observed at currents below 500 µA (see Figure 9.30). At first view, it seems there is no correlation between field emission current and dielectric breakdowns for this type of interrupter. But looking again at the average curves

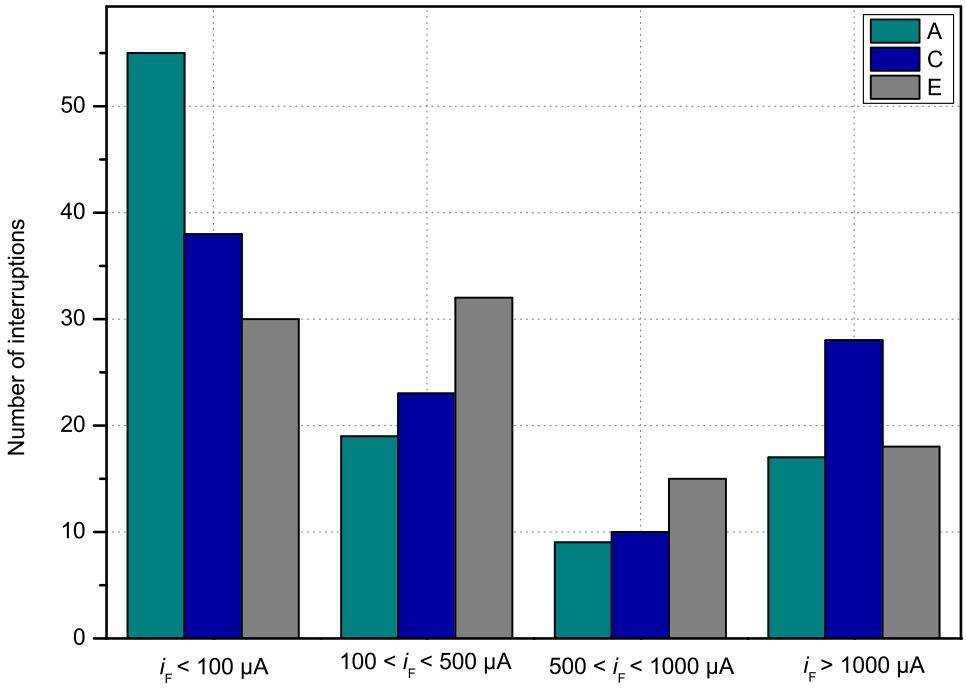

Figure 9.28: Occurrence frequency of different field emission current ranges during 10×10 -measurements for interrupters type “A”, “C”, “E”.

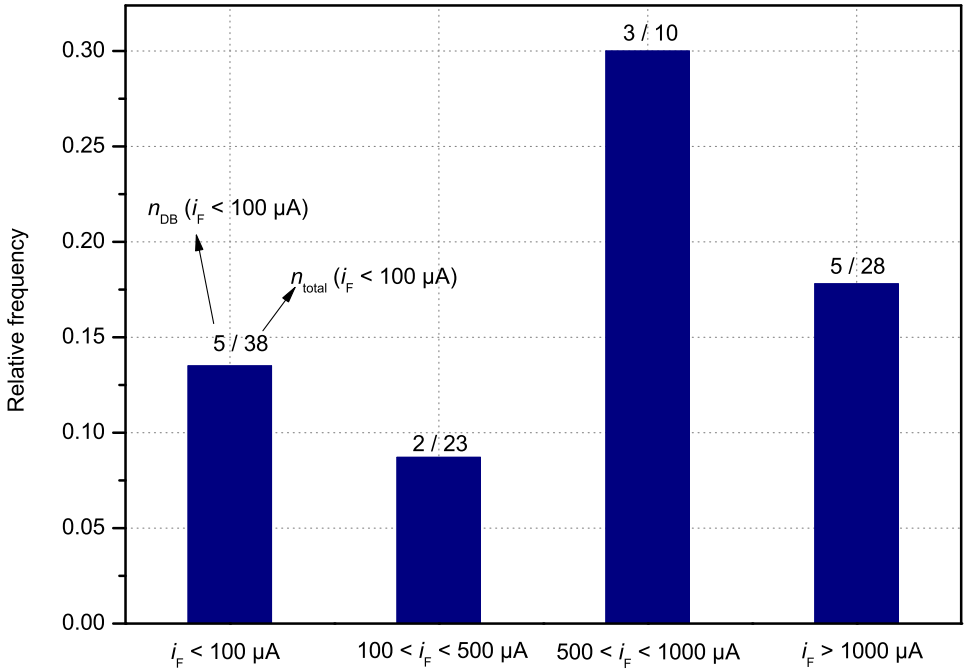

Figure 9.29: Relative frequency of breakdowns for certain ranges of the field emission current, (10×10)-measurement on the interrupter “C”

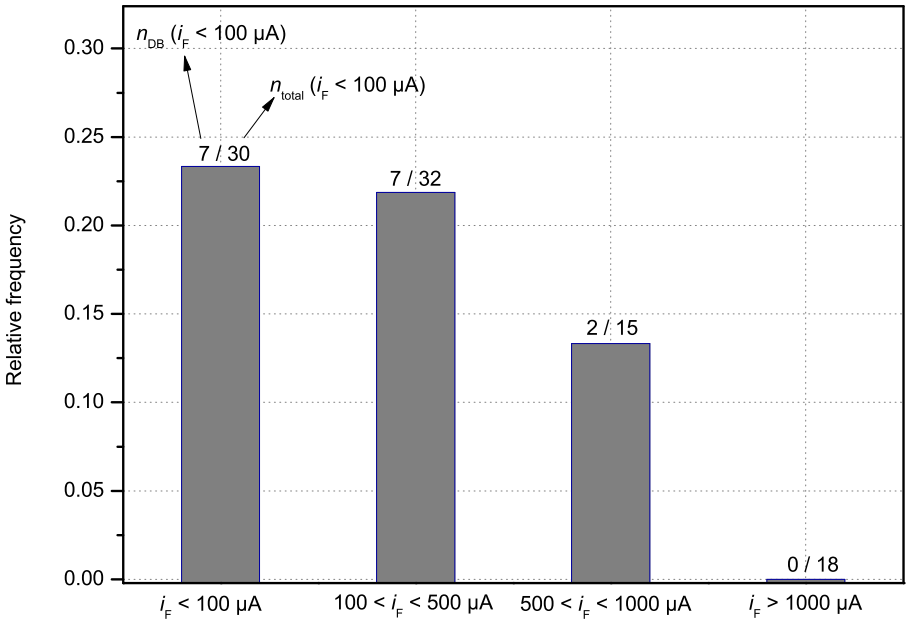

Figure 9.30: Relative frequency of breakdowns for certain ranges of the field emission current, (10 × 10)-measurement on the interrupter "E"

(Figure 9.27) it is obvious that higher average field emission currents are recorded for interrupter "E" than for interrupter "A", where no breakdown at all is observed. Therefore, the average field emission currents indicate also here possible dielectric instabilities of the interrupter (particles presence). In this regard, particles have significant influence. On one hand, they may affect the contact surface condition due to their impact with the contact, and therefore affect the field emission current as well as the dielectric behavior of the interrupter. On the other hand, particles evaporation (see 2.2.3) may result in a direct breakdown without any preceding increase in field emission current.

9.4.2 Influence of gap spacing

As during the measurements on commercial interrupters (manufacturer "M1") no breakdown is observed at all, it is interesting to study the effect of the gap spacing in this regard. For this reason, procedure 3 is performed on interrupters with reduced gap spacings:

- B: $d_r = 8$ mm, $d = 6$ mm
- F: $d_r = 11$ mm, $d = 8$ mm
- G: $d_r = 11$ mm, $d = 4$ mm

where, d_r is the rated gap spacing and d is the actual gap spacing.

Field emission current at reduced gap spacing

Figure 9.31 shows the average field emission current amplitudes measured during procedure 3 on interrupters "F" and "G", having $d = 8$ mm and $d = 4$ mm, respectively. It is observed that the average values of the field emission current non-linearly depend on the gap distance. They are unambiguously (factor of approximately 3.5) higher at shorter contact distances. This is explained by the higher electrical field stress in the gap at shorter distances and same applied recovery voltage. The higher electrical field stress results in more breakdowns for interrupter "G".

Comparing the results of interrupter "A" (see Figure 9.27) and interrupter "F" (having equal gap spacings), it is seen that for both interrupters the average field emission currents are in the same range. Furthermore, no breakdowns are observed during the measurement sets for any of these interrupters.

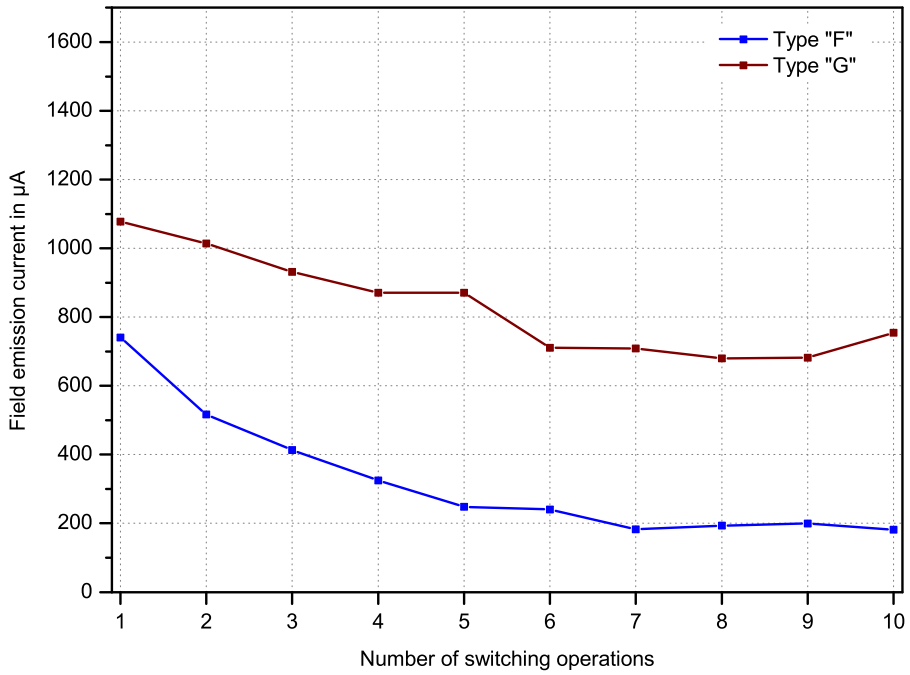

Figure 9.31: Average field emission current amplitudes during (10×10)-measurements for interrupters types "F" ($d = 8$ mm) and "G" ($d = 4$ mm)

Characteristics of dielectric breakdowns during recovery

Figure 9.32 shows the cumulated number of breakdowns during procedure 3 for interrupters "B", "F", "G". For the 24 kV interrupters ("F", "G") it is seen that a reduction of gap

spacing from nominal value $d_r = 11$ mm to $d = 8$ mm ("F") does not result in additional breakdowns during the measurement set (no breakdown out of one hundred interruptions). Further decrease of the gap spacing to $d = 4$ mm ("G") affects the dielectric behavior of the interrupter significantly (fourteen breakdowns out of one hundred interruptions). For the 17.5 kV interrupter ("B"), where the gap spacing is decreased from $d_r = 8$ mm to $d = 6$ mm, only two breakdowns out of one hundred measurements are observed.

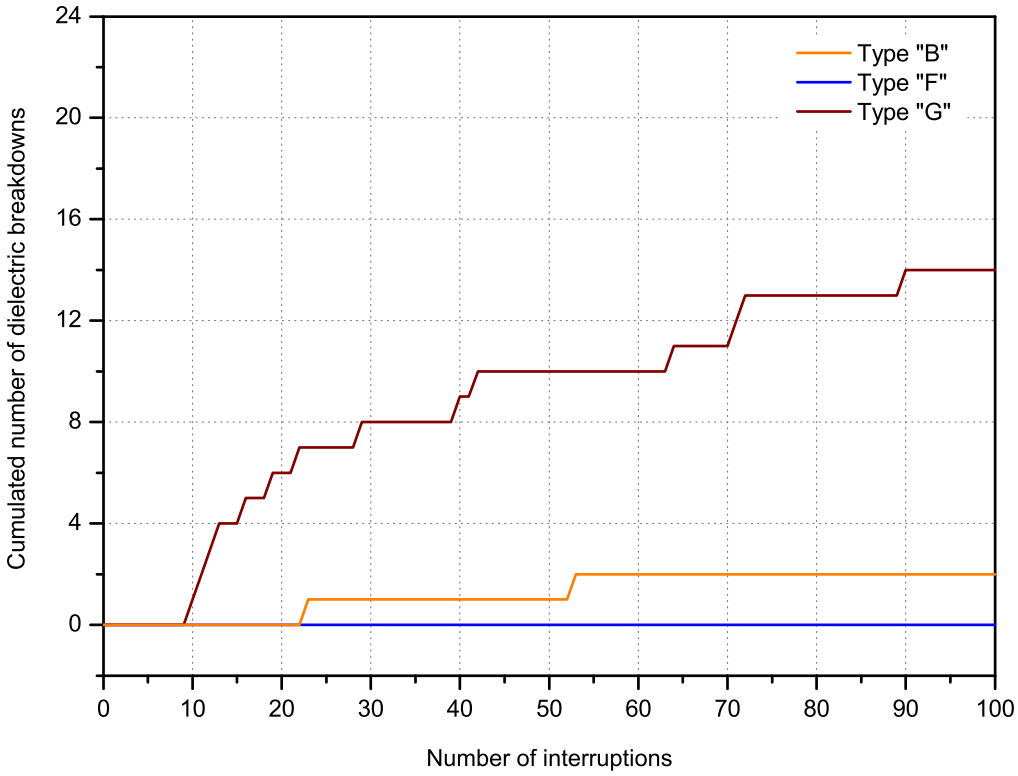

Figure 9.32: Cumulated number of dielectric breakdowns for one interrupter of each type "B" ($d_r = 8$ mm, $d = 6$ mm), "F" ($d_r = 11$ mm, $d = 8$ mm), "G" ($d_r = 11$ mm, $d = 4$ mm) tested acc. to procedure 3

A comparison of the breakdown moments of interrupters "B" and "G" (with reduced gap spacings) with interrupters "C", "D" and "E" (with modified manufacturing process or different manufacturer) are given in **Figure 9.33**. Here, two different kinds of dielectric breakdowns can be clearly distinguished:

1. Breakdowns in the first recovery cycle ($t_{DB} \leq 20$ ms, cyan colors): These breakdowns occur due to the initial high electrical field stress i.e. short gap spacing like interrupters "B" and "G" or high surface roughness like the unconditioned interrupter "D".

2. Breakdowns in the range 20 ms $< t_{DB} \leq$ 100 ms and $t_{DB} >$ 100 ms (gray colors): These breakdowns occur most likely due to particle effect under high electrical field stress, which may increase the field emission current or lead directly to a breakdown (interrupters “C” and “E”).

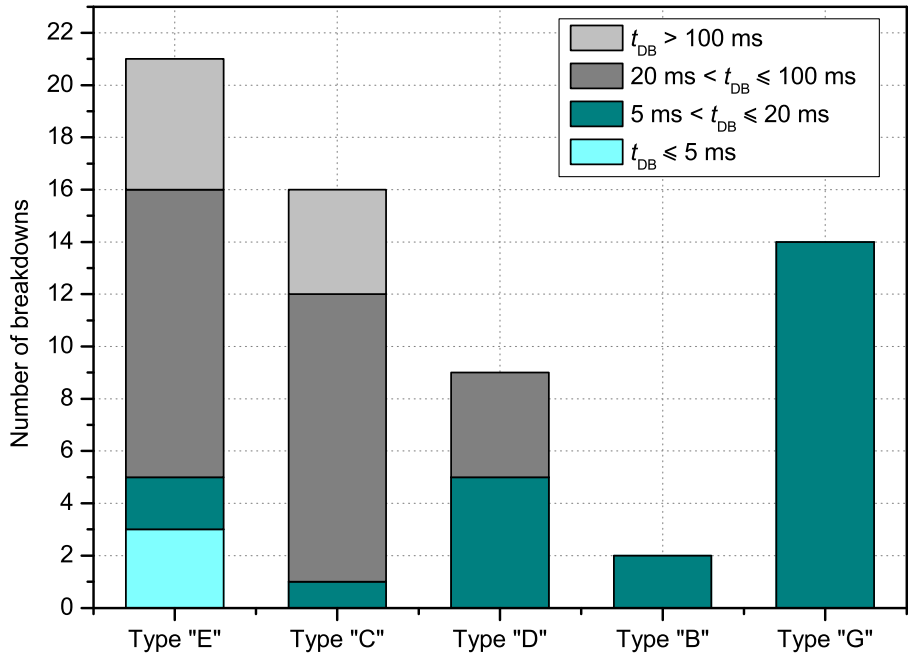

Figure 9.33: Breakdown moments for different interrupters tested acc. to procedure 3, t_{DB}: moment of dielectric breakdown

9.5 Conclusion

Applying the developed measuring system for field emission current measurement after capacitive current switching in high-voltage or full-power test laboratories, it is possible to get deeper insight into dielectric recovery performance of vacuum interrupters. A wide range of field emission current amplitudes has been observed in more than one thousand measurements, which did not lead to a breakdown in commercially manufactured vacuum interrupters (“A”) produced by manufacturer M1.

For modified interrupters type “D” (without conditioning) dielectric breakdowns are observed more frequently at the beginning of the measurement sets. The number of breakdowns is decreased later on due to the conditioning effect of the breakdowns as well as the breaking current. They also occur either in the first or second recovery cycle, but never

later. These breakdowns seem to be a kind of conditioning breakdowns and occur due to the high cathode roughness, as the interrupters contacts were not conditioned during manufacturing process, and consequently high surface electrical field stress.

Comparable type of dielectric breakdowns are also observed by commercial interrupters with reduced gap spacing e.g. type "G" ($d_r = 11$ mm, $d = 4$ mm). Here, early dielectric breakdowns only in the first recovery cycle are observed. The origin of these breakdowns is also the original high electrical field stress and field emission current because of too low gap spacing.

Another type of dielectric breakdowns are observed by interrupters "C" (manufactured in non-clean room condition) and "E" (commercially manufactured by manufacturer M2). They show the highest number of breakdowns during all measurement sets (twenty two breakdowns for "E" and twenty breakdowns for "C"). Here, breakdowns mostly occurred after a time of hundred milliseconds or even later. Furthermore, high average field emission currents are recorded compared to commercial interrupters "A" from manufacturer M1.

For modified interrupters type "C" dielectric breakdowns are observed more frequently after field emission current amplitudes above 500 µA. However, no fix and clear relationship can be established between breakdown probability and field emission current in such interrupters. For interrupter type "E", more breakdowns occurred at field emission current amplitudes below 500 µA. Nevertheless, an average high field emission current is also recorded for this interrupter, which indicates its dielectric instabilities. For both types of interrupters "C" and "E", particles have an important effect on the dielectric property of the interrupter. Under high enough electrical field stress, they may either have an indirect influence i.e. varying the field emission characteristics (particle induced field emission current) or lead directly to a breakdown after their evaporation.

Therefore, the average value of the field emission current is a good measure for the dielectric properties of the interrupter. In all measurement sets higher average field emission currents are measured for interrupters also having a higher number of breakdowns. However, one single measurement is not adequate to forecast the interrupter behavior. A higher number of measurements and statistical evaluation are necessary.

The dielectric impact of a making arc on the surface micro-topology (de-conditioning), as well as the subsequent surface conditioning by the breaking arc can be mapped in a convincing way. The investigations have shown, that the inrush current has a large de-conditioning effect on the interrupter contacts, clearly related to its amplitude. In case of higher inrush making current, higher field emission current is observed after current interruption. Furthermore, it is observed that the capacitive arc current has a positive

conditioning effect on the contacts surface, which is clearly related to the arc's energy i.e. arc's amplitude and time duration. After short arcing time or low breaking arc current the field emission current is much higher than after longer arcing time or higher breaking arc current.

10 Conclusion and Summary

With regard to the environmental issues, many investigations have been performed in different countries in the last years to develop vacuum circuit breakers for transmission voltages as a possible replacement for SF_6. At the moment vacuum breakers are most dominant for applications at medium voltage levels. However, the existing medium voltage vacuum technology cannot be directly applied to the transmission voltage levels. Many important design features face more difficulties at high voltage levels. In this work, two issues of special importance for the applicability of vacuum circuit breakers to higher system voltage levels are investigated: diagnostic of vacuum quality ("DVQ") and impact of capacitive switching ("ICS").

A special system is developed for measuring a very wide range of field emission current amplitudes ($10\,\mu A \cdots 5\,mA$) immediately after HF current arc-polishing (for DVQ) as well as after capacitive current switching (for ICS) in high-voltage or full-power test laboratories. By using anti-parallel diodes the high current and the low field emission current, which differ by several orders of magnitude in amplitude, can be measured separately. Furthermore, the required compensation tool (hardware/online method) is developed for the compensation of the capacitive component of the total current due to the interrupter's stray capacitance. This method is then compared with the software/offline method (developed by project-partner (KEMA), which is more suitable for applications under more severe electromagnetic interferences. The measured field emission current is validated by application of the Fowler-Nordheim equation (FNE) in all cases. The current/voltage relationship follows perfectly the Fowler-Nordheim theory.

10.1 Diagnostic of vacuum quality (DVQ)

In spite of different investigations over the last decades, still no appropriate tool for the diagnostic of the vacuum state in interrupters after several years of service has been established. While the lack of such tool is not necessarily an essential issue in medium voltage

levels, it might become important for transmission system application. As the interrupter becomes larger in size at higher voltages, there are more difficulties to be handled and more careful designs of the components, seals, and assembly techniques are required. Moreover, despite the vacuum interrupter success in real service for more than 30 years in medium voltage levels, the users in the transmission voltage levels often want to know more about the up-to-date state of the high-voltage devices during their whole service life. According to current findings of the Cigré working group A3.27 "The impact of the application of vacuum switchgear at transmission voltages" (established 2009; work not yet finished), besides some technical and economical concerns, the non-availability of vacuum quality diagnostic tools might be one of the reasons for transmission system operators not to apply vacuum circuit breakers in their high-voltage transmission systems.

The inherent high functional reliability of vacuum interrupters depends on the high degree of vacuum, persisting for a long time. After some years of service the internal pressure might increase due to out-gassing from materials inside the interrupter, gas permeation through the insulation housing and metallic flanges or small gas leakages (e.g. caused by undue mechanical stress). If the internal pressure of the interrupter reaches the critical levels (in the range of $10^{-4} \cdots 10^{-2}$ mbar), the current breaking capability and finally the insulation strength of the interrupter is not adequate any more. Therefore, an applicable, simple on-site diagnostic method for the internal pressure verification, without demounting the interrupter from the switchgear is still looked for.

One idea, published earlier, is based on the analysis of the changing rate of field emission currents immediately after arc-polishing of the contacts (field emission analysis (FEA) method). While the absolute value of the field emission current has no simple dependence on the internal pressure, this is the case for the current changing rate. The re-adsorption process of a gas layer on a metal surface (after arc-polishing) distinctly depends on internal pressure. The field emission current decays with time, and the relevant time constant is shorter for higher internal pressures. Therefore, if the gas layer is forced to be removed from the contact surface with the help of arc-polishing by spark-over of the electrodes and a subsequent defined current flow, afterwards the time response of re-adsorption of the gas layer can be observed by measuring the field emission current over time.

It was the goal of this project to systematically investigate if this method, so far only tried out on model configurations, is applicable to commercial interrupters having complex gap and contacts geometries, and if the method is stable and robust enough to serve as basis of a future on-site diagnostic method which then would have to be developed. It was not the goal to actually perform the development of such method or to find a superseded method for internal pressure verification.

For this purpose, an experimental test circuit was developed that allows arc-polishing at different parameters (amplitude, frequency of the arc current), subsequent flow of field emission current and current analyses. Numerous test samples were investigated: commercial interrupters from different manufacturers with increased internal pressures, as well as a model vacuum interrupter (MVI) with different electrode configurations (plate-plate, tip-plate) and electrode materials (Cu, CuCr). In the model vacuum interrupter also the internal pressure and the residual gas type could be varied.

As result of these investigations, it can be summarized that for commercially available vacuum interrupters it was not possible at all to define a test method or any test parameter configuration based on the chosen method, respectively, which would reproducibly cause a decay of the field emission current after arc polishing. In only 3% (commercial interrupters) and 5% (MVI with plate-plate electrodes) of all cases the effect of decaying of field emission current was observed. This is mainly explained by the fact that it is essential that the arc-polishing (removing of the gas molecules from the contact surface) exactly takes place on cathode regions, which would contribute later to the field emission current process. Otherwise, field emission current would flow from emitters that were not cleaned before by means of the arc, and thus no change in the field emission current will later be observed. Consequently, on a flat electrode surface (as it is the case in a vacuum interrupter) it will be just a matter of statistics if the effect of interest can be observed or not.

It was found that the yield is much higher for inhomogeneous electrode configurations (tip-plate) where the locations of arc-polishing and origin of the subsequent field emission current are more likely the same. Here, an inverse dependency between the decisive decay time constant τ_2 of the field emission current and the internal pressure is found. At higher internal pressure, smaller decay time constants are measured, which is due to the faster gas re-adsorption process. Nevertheless, a sufficiently high number of measurements (at least twenty) must be performed for correct evaluation of the internal pressure. It is observed that the mean value of the decay time constant τ_2 (calculated from twenty measurements) is in a good agreement with the calculated formation time of a mono molecular gas layer on a solid surface.

But even in the investigated extreme case of a tip-plate electrode, the effect would occur in only 85% of all cases. Regarding further that due to the observed wide stray of the decisive time constant τ_2 at least twenty successful measurements are required for a statistically reliable evaluation (meaning that on a commercial interrupter 700 trials would be necessary, which is a totally unacceptable value), the investigated method has no practical meaning for monitoring purposes. Though the effects, which were published earlier, are basically

present, the reproducibility is unfortunately too low. The search for a practical on-site diagnostic tool must therefore go on.

10.2 Impact of capacitive switching (ICS)

A very important issue for development of high voltage vacuum circuit breakers is their dielectric behavior after switching of capacitive loads. For utilization of vacuum interrupters in transmission systems, the restrike phenomena (dielectric breakdown) must be well understood and related problems be solved. Even in the medium voltage levels, there are severe requirements for the capacitive test duty according to the IEC circuit breaker standard [IEC6 08]. To design an interrupter with very low probability of restrikes, especially at higher voltages, more investigations on the dielectric performance of the interrupter during recovery is required. Here, more information (than "pass" or "not pass") during the measurement is necessary, which identifies the different electrical activities (especially field emission current) in the vacuum gap during the recovery phase of the interrupter.

Switching of capacitive loads results in an increased dielectric stress of the interrupter (about 2 to 2.5 p.u.). While most vacuum interrupters are able to withstand the unidirectional capacitive recovery voltage during their service life, once in a while a breakdown will occur. In case multiple breakdowns happen at voltage peaks, the capacitive load can be charged to a multiple of the system voltage peak value. Multiple breakdowns may lead to very high overvoltages, which may cause damage to the switchgear insulation and to the capacitive load.

To find out the impact of capacitive switching on the dielectric behavior of vacuum interrupters, and to have more detailed information on the origin of restrikes, measurements of very low field emission currents immediately after interruption of capacitive currents during the complete period of the dielectric recovery are performed both in a high-voltage experimental circuit as well as in a full-power test-circuit. Numerous test samples were investigated: commercial interrupters from different manufacturers (up to 36 kV rated voltage) as well as non-regular interrupters each having certain process modifications.

As result of these investigations, it can be summarized, that the impact of the inrush (making) current on the field emission current during recovery is observed to be large and to be clearly related to its amplitude. Furthermore, it is seen that the capacitive arc current and its time duration have significant influence on the field emission current during recovery. After short arcing time the field emission current is much higher than after longer arcing time. The dielectric impact of the making arc on the surface micro-topology, as well

the subsequent surface conditioning by the breaking arc can be mapped in a convincing way.

More than one thousand measurements did not lead to a breakdown in commercially manufactured vacuum interrupters ("A") produced by manufacturer M1. For interrupters manufactured intentionally without conditioning process ("D") and commercial interrupters with reduced gap spacing ("G": $d_\mathrm{r} = 11\,\mathrm{mm}$, $d = 4\,\mathrm{mm}$ and "B": $d_\mathrm{r} = 8\,\mathrm{mm}$, $d = 6\,\mathrm{mm}$) early dielectric breakdowns (in the first recovery cycle) are mostly observed. These breakdowns occur due to the original high electrical field stress because of short gap spacing like interrupters "B" and "G" or high surface roughness like the unconditioned interrupter "D".

Another type of dielectric breakdowns are observed for interrupters "C" (intentionally manufactured in non-clean room condition) and "E" (commercial one from manufacturer M2). They show the highest number of breakdowns during all measurement sets as well as the highest average field emission currents. Here, breakdowns mostly occurred after time durations of hundred milliseconds or even later. It is supposed that this kind of dielectric breakdowns occurs due to the particles which are more likely present in these interrupters. Observation of the fluctuations in the field emission current during recovery also supports this assumption. On one hand, particles may increase the field emission current during their "in-flight" phase or by their impact to the electrodes, and on the other hand they may even lead to a direct breakdown after evaporation without any preceding increase in field emission current.

It was found that the average value of the field emission current (according to the introduced procedure "(10×10)measurement") is a good measure for dielectric instabilities of the interrupter. In all measurement sets higher average field emission currents are measured on interrupters with also higher number of breakdowns. However, no solid one-by-one relationship can be established between breakdown probability and field emission current in such interrupters. Therefore, one single measurement is not adequate to forecast the interrupter behavior and a higher number of measurements (like in procedure "(10×10)measurement") and statistical evaluation are necessary.

Comparing the measurement results it can also be concluded that the likelihood of restrikes during capacitive switching is a proper figure to control the production quality of vacuum interrupters. Hence, by using this method the stability of the production process of vacuum interrupters can be evaluated.

10.3 Outlook

More measurements for various type of vacuum interrupters from different manufacturers with different manufacturing process have to be carried out using the presented procedure "(10×10)measurement" in order to create a data bank, which then gives information about the average value of the field emission current, its relative frequency and the number of dielectric breakdowns. This data bank can be subsequently used as a proper tool for the evaluation of the interrupter dielectric properties.

Furthermore, using this procedure and the corresponding data bank, the influence of the production process on the interrupters' behavior can be understood better. Therefore, the manufacturers can optimize the process for the capacitive test duty. Especially for applications in high voltage levels, proper production process can be developed.

The phenomenon of fluctuation in the field emission current after current interruption is a new finding that is still not clearly understood. Different hypotheses about their origin are suggested in this work. It is supposed that this phenomenon and its origin has an important influence on the interrupter dielectric behavior. Its deeper understanding may therefore help to solve the problem of restrikes at higher voltage levels. Thus, more investigations in this regard are required.

To understand the impact of the micro-particles, particularly their type (metallic or non-metallic) and size, it is helpful to introduce certain known particles to commercial interrupters during their manufacturing process in clean room condition (controlled uncleaned interrupter). It is then interesting to check the phenomenon of fluctuation as well as breakdown events for such modified interrupters.

Another point are the observed high frequency (HF) spikes (possibly micro-discharges) overlapped to the peak of the field emission current. During the measurements, such HF spikes are detected as the voltage across the interrupter rises. It is important to note, that at certain voltage the spikes were observable only after mechanical switchings and not in case of only applying voltage on interrupter in open position. Measurement of such HF spikes over a long duration of time (more than one second) is a challenging task and requires a measurement system with very high sampling rate. An exact evaluation of these spikes may help to have a better view on the micro-particles and fluctuation phenomena.

Appendix A

Diode-resistor-shunt "DRS"

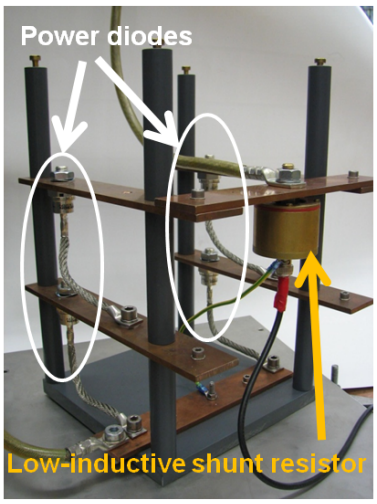

Figure A.1: Photo of the diode-resistor-shunt (DRS)

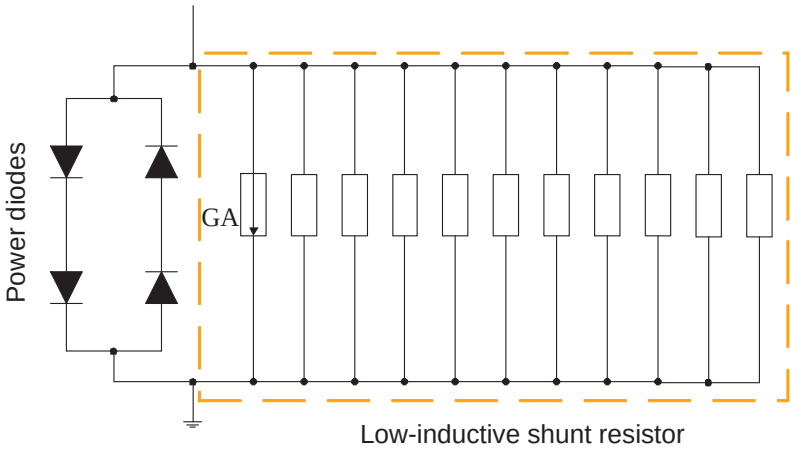

Figure A.2: Circuit diagram of diode-resistor-shunt (DRS), GA: gas-discharge arrester

Appendix B

Compensation

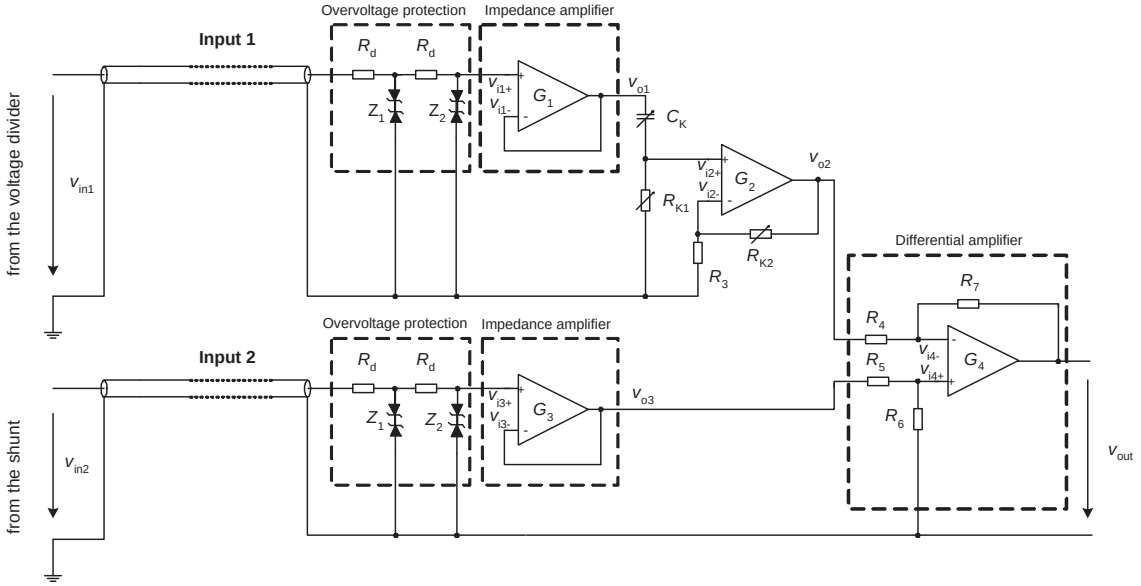

Figure B.1: Electronic compensation circuit.
R_d: decoupling resistor
Z_1 and Z_1: Zener diodes for overvoltage protection
C_k: rotary capacitor ($5 \cdots 100$ pF)
R_k1: potentiometer ($0 \cdots 1$ MΩ)
R_k2: potentiometer ($0 \cdots 1$ kΩ)
$R_3 = 100\,\Omega$
$R_4, R_5, R_6, R_7 = 10\,\mathrm{k}\Omega$

In the following the voltage of different nodes in the cicuit is calculated. Finally, it is shown that the output voltage represents the pure field emission current.

$$v_\mathrm{in1} = v_\mathrm{2,vac} = \frac{v_\mathrm{vac}}{\text{divider ratio}} \tag{B.1}$$

$$v_{\mathrm{in2}} = R_{\mathrm{sh}} \cdot i_{\mathrm{tot}} \tag{B.2}$$

$$v_{\mathrm{o1}} = v_{\mathrm{in1}} \; ; \; v_{\mathrm{o3}} = v_{\mathrm{in2}} \tag{B.3}$$

$$v_{\mathrm{i2+}} \approx R_{\mathrm{k1}} \cdot C_{\mathrm{k}} \cdot \frac{\mathrm{d}v_{o1}}{\mathrm{d}t} \tag{B.4}$$

$$v_{\mathrm{o2}} = v_{\mathrm{i2+}} \cdot \frac{R_{\mathrm{k2}} + R_3}{R_3} \tag{B.5}$$

$$v_{\mathrm{out}} = v_{\mathrm{o3}} - v_{\mathrm{o2}} = v_{\mathrm{in2}} - R_{\mathrm{k1}} \cdot C_{\mathrm{k}} \cdot \frac{R_{\mathrm{k2}} + R_3}{R_3} \cdot \frac{\mathrm{d}v_{\mathrm{in1}}}{\mathrm{d}t} \tag{B.6}$$

$$v_{\mathrm{out}} = v_{\mathrm{in2}} - k_{\mathrm{c}} \cdot R_{\mathrm{sh}} \cdot \frac{\mathrm{d}v_{\mathrm{in1}}}{\mathrm{d}t} \tag{B.7}$$

Where k_{c} is defined as:

$$k_{\mathrm{c}} = R_{\mathrm{k1}} \cdot C_{\mathrm{k}} \cdot \frac{R_{\mathrm{k2}} + R_3}{R_3 \cdot R_{\mathrm{sh}}} \tag{B.8}$$

and $i_{\mathrm{cap,equ}}$ is:

$$i_{\mathrm{cap,equ}} = k_{\mathrm{c}} \cdot \frac{\mathrm{d}v_{\mathrm{in1}}}{\mathrm{d}t} \tag{B.9}$$

With correct adjusting of the rotary capacitor C_{k} and two potentiometer R_{k1} and R_{k2}, it is possible to achieve $i_{\mathrm{cap,equ}} = i_{\mathrm{cap}}$, and thus:

$$v_{\mathrm{out}} = R_{\mathrm{sh}} \cdot i_{\mathrm{F}} \tag{B.10}$$

Appendix C

Middle shield potential measurement

Figure C.1 shows the measurement system. It consists of a coupling capacitor $C_{\mathrm{cou}} = 4\mathrm{pF}$ and a charge amplifier of type "Kistler-5011B".

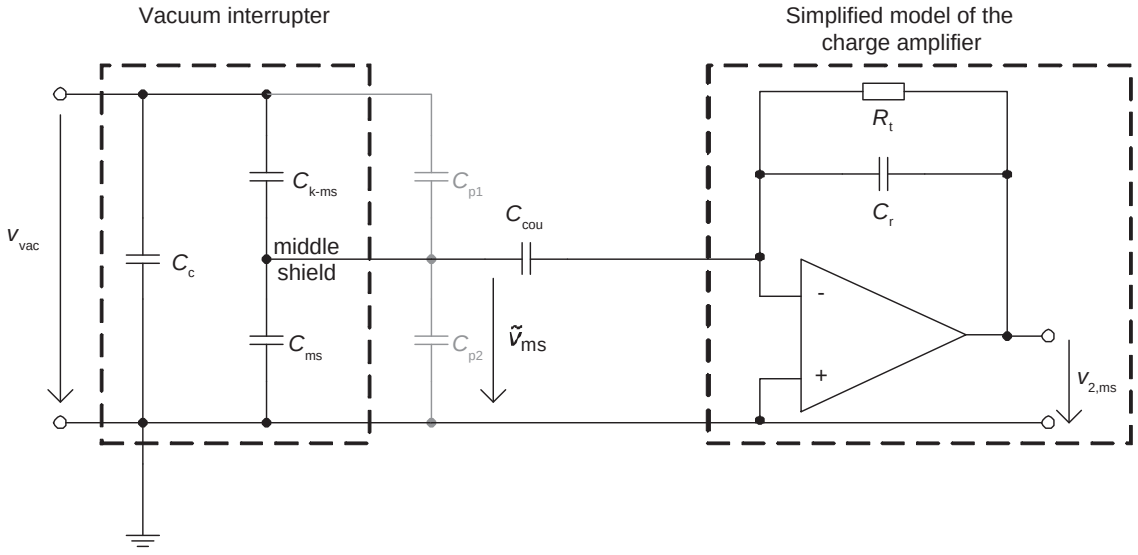

Figure C.1: Measurement system for middle shield potential measurement.
Capacitance between the contacts $C_{\mathrm{c}} = 15\,\mathrm{pF} \pm 25\%$
Capacitance between middle shield and ground contact $C_{\mathrm{ms}} = 25\,\mathrm{pF} \pm 25\%$
Capacitance between middle shield and high voltage contact $C_{\mathrm{k\text{-}ms}} = 15\,\mathrm{pF} \pm 25\%$
Parasitic capacitances $C_{\mathrm{p1}} << C_{\mathrm{k\text{-}ms}}$ and $C_{\mathrm{p2}} << C_{\mathrm{ms}}$
Coupling capacitors $C_{\mathrm{cou}} = 4\,\mathrm{pF}$
Range capacitor $C_{\mathrm{r}} = 100\,\mathrm{nF}$ (adjustable parameter in the charge amplifier)
Time constant resistor $R_{\mathrm{t}} = 1\,\mathrm{G\Omega}$ (adjustable parameter in the charge amplifier)

The charge amplifier acts as an integrator and converts an electric input charge into a usable proportional output voltage. It consists of an inverting voltage amplifier with a high open loop gain and capacitive negative feedback. If the open loop gain is sufficiently high, the output voltage $v_{2,\mathrm{ms}}$ depends on just the input charge Q_i and the range capacitor C_r [Kist 05]:

$$v_{2,\mathrm{ms}} = -Q_\mathrm{i}/C_\mathrm{r} \tag{C.1}$$

The input charge of the amplifier is equal to the charge of the coupling capacitor:

$$Q_\mathrm{i} = \tilde{v}_\mathrm{ms} \times C_\mathrm{cou} \tag{C.2}$$

where, $\tilde{v}_\mathrm{ms}$ is the potential of the middle shield, when the measurement system is connected to the shield. Substituting *equation* C.1 in C.2, it is given:

$$\tilde{v}_\mathrm{ms} = -v_{2,\mathrm{ms}} \times \frac{C_\mathrm{r}}{C_\mathrm{cou}} \tag{C.3}$$

Therefore, measuring the output voltage of the amplifiere $v_{2,\mathrm{ms}}$, the middle shield potential $\tilde{v}_\mathrm{ms}$ can be calculated. To estimate the error due to the connection of the measurement system, the middle shield potential is given here once with ($\tilde{v}_\mathrm{ms}$) and once without (v_ms) the measurement system:

$$v_\mathrm{ms} = v_\mathrm{vac} \times \frac{C_\text{k-ms}}{C_\text{k-ms} + C_\mathrm{ms}} \tag{C.4}$$

$$\tilde{v}_\mathrm{ms} = v_\mathrm{vac} \times \frac{C_\text{k-ms}}{C_\text{k-ms} + C_\mathrm{ms} + C_\mathrm{cou}} \tag{C.5}$$

Thus, from *equations* C.4 and C.5:

$$\frac{\tilde{v}_\mathrm{ms}}{v_\mathrm{ms}} = \frac{C_\text{k-ms} + C_\mathrm{ms}}{C_\text{k-ms} + C_\mathrm{ms} + C_\mathrm{cou}} \tag{C.6}$$

Where, capacitors $C_\text{k-ms}$ and C_ms are defined in Figure C.1. According to the values measured using the impedance analizer, the measurement uncertainty is calculated to be in the range of $-7.5\% \cdots -12\%$. It can be reduced using even smaller coupling capacitors. Here, the influence of the parasitic capacitors C_p1 and C_p2 are neglected. This can be done, as the parasitic capacitances are much lower than capacitances between shield and contacts. It is important to notice, that the calculated measurement uncertainty remains constant during the measurement as long as no changes are introduced to the installed circuit.

Bibliography

[3M 00] 3M. *Online Product Information: 3M Fluorinert Electronic Liquid FC72.* http://www.mgchemicals.com/products/3m-fc72.html from 22.11.2011, 2000.

[Ball 92] J. Ballat. *Untersuchung zum Emissionsstrom-, Konditionierungs- und Schweißverhalten von Vakuum-Schaltstrecken mit CuCr-Kontaktstücken.* PhD thesis, TU Darmstadt, 1992.

[Boxm 95] R. L. Boxman, D. M. Sanders, and P. J. Martin. *Handbook of Vacuum Arc Science and Technology: Fundamentals and Applications.* Noyes Publications, New Jersey, 1995.

[Cigr 10] Cigré. "Working group A3.27: The impact of the application of vacuum switchgear at transmission voltages". *information from internal working documents*, 2010.

[Cigr 94] Cigré. "WG 13.04: Capacitive Current Switching - State of the Art". *Electro*, No. 155, pp. 33–63v, 1994.

[Dams 95] G. C. Damstra, R. P. P. Smeets, and H. B. F. Poulussen. "Pressure Estimation in Vacuum Circuit Breakers". *IEEE Transactions on Dielectrics and Electrical Insulation*, Vol. 2, No. 2, pp. 198 – 201, April 1995.

[Dohn 81] D. Dohnal. *Untersuchung zur Röntgenstrahlung an Hochspannungs-Hochvakuum-Anordnungen.* PhD thesis, TU Braunschweig, 1981.

[Dull 04] E. Dullni, D. Gentsch, I. Kleberg, K. Niayesh, and S. Wenkai. "Switching of Capacitive Currents". *XXIst International Symposium on Discharges and Electrical Insulation in Vacuum (ISDEIV)*, Vol. 2, pp. 407 – 410, September - October 2004.

[Dull 06] E. Dullni, W. Shang, D. Gentsch, I. Kleberg, and K. Niayesh. "Switching of Capacitive Currents and the Correlation of Restrike and Pre-ignition Behavior". *IEEE Transactions on Dielectrics and Electrical Insulation*, Vol. 13, pp. 65 – 71, February 2006.

[Eich 89] J. Eichmeier and H. Heynisch. *Handbuch der Vakuumelektronik*. R. Oldenbourg Verlag, München, Wien, 1989.

[Falk 06] L. T. Falkingham. "Vacuum interrupter design for HV and UHV applications". 2006.

[Fink 95] H. Fink, D. Gentsch, and J. Lipperts. "Quality Control for Vacuum Circuit-Breakers through Residual-Gas Analysis". *ABB Review*, 1995.

[Fron 00] F. R. Frontzek. "Verfahren zur Beurteilung des Innendrucks bei Vakuumschaltkammern". *Elektrie*, pp. 207 – 211, 2000.

[Fron 93a] F. R. Frontzek and D. König. "Measurement of Emission Currents Immediately after Arc Polishing of Contacts - Method for Internal Pressure Diagnostics of Vacuum Interrupters". *IEEE Transactions on Electrical Insulation*, Vol. 28, No. 4, pp. 700 – 705, August 1993.

[Fron 93b] F. R. Frontzek, D. König, and R.Heinemeyer. "Electrical Methods for Verifying Internal Pressure of Vacuum Interrupters after Long-time Service". *IEEE Transactions on Electrical Insulation*, Vol. 28, No. 4, pp. 635 – 641, August 1993.

[Fron 98] F. Frontzek and D. König. "Methods for Internal Pressure Diagnostic of Vacuum Circuit Breakers". *XVIIIth International Symposium on Discharges and Electrical Insulation in Vacuum (ISDEIV)*, Vol. 2, pp. 467–472, 1998.

[Gier 01] S. Giere, H. C. Kärner, and H. Knobloch. "Dielectric Strength of Double and Single-Break Vacuum Interrupters". *IEEE Transactions on Dielectrics and Electrical Insulation*, Vol. 8, No. 1, pp. 43 – 47, February 2001.

[Haug 90] R. Haug, T. Kouakou, and J. Doremieux. "Phenomena preceding arc ignition between opening contacts: Experimental Study and Theoretical Approach". *Proceedings of the Thirty-Sixth IEEE Holm Conference on Electrical Contacts*, pp. 543 – 549, August 1990.

[Hein 89] R. Heinemeyer. *Untersuchungen zum Einfluß von Fremdgasen auf das elektrische Verhalten von Cu- und CuCr-Elektroden im Vakuum*. PhD thesis, TU Darmstadt, 1989.

[Heuc 10] K. Heuck, K. D. Dettmann, and D. Schulz. *Elektrische Energieversorgung: Erzeugung, Übertragung und Verteilung elektrischer Energie für Studium und Praxis*. Vieweg and Teubner, 8 Ed., 2010.

[Itur 09] A. Iturregi, E. Torres, I. Zamora, and O. Abarrategui. "High Voltage Circuit Breakers: SF6 vs. Vacuum". *International Conference on Renewable Energies and Power Quality*, April 2009.

[Jutt 71] B. Jüttner. *Der Vordurchschlagsstrom von ausgedehnten Metallelektroden im Hochvakuum.* PhD thesis, Humboldt Universität, Berlin, 1971.

[Jutt 72] B. Jüttner, W. Rohrbeck, and H. Wolff. "Pressure dependence of pre-breakdown currents due to sorption processes". *Vth Int. Symp. on Discharges and Electrical Insulation in Vacuum (ISDEIV)*, pp. 65 – 69, August - September 1972.

[Kama 06] M. Kamarol, S. Ohtsuka, H. Saitou, M. Sakaki, and M. Hikita. "Diagnosis of Vacuum Degree in Vacuum Interrupter Based on Partial Discharge". *XXIInd Int. Symp. On Discharge and Electrical Insulation in Vacuum (ISDEIV)*, 2006.

[Kist 05] Kistler. *Betriebsanleitung: Labor-Ladungsverstärker Type 5011B.* Kistler Instrumente AG, 2005.

[Korn 07] F. Körner, M. Lindmayer, M. Kurrat, and D. Gentsch. "Contact behavior in vacuum under capacitive switching duty". *IEEE Transactions on Dielectrics and Electrical Insulation*, Vol. 14, No. 3, pp. 643 – 648, June 2007.

[Korn 08] F. Körner. *Kontaktverhalten von Vakuumschaltern beim kapazitiven Schalten. 3*, TU Braunschweig, 2008.

[Kuch 05] A. Küchler. *Hochspannungstechnik: Grundlagen - Technologie - Anwendungen.* Springer-Verlag Berlin Heidelberg, 2005.

[Laff 80] J. M. Lafferty. *Vacuum Arcs: Theory and Application.* John Wiley and Sons, New York, Chichester, Brisbane, Toronto, 1980.

[Lane 06] E. P. A. V. Lanen, R. P. P. Smeets, M. Popov, and L. van der Sluis. "Current-Zero Characteristics of a Vacuum Circuit Breaker at Short-Circuit Current Interruption". *XXIInd International Symposium on Discharges and Electrical Insulation in Vacuum (ISDEIV)*, 2006.

[Lane 08] E. P. A. V. Lanen. *The Current Interruption Process in Vacuum: Analysis of the Currents and Voltages of Current-Zero Measurements.* PhD thesis, TU Delft, January 2008.

[Lath 72] R. V. Latham. "Micro-particle charge acquisition and reversal at impact". *Journal Physic D: Application Physic*, Vol. 5, pp. 2044 –2054, 1972.

[Lath 81] R. V. Latham. *High Voltage Vacuum Insulation: The Physical Basis.* Academic Press, London, New York, Toronto, Sydney, San Francisco, 1981.

[Lath 95] R. V. Latham. *High Voltage Vacuum Insulation: Basic Concepts and Technological Practice.* Academic Press, London, San Diego, New York, Boston, Sydney, Tokyo, Toronto, 1995.

[Lipp 03] H. J. Lippmann. *Schalten im Vakuum, Physik und Technik der Vakuumschalter.* VDE Verlag GmbH, 2003.

[Mill 89] H. C. Miller. "A Review of Anode Phenomena in Vacuum Arcs". *Contrib. Plasma Physic 29*, Vol. 3, pp. 223 – 249, 1989.

[Mull 04] A. Müller. *Mittelspannungstechnik: Schaltgeräte und Schaltanlagen.* Siemens AG, März 2004.

[Niay 01] K. Niayesh. "Reignitions in short vacuum gaps after interruption of high-frequency currents caused by ion bombardment". *IEEE Transactions on Plasma Science*, Vol. 29, pp. 69 – 74, February 2001.

[Ohki 07] Y. Ohki. "Japan AE Power Systems Develops High-Voltage, Vacuum Circuit Breakers". *IEEE Electrical Insulation Magazine*, Vol. 23, pp. 48 – 49, January - February 2007.

[Puch 97] V. F. Puchkarev and M. B. Bochkarev. "High Current Density Spotless Vacuum Arc as a Glow Discharge". *IEEE Transactions on Plasma Science*, Vol. 25, No. 4, pp. 593 – 597, August 1997.

[Pupp 91] W. Pupp and H. K. Hartmann. *Vakuumtechnik - Grundlagen und Anwendungen.* Carl Hanser Verlag, 1991.

[Renz 06] R. Renz. "High Voltage Vacuum Interrupters; Technical and Physical Feasibility versus Economical Efficiency". *XXIInd International Symposium on Discharges and Electrical Insulation in Vacuum (ISDEIV)*, Vol. 1, pp. 257 – 262, September 2006.

[Renz 07] R. Renz, D. Gentsch, H. Fink, P. Slade, and M. Schlaug. "Vacuum Interrupters - Sealed for Life". *Nineteenth International Conference on Electricity Distribution (CIRED)*, May 2007.

[Ried 67] W. Rieder. *Plasma und Lichtbogen.* Friedr. Vieweg and Sohn GmbH Verlag, Braunschweig, 1967.

[Ryu 10] J. Ryu, Y. Kim, S. Tak, J. Kim, C. Park, M. Kim, S. Park, and W. Song. "The Challenge of SF6 Gasless Type Switchgear for Distribution and Transmission Voltage Class in Korea". *Cigré A3 308*, 2010.

[Scha 02] E. Schade and E. Dullni. "Recovery of Breakdown Strength of a Vacuum Interrupter after Extinction of High Currents". *IEEE Transactions on Dielectrics and Electrical Insulation*, Vol. 9, pp. 207 – 215, April 2002.

[Sche 06] H. Schellekens and G. Gaudart. "High-Voltage Vacuum Circuit Breaker a Feasibility Study". *XXIInd Int. Symp. on Discharges and Electrical Insulation in Vacuum (ISDEIV)*, Vol. 1, pp. 263 – 266, September 2006.

[Schm 87] H. Schmidt. *Über das Isoliervermögen von Vakuumschaltstrecken mit unterschiedlich vorbeanspruchten Kupfer-Chrom-Kontaktstücken.* PhD thesis, TU Darmstadt, 1987.

[Slad 07] P. G. Slade, R. K. Smith, and E. D. Taylor. "The effect of contact closure in vacuum with fault current on prestrike arcing time, contact welding and the field enhancement factor". *Proceeding of the 53th IEEE Holm Conference on Electrical Contacts*, 2007.

[Slad 08] P. G. Slade. *The Vacuum Interrupter: Theory, Design, and Application.* CRC Press, Boca, Raton, London, New York, 2008.

[Smee 00] R. Smeets and A. Lathouwers. "Capacitive Current Switching Duties of High-Voltage Circuit Breakers: Background and Practice of New IEC Requirements". *IEEE Power Engineering Society*, Vol. 3, pp. 2123 – 2128, January 2000.

[Smee 99] R. Smeets. *Patent 99202407.5-2214: Vakuumqualitätprüfeinrichtung und Verfahren für Vakuumschaltkammern.* 1999.

[Sydo 02] S. V. Sydorenkov, A. S. Baturin, and E. P. Sheshin. "Field Emission Method of Pressure Dynamics Registration in Vacuum Interrupters". *XXth Int. Symp. On Discharge and Electrical Insulation in Vacuum (ISDEIV)*, pp. 568 – 571, 2002.

[Walc 02] K. Walczak. "Method for Vacuum State Evaluation Based on Analysis of Dynamics Changes of Electron Field Emission Current and X-Radiation in Time". *XXth Int. Symp. On Discharge and Electrical Insulation in Vacuum (ISDEIV)*, pp. 231 – 234, 2002.

[Walc 99] K. Walczak, J.Janiszewski, and H. Moscicka-Grzesiak. "Evaluation of Internal Pressure of Vacuum Interrupters Based on Dynamics Changes of Electron Field Emission Current and X-Radiation". *Eleventh International Symposium on High Voltage Engineering*, Vol. 5, pp. 192 – 195, August 1999.

[Wang 06] J. Wang, Z. Liu, S. Xiu, Z. Wang, S. Yuan, L. Jin, H. Zhou, and R. Yang. "Development of High Voltage Vacuum Circuit Breakers in China". *XXIInd International Symposium on Discharges and Electrical Insulation in Vacuum (ISDEIV)*, Vol. 1, pp. 247 – 252, September 2006.

[Will 72] D. W. Williams and W. T. Williams. "Effect of electrode surface finish on electrical breakdown in vacuum". *Journal Physic D: Application Physic*, Vol. 5, pp. 1845 –1854, 1972.

[Wutz 00] M. Wutz, H. Adam, W. Walcher, and K. Jousten. *Handbuch Vakuumtechnik - Theorie und Praxis*. Friedr. Vieweg and Sohn Verlagsgesellschaft mbH, 7. auflage Ed., 2000.

[Xing 10] F. Xing-ming, D. Guang-bo, H. Zhi-Chao, L. Xu-dong, Z. Xin, and Z. Ji-yan. "A Smart System for Vacuum Interrupters Inner Pressure On-line Condition Monitor Based on Zigbee". *XXIVth International Symposium on Discharges and Electrical Insulation in Vacuum (ISDEIV)*, pp. 142 – 145, August - September 2010.

[Ziom 93] W. Ziomek and H. Moscicka-Grzesiak. "Relation of Breakdown Voltage and Prebreakdown Microdischarge Parameters in Vacuum". *IEEE Transactions on Electrical Insulation*, Vol. 28, No. 4, August 1993.

[Ziyu 06] Z. Ziyu, S. Huanshneg, J. Xiuchen, M. Naixiang, L. Liwen, J. Yansong, and L. Man. "Study on New Method for Measurement of Internal Pressure of Vacuum Interrupters". *XXIInd Int. Symp. On Discharge and Electrical Insulation in Vacuum (ISDEIV)*, 2006.

Standards

[IEC6 08] IEC62271-100. *International Standard on high-voltage switchgear and control-gear,*. 2.1 Ed., 2008.

[IEC6 93] IEC60071-1. *Insulation co-ordination - Part 1: Definitions, principles and rules.* 7.0 Ed., 1993.

Own publications

[Kooc 08] M. Koochack-Zadeh and V. Hinrichsen. "Diagnostics of the Vacuum Condition in Medium Voltage Vacuum Circuit Breakers". *IEEE International Symposium on Electrical Insulation*, pp. 728 – 731, June 2008.

[Kooc 09a] M. Koochack-Zadeh, K. Harada, V. Hinrichsen, H. Ikeda, and M. Hikita. "Insulation Properties of Vacuum Interrupters after Short-Circuit Current Interruption". *IEEJ Japan Conference*, March 2009.

[Kooc 09b] M. Koochack-Zadeh, V. Hinrichsen, H. Ikeda, and M. Hikita. "Insulation Properties of Vacuum Interrupters after Short-Circuit Current Interruption". *16th International Symposium on High Voltage Engineering*, August 2009.

[Kooc 10a] M. Koochack-Zadeh, V. Hinrichsen, H. Ikeda, M. Hikita, and K. Harada. "Effect of Short Circuit Switching on Dielectric Properties of Vacuum Interrupters". *IEEE PES Conference*, April 2010.

[Kooc 10b] M. Koochack-Zadeh, V. Hinrichsen, and S. Kuivenhoven. "Measurement of Field Emission Current during Switching of Capacitive Current in Vacuum". *24th International Symposium on Discharge and Electrical Insulation in Vacuum (ISDEIV)*, August - September 2010.

[Kooc 10c] M. Koochack-Zadeh, V. Hinrichsen, R. Smeets, and A. Lawall. "The Impact of Capacitor Bank Inrush Current on Field Emission Current in Vacuum". *24th International Symposium on Discharge and Electrical Insulation in Vacuum (ISDEIV)*, pp. 210 – 213, August - September 2010.

[Kooc 11] M. Koochack-Zadeh, V. Hinrichsen, R. Smeets, and A. Lawall. "Field Emission Currents in Vacuum Breakers after Capacitive Switching". *IEEE Transactions on Dielectrics and Electrical Insulation*, June 2011.

Coordinated student research projects and diploma theses

[1] Thomas Rettenmaier. *Untersuchung der Feldemissionsströme an Vakuumschaltkammern mit erhöhtem Innendruck.* Number 1817. Darmstadt, 2008.

[2] Vukasin Basara. *Dielektrisches Verhalten von Vakuumschaltern während der Stromunterbrechung - Stand der Forschung.* Number 1821. Darmstadt, 2008.

[3] Kai Gorlt. *Aufbau und Inbetriebnahme eines Versuchsstandes zur Untersuchung des dielektrischen Verhaltens von Vakuumschaltern während der Stromunterbrechung mit Hilfe eines kombinierten Wechselspannungs- und Stromkreises.* Number 1825. Darmstadt, 2008.

[4] Jonas Schulze. *Dielektrisches Verhalten von Vakuumschaltkammern während der Stromunterbrechung bei kapazitiver Last.* Number 1835. Darmstadt, 2009.

[5] Benjamin Baum. *Aufbau und Inbetriebnahme von Messaufbauten zur Messung des Mittelschirmpotentials und der hochfrequenten Anteile des Emissionsstroms bei Vakuumschaltern.* Number 1846. Darmstadt, 2010.

Curriculum Vitae

Masoumeh KOOCHACK ZADEH
born on 13.12.1979 in Tehran

from 03.2011	Technical Asset Manager Tennet TSO GmbH, Lehrte, Germany
02.2006 - 01.2011	Scientific Assistant at High Voltage Laboratories, Technischen Universität Darmstadt, Germany
04.2005 - 06.2005	Industry Internship, Siemens AG, Berlin, Germany
10.2003 - 01.2006	Student at the Faculty of Electrical Power Engineering, Technischen Universität Darmstadt, Germany Degree: Master of Science
10.1998 - 06.2003	Student at the Faculty of Electrical Power Engineering, Amir Kabir University of Technology, Iran Degree: Bachelor of Science

Erklärung laut §9 PromO

Ich versichere hiermit, dass ich die vorliegende Dissertation allein und nur unter Verwendung der angegebenen Literatur verfasst habe. Die Arbeit hat bisher noch nicht zu Prüfungszwecken gedient.

Darmstadt, den 18. Januar 2011

Masoumeh KOOCHACK ZADEH